Studies in Engineering Mechanics

Report No. 28

AN INVESTIGATION OF DYNAMIC INSTABILITY OF STIFFENED RECTANGULAR PLATES

by

Roger C. Duffield

and

Nicholas Willems

March 1968

CRES

THE UNIVERSITY OF KANSAS • CENTER FOR RESEARCH INC
ENGINEERING SCIENCE DIVISION • LAWRENCE, KANSAS

Studies in Engineering Mechanics
Report No. 28

AN INVESTIGATION OF DYNAMIC INSTABILITY OF STIFFENED RECTANGULAR PLATES

by

Roger C. Duffield
and
Nicholas Willems

March 1968

The University of Kansas
Center for Research in Engineering Science
Lawrence, Kansas

ACKNOWLEDGEMENTS

The writers wish to acknowledge the support from NASA under grant NsG 298 which made this investigation possible. Thanks are expressed to The University of Kansas Center for Research, Inc., Engineering Science Division, and to the University of Kansas Computation Center for their administrative and technical assistance. In addition, thanks are due the Computer Research Center of the University of Missouri-Columbia for allowing the use of their computer in completing this project.*

---

*This report represents the results of the Ph.D. thesis by Roger C. Duffield, Assistant Professor of Mechanical and Aerospace Engineering at the University of Missouri-Columbia, under the supervision of Dr. Nicholas Willems, Professor of Civil Engineering at The University of Kansas.

TABLE OF CONTENTS

		Page
List of Illustrations		iii
1. Introduction		1
	1.1 Objective of the Investigation	1
	1.2 Historical Background	1
2. Theoretical Analysis		3
	2.1 Assumption	3
	2.2 Basic Energy Expressions	3
	2.3 Hamilton's Principle	4
	2.4 General Formulation of the Problem	5
	2.5 Matrix Formulation	10
	2.6 Solution of the System of Differential Equations	33
	2.7 Special Cases	40
3. Experimental Investigation		44
	3.1 The Apparatus	44
	3.2 Experimental Procedure	50
4. Evaluation of Results		51
	4.1 Theoretical Results	51
	4.2 Experimental Results	59
	4.3 Evaluation of Results	65
5. Conclusions		73

LIST OF ILLUSTRATIONS

Fig. No.	Description	Page
1	Periodically Loaded Stiffened Plate	7
2	Uniformly Spaced Stiffeners	15
3	First Static Instability Mode	45
4	Second Static Instability Mode	45
5	Test Arrangement	46
6	Line Drawing - Test Apparatus	47
7	First Test Specimen	48
8	Second Test Specimen	48
9	Schematic of Experimental Arrangement	49
10	Case No. 1	52
11	First Spatial Mode, Case No. 1	52
12	Second Spatial Mode, Case No. 1	53
13	Third Spatial Mode, Case No. 1	53
14	Mathieu's Results	54
15	Case No. 2	55
16	First Spatial Mode, Case No. 2	55
17	Second Spatial Mode, Case No. 2	56
18	Third Spatial Mode, Case No. 2	56
19	Case No. 3	57
20	First Spatial Mode, Case No. 3	57
21	Second Spatial Mode, Case No. 3	58
22	Third Spatial Mode, Case No. 3	58
23	Fourth Spatial Mode, Test No. 1	61
24	Fifth Spatial Mode, Test No. 2	61

25	Transient Motion from the Principal Region of Instability to the Lower Stability Region	63
26	Transient Motion from the Upper Stability Region to the Principal Region of Instability (Beat)	63
27	Transient Motion from the Upper Stability Region to the Principal Region of Instability	64
28	Transient Motion from the Principal Region of Instability to the Upper Stability Region	64
29	Transient Motion from the Second Temporal Mode of Instability to the Lower Stability Region	66
30	Transient Motion from the Second Temporal Mode of Instability to the Upper Stability Region	66
31	Typical Instability Regions in the (P_1, Θ) Parameter Space (with damping)(18)	68
32	Nonlinear Effects on the Instability Region, in the (Θ ,A) Parameter Space	68
33	Superposition of Spatial Modes, Case No. 2	
34	Transient Motion from the Principal Mode of the First Spatial Mode to the Second Temporal Mode Region of the Second Spatial Mode	70
35	Combined Motion Between the Principal Mode of the First Spatial Mode and the Second Temporal Mode Region of the Second Spatial Mode	71

1. INTRODUCTION

1.1 Objective of the Investigation

The objective of this investigation is to determine theoretically the boundaries of the regions of parametric instability for principal resonance of a simply supported stiffened rectangular plate subjected to periodic in-plane boundary forces. The effects of size and location of the stiffeners on the boundaries of the regions of parametric instability are also studied. Experimental verification is obtained for stiffened plates with a single centrally located stiffener transverse to an in-plane boundary force acting on two opposite edges.

1.2 Historical Background

Parametric instability mainly concerns the study of the response of a mechanical or elastic system to certain types of periodic loads. The term "parametric instability" stems from the fact that the time-dependent load appears in the coefficients (parameters) of the differential equation of motion of the system.

The problem of parametric instability has been studied by several investigators (1, 2, 3, 4). A complete history of the parametric instability of elastic systems through 1951 is given by Beilin and Dzhanelidze (5).* A more recent review of the history is given by Evan-Iwanowski (6, 7).

An article by Beliaev (8), published in 1924, is considered to be the first analysis of parametric instability of a structure. He studied the parametric response of a simply-supported beam subjected to periodic axial loads of the type $P(t) = P_o + P_t \cos \theta t$.

The nonlinear problem associated with the parametric response of an elastic column was studied by Weidenhammer (9,10), by Bolotin (11, 12), and by Grybos (13). Bolotin and Grybos not only studied the nonlinear effects in the principal region of instability but also the higher order parametric instability regions.

Experimental verification of the principal region of parametric resonance reported by Beliaev and others was first obtained by Utida and Sezawa (14). Bolotin (11), verified the existence of the principal region of parametric resonance and he also verified the behavior of the column within the region of instability. The most extensive experimental investigation of the boundaries of the principal region was performed by Somerset (15, 16), in 1964, who was the first to take P_o, P_1 and θ of the axial load, $P(t) = P_o + P_1 \cos \theta t$, to be independent variables.

The research in the area of parametric instability of plate structures is not as extensive as for columns. The first investigation on rectangular plates was done in 1936 by Einaudi (17).

Bolotin (18, 19), was the first to investigate nonlinear problems of parametric response of a rectangular elastic plate. Somerset (20, 21, 22) in 1965 reinvestigated Bolotin's nonlinear problems, and his investigation

---

* Numbers in parenthesis designate references listed in the Bibliography.

is mainly concerned with an experimental study of the nonlinear problem. This experimental study is the only experimental work that has been performed in the area of plates prior to the work done in the investigation presented here.

Vu and Lai (23, 24), 1966, investigated the linear and nonlinear problems of parametric response of a sandwich plate. Ambratsumyan and Gnuni (25,26), 1961, studied the linear and nonlinear problem for an infinitely long three layered plate and took into account linear damping. The nonlinear problem for three layered plates was also studied by Schmidt (27) in 1965.

Research in the proximity of the area of parametric instability of stiffened plates was done by Ambratsumyan and Khachaturian (28, 29) in 1959 and 1960. They studied the vibrational and dynamic stability characteristics of rectangular anisotropic plates using a theory not based on Kirchhoff's hypothesis.

2. THEORETICAL ANALYSIS

2.1 Assumption

There are several mathematical models which can be used to represent a stiffened plate system. In this investigation the mathematical model consists of discrete elements which are the plate and the stiffeners.

The investigation presented in this analysis is limited to a dynamic system so constructed that the stiffeners are attached to the plate in such a manner that the middle-surface of the stiffeners coincides with the middle-surface of the plate. It is assumed that the assumptions of both the classical plate and beam theories hold for this system. It is also assumed that:

(1) the stiffeners are composed of thin walled open members and their torsional rigidities, GJ, are taken to be negligible

(2) the effects of rotary inertia on the system are negligible

In this investigation in the in-plane loading is taken to be periodic in nature. The magnitude of the in-plane loading, applied at the boundaries of the system, will propagate at the speed of the longitudinal frequency of the system. If the frequency of the periodic in-plane boundary loading is taken to be considerably below that of the longitudinal frequency, it is reasonable to assume that the magnitude of the loading is independent of the space coordinates of the system. This implies that the whole system instantaneously senses the magnitude of the loading and that the in-plane inertia effects due to the periodic in-plane boundary loading are negligible.

2.2 Basic Energy Expressions

The total potential energy of the system is the sum of the strain energies and external potential energies. In this investigation the external in-plane forces are limited to those which are expressable in terms of a time dependent potential. Thus:

$$V=\frac{D}{2}\int_0^a\int_0^b\left\{\left(\frac{\partial^2 w}{\partial x^2}+\frac{\partial^2 w}{\partial y^2}\right)^2-2(1-\nu)\left[\frac{\partial^2 w}{\partial x^2}\frac{\partial^2 w}{\partial y^2}-\left(\frac{\partial^2 w}{\partial x\partial y}\right)^2\right]\right\}dx\,dy-$$

$$-\frac{1}{2}\int_0^a\int_0^b\left[N_x\left(\frac{\partial w}{\partial x}\right)^2+N_y\left(\frac{\partial w}{\partial y}\right)^2\right]dx\,dy+\sum_{i=1}^{R}\frac{E_{ri}I_{ri}}{2}\int_0^a\left(\frac{\partial^2 w}{\partial x^2}\right)^2_{y=y_i}dx+$$

$$+\sum_{K=1}^{P}\frac{E_{sK}I_{sK}}{2}\int_0^b\left(\frac{\partial^2 w}{\partial y^2}\right)^2_{x=x_K}dy-\sum_{i=1}^{R}\frac{P_{ri}}{2}\int_0^a\left(\frac{\partial w}{\partial x}\right)^2_{y=y_i}dx-$$

$$-\sum_{K=1}^{P}\frac{P_{SK}}{2}\int_{0}^{b}\left(\frac{\partial w}{\partial y}\right)^{2}_{x=x_K}dy \qquad (1)$$

The total kinetic energy of the system is the sum of the kinetic energies of the plate and the stiffeners which results in:

$$T=\frac{1}{2}\int_{0}^{a}\int_{0}^{b}\left[\rho_p h\left(\frac{\partial w}{\partial t}\right)^2\right]dx\,dy+\frac{1}{2}\sum_{i=1}^{R}\int_{0}^{a}\left[\rho_{ri}A_{ri}\left(\frac{\partial w}{\partial t}\right)^2_{y=y_i}\right]dx+$$

$$+\frac{1}{2}\sum_{K=1}^{P}\int_{0}^{b}\left[\rho_{SK}A_{SK}\left(\frac{\partial w}{\partial t}\right)^2_{x=x_K}\right]dy \qquad (2)$$

2.3 Hamilton's Principle

The dynamic behavior of a continuous system can be formulated in terms of Hamilton's principle. This principle is used as the basis for the determination of the solutions to the problems under study in this investigation. The mathematical statement of Hamilton's principle for a conservative system is:

$$\delta A=0 \qquad (3)$$

in which

$$A=\int_{t_1}^{t_2}L\,dt \qquad (4)$$

and

$$L=T-V \qquad (5)$$

The formulation of the dynamic behavior for the systems under investigation in terms of Hamilton's principle can be obtained by the substitution of Eqs. (1) and (2) into Eq. (3), which results in:

$$\delta A=\delta\int_{t_1}^{t_2}\left\{\frac{\rho_p h}{2}\int_{0}^{a}\int_{0}^{b}\left(\frac{\partial w}{\partial t}\right)^2dx\,dy+\sum_{i=1}^{R}\frac{\rho_{ri}A_{ri}}{2}\int_{0}^{a}\left(\frac{\partial w}{\partial t}\right)^2_{y=y_i}dx+\sum_{K=1}^{P}\frac{\rho_{SK}A_{SK}}{2}\int_{0}^{b}\left(\frac{\partial w}{\partial t}\right)_{x=x_K}dy-\right.$$

$$\left.-\frac{D}{2}\int_{0}^{a}\int_{0}^{b}\left\{\left(\frac{\partial^2 w}{\partial x^2}+\frac{\partial^2 w}{\partial y^2}\right)^2-2(1-\nu)\left[\frac{\partial^2 w}{\partial x^2}\frac{\partial^2 w}{\partial y^2}-\left(\frac{\partial^2 w}{\partial x\partial y}\right)^2\right]\right\}dx\,dy+\right.$$

$$+\frac{1}{2}\int_0^a\int_0^b\left[N_x\left(\frac{\partial w}{\partial x}\right)^2+N_y\left(\frac{\partial w}{\partial y}\right)^2\right]dx\,dy-\sum_{i=1}^{R}\frac{E_{ri}I_{ri}}{2}\int_0^a\left(\frac{\partial^2 w}{\partial x^2}\right)^2_{y=y_i}dx-$$

$$-\sum_{K=1}^{P}\frac{E_{sK}I_{sK}}{2}\int_0^b\left(\frac{\partial^2 w}{\partial y^2}\right)^2_{x=x_K}dy+\sum_{i=1}^{R}\frac{P_{ri}}{2}\int_0^a\left(\frac{\partial w}{\partial x}\right)^2_{y=y_i}dx+\sum_{K=1}^{P}\frac{P_{sK}}{2}\int_0^b\left(\frac{\partial w}{\partial y}\right)^2_{x=x_K}dy=0 \quad (6)$$

2.4 General Formulation of the Problem

For a holonomic system, Hamilton's principle yields the Euler equations for the integral A which are differential equations of motion. If the system has a finite number of generalized coordinates q_k, Lagrange's equations of motion for a conservative system are:

$$\frac{d}{dt}\frac{\partial L}{\partial \dot{q}_K}-\frac{\partial L}{\partial q_K}=0 \quad (7)$$

This equation is used to obtain an approximate solution to the problem under investigation. This approach is sometimes referred to as the Rayleigh-Ritz method or the assumed modes method.

A solution is assumed for the problem in the form of a series composed of a linear combination of functions ϕ_i, which are functions of the spatial coordinates, multiplied by time-dependent generalized coordinates $q_i(t)$, that is

$$w(x,y,t)=\sum_{i=1}^{n}q_i(t)\,\phi_i(x,y) \quad (8)$$

The functions ϕ_i must form a complete set of functions over the region R of the plate and because the problem is formulated in terms of Hamilton's principle they must at least satisfy the prescribed boundary conditions, but not necessarily the natural boundary conditions.

A set of functions, ϕ_i, that are complete over the region of the stiffened plate $0\le x\le a$ and $0\le y\le b$ and which satisfy the simply supported boundary conditions are

$$\phi_{mn}(x,y)=\sin\frac{m\pi x}{a}\sin\frac{n\pi y}{b} \quad (9)$$

Thus, according to Eq. (8) the assumed form for w (x,y,t) is

$$w(x,y,t)=\sum_{m=1}^{\infty}\sum_{n=1}^{\infty}q_{mn}(t)\sin\frac{m\pi x}{a}\sin\frac{n\pi y}{b} \quad (10)$$

The first step for the solution is the determination of the Lagrangian function L in terms of the functions $q_{mn}(t)$. The substitution of Eq. (10) into Eqs. (1) and (2) and then the corresponding substitution of Eqs. (1) and (2) into Eq. (5) gives:

$$L=\frac{\rho_p hab}{8}\sum_{m=1}^{\infty}\sum_{n=1}^{\infty}\left[\dot{q}_{mn}(t)\right]^2+\sum_{i=1}^{R}\frac{\rho_{ri}A_{ri}a}{4}\sum_{m=1}^{\infty}\sum_{n=1}^{\infty}\dot{q}_{mn}(t)\sin\frac{n\pi y_i}{b}\cdot$$

$$\cdot\sum_{u=1}^{\infty}\dot{q}_{mu}(t)\sin\frac{u\pi y_i}{b}+\sum_{K=1}^{P}\frac{\rho_{sK}A_{sK}b}{4}\sum_{m=1}^{\infty}\sum_{n=1}^{\infty}\dot{q}_{mn}(t)\sin\frac{m\pi x_K}{a}\cdot$$

$$\cdot \sum_{v=1}^{\infty} \ddot{q}_{vn}(t) \sin \frac{v\pi x_k}{a} - \left\{ \frac{ab\pi^4 D}{8} \sum_{m=1}^{\infty} \sum_{n=1}^{\infty} \left[q_{mn}(t) \right]^2 \left[\frac{m^2}{a^2} + \frac{n^2}{b^2} \right]^2 - \right.$$

$$- \frac{\pi^2}{8} \sum_{m=1}^{\infty} \sum_{n=1}^{\infty} \left[q_{mn}(t) \right]^2 \left[\frac{m^2 b}{a} N_x(t) + \frac{n^2 a}{b} N_y(t) \right] + \frac{\pi^4}{4a^3} \sum_{i=1}^{R} E_{ri} I_{ri} \cdot$$

$$\cdot \sum_{m=1}^{\infty} \sum_{n=1}^{\infty} m^4 q_{mn}(t) \sin \frac{n\pi y_i}{b} \sum_{u=1}^{\infty} q_{mu}(t) \sin \frac{u\pi y_i}{b} + \frac{\pi^4}{4b^3} \sum_{k=1}^{P} E_{sk} I_{sk} \cdot$$

$$\cdot \sum_{m=1}^{\infty} \sum_{n=1}^{\infty} n^4 q_{mn}(t) \sin \frac{m\pi x_k}{a} \sum_{v=1}^{\infty} q_{vn}(t) \sin \frac{v\pi x_k}{a} - \frac{\pi^2}{4a} \sum_{i=1}^{R} P_{ri}(t) \cdot$$

$$\cdot \sum_{m=1}^{\infty} \sum_{n=1}^{\infty} m^2 q_{mn}(t) \sin \frac{n\pi y_i}{b} \sum_{u=1}^{\infty} q_{mu}(t) \sin \frac{u\pi y_i}{b} - \frac{\pi^2}{4b} \sum_{k=1}^{P} P_{sk}(t) \cdot$$

$$\left. \cdot \sum_{m=1}^{\infty} \sum_{n=1}^{\infty} n^2 q_{mn}(t) \sin \frac{m\pi x_k}{a} \sum_{v=1}^{\infty} q_{vn}(t) \sin \frac{v\pi x_k}{a} \right\} \text{------} \quad (11)$$

In the determination of Eq. (11) summation and integration signs are interchanged. This is done on the basis that w is a fourtimes continuously differentiable function over the region of the stiffened plate.

In this investigation only harmonic in-plane edge forces are considered, which can be expressed as (see also Fig. 1)

$$N_x(t) = N_{xo} + N_{xt} \cos \Theta t \quad \text{-------} \quad (12)$$

and

$$N_y(t) = N_{yo} + N_{yt} \cos \Theta t \quad \text{-------} \quad (13)$$

in which Θ is the circular frequency of the time-dependent component of the forces, N_{xo} and N_{yo} are the static components of the forces, and N_{xt} and N_{yt} are the magnitudes of the variable components of the forces in the x and y directions respectively. The expression for the forces acting on the ends of the i^{th} rib and k^{th} stringer respectively can be written as

$$P_{ri}(t) = \bar{P}_{ri} + P'_{ri} \cos \Theta t \quad \text{--------} \quad (14)$$

and

$$P_{sk}(t) = \bar{P}_{sk} + P'_{sk} \cos \Theta t \quad \text{--------} \quad (15)$$

in which the bar denotes the static component of the force and the prime denotes the magnitude of the variable component of the force. For computation reasons, it is convenient to express Eqs. (14) and (15) in

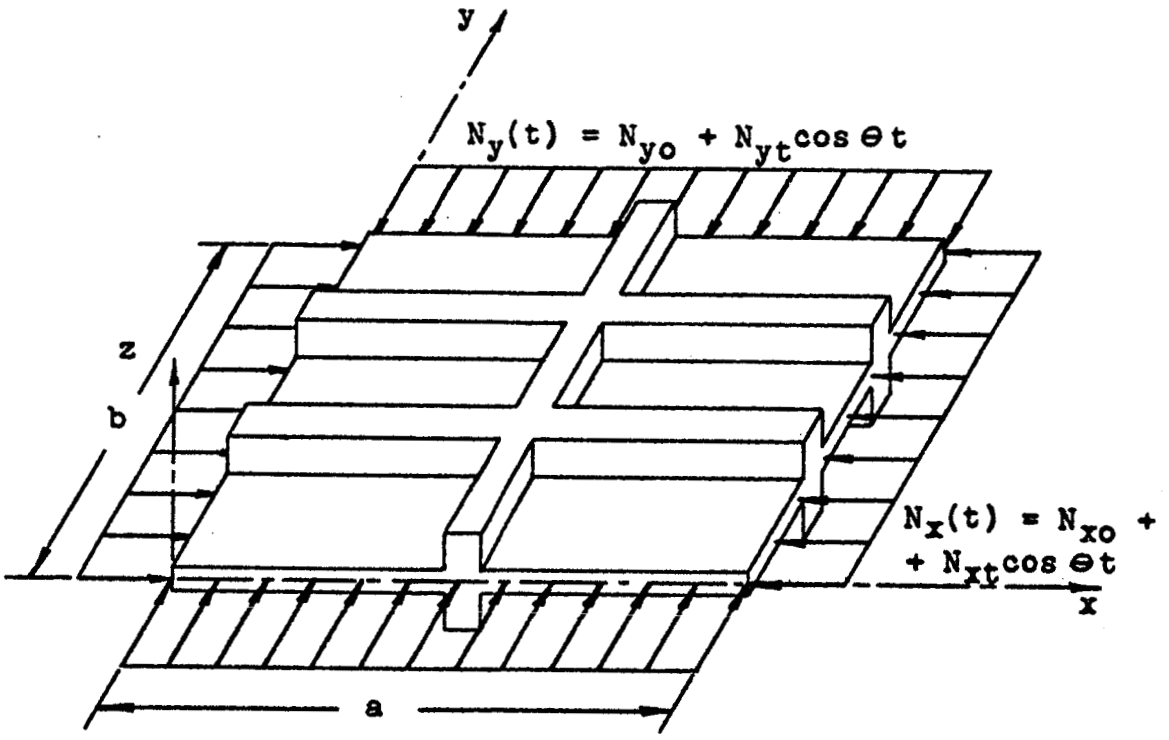

Fig. 1 Periodically Loaded Stiffened Plate

the form

$$P_{ri}(t) = \frac{A_{ri}}{h}\left[\bar{\nu}_{ri} N_{xo} + \nu'_{ri} N_{xt} \cos\theta t\right] - - - - - \quad (16)$$

and

$$P_{sk}(t) = \frac{A_{sk}}{h}\left[\bar{\nu}_{sk} N_{yo} + \nu'_{sk} N_{yt} \cos\theta t\right] - - - - - \quad (17)$$

in which $\bar{\nu}_{ri}$, ν'_{ri} , $\bar{\nu}_{sk}$, and ν'_{sk} are proportionality constants which relate the magnitude of the stiffener loading to the magnitude of the plate loading.

The substitution of Eqs. (12, 13, 16) and (17) into Eq. (11) and next the corresponding substitution of Eq. (11) into Eq. (7) gives

$$\frac{a^4 \rho h}{4\beta\pi^4 D}\ddot{q}_{mn}(t) + \sum_{i=1}^{R}\frac{a^3 \rho_{ri} A_{ri}}{2\pi^4 D}\sin\frac{n\pi y_i}{b}\sum_{u=1}^{\infty}\ddot{q}_{mu}(t)\sin\frac{u\pi y_i}{b} +$$

$$+\sum_{k=1}^{P}\frac{a^3 \rho_{sk} A_{sk}}{2\beta\pi^4 D}\sin\frac{m\pi x_k}{a}\sum_{v=1}^{\infty}\ddot{q}_{vn}(t)\sin\frac{v\pi x_k}{a} + \frac{1}{4\beta}\left[m^2 + n^2\beta^2\right]^2 q_{mn}(t) +$$

$$+\sum_{i=1}^{R}\frac{E_{ri} I_{ri} m^4}{2aD}\sin\frac{n\pi y_i}{b}\sum_{u=1}^{\infty} q_{mu}(t)\sin\frac{u\pi y_i}{b} + \sum_{k=1}^{P}\frac{\beta^3 E_{sk} I_{sk} n^4}{2aD}\cdot$$

$$\cdot \sin\frac{m\pi x_k}{a}\sum_{v=1}^{\infty} q_{vn}(t)\sin\frac{v\pi x_k}{a} - \frac{a^2 m^2}{4\beta\pi^2 D}\left(N_{xo} + N_{xt}\cos\theta t\right) q_{mn}(t) -$$

$$-\frac{\beta a^2 n^2}{4\pi^2 D}\left(N_{yo} + N_{yt}\cos\theta t\right) q_{mn}(t) - \sum_{i=1}^{R}\frac{a m^2 A_{ri}}{2\pi^2 h D}\left(\bar{\nu}_{ri} N_{xo} + \nu'_{ri} N_{xt}\cos\theta t\right)\cdot$$

$$\cdot \sin\frac{n\pi y_i}{b}\sum_{u=1}^{\infty} q_{mu}(t)\sin\frac{u\pi y_i}{b} - \sum_{k=1}^{P}\frac{\beta a n^2 A_{sk}}{2\pi^2 h D}\left(\bar{\nu}_{sk} N_{yo} + \nu'_{sk} N_{yt}\cos\theta t\right)\cdot$$

$$\cdot \sin\frac{m\pi x_k}{a}\sum_{v=1}^{\infty} q_{vn}(t)\sin\frac{v\pi x_k}{a} = 0 \quad (m, n = 1, 2, 3 - - - -\infty) - - - (18)$$

in which $\beta = a/b$. In order to express Eq. (18) in a more workable form the following relationships are introduced

$$\rho_{ri} = \epsilon_{ri}\rho_p \;,\; \rho_{sk} = \epsilon_{sk}\rho_p \quad - - - - - - - - - - - - - \quad (19)$$

and

$$N_{yo} = \bar{u} N_{xo} \;,\; N_{yt} = u' N_{xt} \quad - - - - - - - - - - - - - \quad (20)$$

in which ϵ_{ri} and ϵ_{rs} are proportionality factors relating the magnitude

of the mass densities of the stiffeners to the magnitude of the mass density of the plate and $\bar{\mu}$ and μ' are proportionality factors relating the magnitudes of the static and variable components respectively of the in-plane loading on the plate in the x-direction to the corresponding components in the y-direction. The substitution of Eqs. (19) and (20) into Eq. (18) along with the introduction of a set of parameters gives

$$\frac{M}{\beta}\ddot{q}_{mn}(t)+\frac{2M}{\beta}\sum_{i=1}^{R}\epsilon_{ri}\lambda_{ri}\sin\frac{n\pi y_i}{b}\sum_{u=1}^{\infty}q_{mu}(t)\sin\frac{u\pi y_i}{b}+$$

$$+\frac{2M}{\beta}\sum_{K=1}^{P}\epsilon_{sK}\lambda_{sK}\sin\frac{m\pi x_K}{a}\sum_{v=1}^{\infty}\ddot{q}_{vn}(t)\sin\frac{v\pi x_K}{a}+\frac{1}{4\beta}\left[m^2+n^2\beta^2\right]q_{mn}(t)+$$

$$+\frac{m^4}{2\beta}\sum_{i=1}^{R}J_{ri}\sin\frac{n\pi y_i}{b}\sum_{u=1}^{\infty}q_{mu}(t)\sin\frac{u\pi y_i}{b}+\frac{\beta^3n^4}{2}\sum_{K=1}^{P}J_{sK}\sin\frac{m\pi x_K}{a}\cdot$$

$$\cdot\sum_{v=1}^{\infty}q_{vn}(t)\sin\frac{v\pi x_K}{a}-\left[\frac{\beta m^2}{4}+\frac{\beta^3n^2\bar{\mu}}{4}\right]\bar{\alpha}q_{mn}(t)-\left[\frac{\beta m^2}{4}+\frac{\beta^3n^2\mu'}{4}\right]\cdot$$

$$\cdot\alpha'\cos\theta t\,q_{mn}(t)-\frac{\beta m^2}{2}\sum_{i=1}^{R}\lambda_{ri}\left(\bar{v}_{ri}\bar{\alpha}+v_{ri}'\alpha'\cos\theta t\right)\sin\frac{n\pi y_i}{b}\cdot$$

$$\cdot\sum_{u=1}^{\infty}q_{mu}(t)\sin\frac{u\pi y_i}{b}-\frac{\beta^3n^2}{2}\sum_{K=1}^{P}\lambda_{sK}\left(\bar{v}_{sK}\bar{\mu}\bar{\alpha}+v_{sK}'\mu'\alpha'\cos\theta t\right)\sin\frac{m\pi x_K}{a}\cdot$$

$$\cdot\sum_{v=1}^{\infty}q_{vn}(t)\sin\frac{v\pi x_K}{a}=0\qquad(m,n=1,2,3----,\infty)\text{---}\quad(21)$$

in which

$$M=\frac{a^4\rho_p h}{4\pi^4 D}\text{ ---------}\quad(22)$$

$$\lambda_{ri}=\frac{A_{ri}}{bh}\text{ ------}\quad(23)$$

$$\lambda_{sK}=\frac{A_{sK}}{ah}\text{ ----------}\quad(24)$$

$$J_{ri}=\frac{E_{ri}I_{ri}}{bD}\text{ ---------}\quad(25)$$

$$J_{sk} = \frac{E_{sk} I_{sk}}{aD} \quad \text{---------} \quad (26)$$

$$\bar{\alpha} = \frac{b^2 N_{xo}}{\pi^2 D} \quad \text{---------} \quad (27)$$

and

$$\alpha' = \frac{b^2 N_{yo}}{\pi^2 D} \quad \text{---------} \quad (28)$$

2.5 Matrix Formulation

a. Random Stiffener Size and Material Properties

The generalized coordinates $q_{mn}(t)$ can be represented by a square matrix

$$[\bar{Q}] = q_{mn}(t) = \begin{bmatrix} q_{11} & q_{12} & \cdots & q_{1n} \\ q_{21} & q_{22} & \cdots & q_{2n} \\ \vdots & \vdots & & \vdots \\ q_{m1} & q_{m2} & \cdots & q_{mn} \end{bmatrix} \quad \text{------} \quad (29)$$

for m, n = 1,2,3,----,∞. However, in order to express Eq. (21) in matrix notation it is necessary to represent the set of functions $q_{mn}(t)$ by a column matrix which is composed of the column's of $[\bar{Q}]$ as follows

$$\{Q\} = \begin{Bmatrix} q_{11} \\ \vdots \\ q_{m1} \\ q_{12} \\ \vdots \\ q_{m2} \\ q_{1n} \\ \vdots \\ q_{mn} \end{Bmatrix} \quad \text{----------} \quad (30)$$

With $q_{mn}(t)$ represented in this form Eq. (21) in matrix notation can be written as

$$M[V]\{\ddot{Q}\} + \left[[K] - \bar{\alpha}[S] - \alpha' \cos \theta t [T]\right]\{Q\} = 0 \quad \text{---} \quad (31)$$

in which

$$[V] = V_{mn,vu} = \begin{cases} \frac{1}{\beta} + \frac{2}{\beta}\sum_{i=1}^{R} \epsilon_{ri}\lambda_{ri} \sin n\pi\eta_i \sin u\pi\eta_i + & m=v,\ n=u \\ + \frac{2}{\beta}\sum_{k=1}^{P} \epsilon_{sk}\lambda_{sk} \sin m\pi\xi_k \sin v\pi\xi_k\,, & m=v,\ n=u \\ \frac{2}{\beta}\sum_{i=1}^{R} \epsilon_{ri}\lambda_{ri} \sin n\pi\eta_i \sin u\pi\eta_i\,, & m=v,\ n\neq u \\ \frac{2}{\beta}\sum_{k=1}^{P} \epsilon_{sk}\lambda_{sk} \sin m\pi\xi_k \sin v\pi\xi_k\,, & m\neq v,\ n=u \\ 0\,, & m\neq v,\ n\neq u \end{cases} \quad -- \quad (32)$$

$$[K] = K_{mn,vu} = \begin{cases} \frac{1}{4\beta}\left[m^2+n^2\beta^2\right] + \frac{m^4}{2\beta}\sum_{i=1}^{R} J_{ri} \sin n\pi\eta_i \sin u\pi\eta_i + & m=v,\ n=u \\ + \frac{n^4\beta^3}{2}\sum_{k=1}^{P} J_{sk} \sin m\pi\xi_k \sin v\pi\xi_k\,, & m=v,\ n=u \\ \frac{m^4}{2\beta}\sum_{i=1}^{R} J_{ri} \sin n\pi\eta_i \sin u\pi\eta_i\,, & m=v,\ n\neq u \\ \frac{n^4\beta^3}{2}\sum_{k=1}^{P} J_{sk} \sin m\pi\xi_k \sin v\pi\xi_k\,, & m\neq v,\ n=u \\ 0\,, & m\neq v,\ n\neq u \end{cases} \quad -- \quad (33)$$

$$[S] = S_{mn,vu} = \begin{cases} \left[\frac{\beta m^2}{4} + \frac{\beta n^2\bar{u}}{4}\right] + \frac{\beta m^2}{2}\sum_{i=1}^{R} V'_{ri}\lambda_{ri} \sin n\pi\eta_i \sin u\pi\eta_i + & \\ + \frac{\beta^3 n^2 u'}{2}\sum_{k=1}^{P} V'_{sk}\lambda_{sk} \sin m\pi\xi_k \sin v\pi\xi_k\,, & m=v,\ n=u \\ \frac{\beta m^2}{2}\sum_{i=1}^{R} V'_{ri}\lambda_{ri} \sin n\pi\eta_i \sin u\pi\eta_i\,, & m=v,\ n\neq u \\ \frac{\beta^3 n^2 u'}{2}\sum_{k=1}^{P} V'_{sk}\lambda_{sk} \sin m\pi\xi_k \sin v\pi\xi_k\,, & m\neq v,\ n=u \\ 0\,, & m\neq v,\ n\neq u \end{cases} \quad -- \quad (34)$$

$$[T]=t_{mn,vu}=\begin{cases}\left[\frac{\beta m^2}{4}+\frac{\beta^3 n^2 u'}{4}\right]+\frac{\beta m^2}{2}\sum_{i=1}^{R} V_{ri}'\lambda_{ri}\sin n\pi\eta_i\sin u\pi\eta_i+ \\ +\frac{\beta^3 n^2 u'}{2}\sum_{K=1}^{P} V_{sK}'\lambda_{sK}\sin m\pi\xi_K\sin v\pi\xi_K, & \begin{matrix}m=v\\ n=u\end{matrix} \\ \frac{\beta m^2}{2}\sum_{i=1}^{R} V_{ri}'\lambda_{ri}\sin n\pi\eta_i\sin u\pi\eta_i, & \begin{matrix}m=v\\ n\neq u\end{matrix} \\ \frac{\beta^3 n^2 u'}{2}\sum_{K=1}^{P} V_{sK}\lambda_{sK}\sin m\pi\xi_K\sin v\pi\xi_k, & \begin{matrix}m\neq v\\ n=u\end{matrix} \\ 0, & \begin{matrix}m\neq v\\ n\neq u\end{matrix}\end{cases} \qquad (35)$$

and

$$y_i=\eta_i b,\ x_K=\xi_K a \qquad (36)$$

An examination of Eq. (21) reveals that when there are no stringers on the stiffened plate, which implies that λ_{sk} = Jsk = 0, the equation reduces to the form

$$\frac{M}{\beta}\ddot{q}_{mn}(t)+\frac{2M}{\beta}\sum_{i=1}^{R}\epsilon_{ri}\lambda_{ri}\sin\frac{n\pi y_i}{b}\sum_{u=1}^{\infty}\ddot{q}_{mu}(t)\sin\frac{u\pi y_i}{b}+$$

$$+\frac{1}{4\beta}\left[m^2+n^2\beta^2\right]q_{mn}(t)+\frac{m^4}{2\beta}\sum_{i=1}^{R}J_{ri}\sin\frac{n\pi y_i}{b}\sum_{u=1}^{\infty}q_{mu}(t)\sin\frac{u\pi y_i}{b}-$$

$$-\left[\frac{\beta m^2}{4}+\frac{\beta^3 n^2\bar{u}}{4}\right]\bar{\alpha}\,q_{mn}(t)-\left[\frac{\beta m^2}{4}+\frac{\beta^3 n^2 u'}{4}\right]\alpha' q_{mn}(t)-\frac{\beta m^2}{2}\sum_{i=1}^{R}\lambda_{ri}\cdot$$

$$\cdot\left(\bar{V}_{ri}\bar{\alpha}+V_{ri}'\alpha'\cos\theta t\right)\sin\frac{n\pi y_i}{b}\sum_{u=1}^{\infty}q_{mu}(t)\sin\frac{u\pi y_i}{b}=0,\ (m,n=1,--\infty) \qquad (37)$$

In the set of infinite equations given by Eq. (21), the set of functions $q_{mn}(t)$ are coupled only by the subscript n. Thus, the original set of infinite ordinary differential equations reduces to m subsets of ordinary coupled differential equations with periodic coefficients. Equation (37) reduces to the same general matrix form as given by Eq. (31) except that there exists an equation of this type for each m = 1, ---, ∞, which is given by

$$M[V]\{\ddot{Q}\}+\left[[K]-\bar{\alpha}[S]-\alpha'\cos\theta t[T]\right]\{Q\}=0 \qquad (38)$$

in which

$$\{Q\}=\begin{Bmatrix}q_{m1}\\ q_{m2}\\ \vdots\\ q_{mK}\\ \vdots\\ q_{mn}\end{Bmatrix} \qquad (39)$$

$$[V]=V_{mn,vu}=\begin{cases}\frac{1}{\beta}+\frac{2}{\beta}\sum_{i=1}^{R}\epsilon_{ri}\lambda_{ri}\sin n\pi\eta_i\sin u\pi\eta_i, & \begin{matrix}m=v\\n=u\end{matrix}\\ \frac{2}{\beta}\sum_{i=1}^{R}\epsilon_{ri}\lambda_{ri}\sin n\pi\eta_i\sin u\pi\eta_i, & \begin{matrix}m=v\\n\neq u\end{matrix}\end{cases} \quad -- (40)$$

$$[K]=K_{mn,vu}=\begin{cases}\frac{1}{4\beta}\left[m^2+n^2\beta^2\right]^2+\frac{m^4}{2\beta}\sum_{i=1}^{R}J_{ri}\sin n\pi\eta_i\sin u\pi\eta_i, & \begin{matrix}m=v\\n=u\end{matrix}\\ \frac{m^4}{2\beta}\sum_{i=1}^{R}J_{ri}\sin n\pi\eta_i\sin u\pi\eta_i, & \begin{matrix}m=v\\n=u\end{matrix}\end{cases} \quad -- (41)$$

$$[S]=S_{mn,vu}=\begin{cases}\frac{\beta m^2}{4}+\frac{\beta^3 n^2 u}{4}+\frac{\beta m^2}{2}\sum_{i=1}^{R}\bar{v}_{ri}\lambda_{ri}\sin n\pi\eta_i\sin u\pi\eta_i, & \begin{matrix}m=v\\n=u\end{matrix}\\ \frac{\beta m^2}{2}\sum_{i=1}^{R}v'_{ri}\lambda_{ri}\sin n\pi\eta_i\sin u\pi\eta_i, & \begin{matrix}m=v\\n=u\end{matrix}\end{cases} \quad -- (42)$$

and

$$[T]=t_{mn,vu}\begin{cases}\frac{\beta m^2}{4}+\frac{\beta^3 n^2 u'}{4}+\frac{\beta m^2}{2}\sum_{i=1}^{R}v'_{ri}\lambda_{ri}\sin n\pi\eta_i\sin u\pi\eta_i, & \begin{matrix}m=v\\n\neq u\end{matrix}\\ \frac{\beta m^2}{2}\sum_{i=1}^{R}v'_{ri}\lambda_{ri}\sin n\pi\eta_i\sin u\pi\eta_i, & \begin{matrix}m=v\\n\neq u\end{matrix}\end{cases} \quad -- (43)$$

Equation (21) again shows that when the stiffened plate contains no ribs, which implies that $\lambda_{ri} = J_{ri} = 0$, the equation reduces to

$$M[V]\{\ddot{Q}\}+\left[[K]-\bar{\alpha}[S]-\alpha'\cos\theta+[T]\right]\{Q\}=0 \quad ------ \quad (44)$$

in which

$$\{Q\}=\begin{Bmatrix}q_{1n}\\q_{2n}\\q_{kn}\\q_{mn}\end{Bmatrix} \quad ---------- \quad (45)$$

$$[V]=V_{mn,vu}=\begin{cases}\frac{1}{\beta}+\frac{2}{\beta}\sum_{K=1}^{P}\epsilon_{sK}\lambda_{sK}\sin m\pi\xi_K\sin v\pi\xi_K, & \begin{matrix}m=v\\n\neq u\end{matrix}\\ \frac{2}{\beta}\sum_{K=1}^{P}\epsilon_{sK}\lambda_{sK}\sin m\pi\xi_K\sin v\pi\xi_K, & \begin{matrix}m=v\\n\neq u\end{matrix}\end{cases} \quad -- (46)$$

$$[K] = K_{mn,vu} = \begin{cases} \frac{1}{\beta} + \frac{2}{\beta}\sum_{K=1}^{P} \epsilon_{sK}\lambda_{sK}\,\mathrm{Sin}\,m\pi\zeta_K\,\mathrm{Sin}\,v\pi\zeta_K, & \begin{matrix} m=v \\ n\neq u \end{matrix} \\ \frac{2}{\beta}\sum_{K=1}^{P} \epsilon_{sK}\lambda_{sK}\,\mathrm{Sin}\,m\pi\zeta_K\,\mathrm{Sin}\,v\pi\zeta_K, & \begin{matrix} m=v \\ n\neq u \end{matrix} \end{cases} \quad \text{--(47}$$

$$[S] = S_{mn,vu} = \begin{cases} \left[\frac{\beta m^2}{4} + \frac{\beta^3 n^2 \bar{u}}{4}\right] + \frac{\beta^3 n^2 \bar{u}}{2}\sum_{K=1}^{P} \bar{V}_{sK}\lambda_{sK}\,\mathrm{Sin}\,m\pi\zeta_K\,\mathrm{Sin}\,v\pi\zeta_K, & \begin{matrix} m=v \\ n\neq u \end{matrix} \\ \frac{\beta^3 n^2 \bar{u}}{4}\sum_{K=1}^{P} \bar{V}_{sK}\lambda_{sK}\,\mathrm{Sin}\,m\pi\zeta_K\,\mathrm{Sin}\,v\pi\zeta_K, & \begin{matrix} m=v \\ n=u \end{matrix} \end{cases} \quad \text{--(48)}$$

$$[T] = t_{mn,vu} = \begin{cases} \left[\frac{\beta m^2}{4} + \frac{\beta^3 n^2 u'}{4}\right] + \frac{\beta^3 n^2 u'}{4}\sum_{K=1}^{P} V'_{sK}\lambda_{sK}\,\mathrm{Sin}\,m\pi\zeta_K\,\mathrm{Sin}\,v\pi\zeta_K, & \begin{matrix} m=v \\ n\neq u \end{matrix} \\ \frac{\beta^3 n^2 u'}{4}\sum_{K=1}^{P} V'_{sK}\lambda_{sK}\,\mathrm{Sin}\,m\pi\zeta_K\,\mathrm{Sin}\,v\pi\zeta_K, & \begin{matrix} m=v \\ n\neq u \end{matrix} \end{cases} \quad \text{--(49)}$$

Equation (44) reduces to the same general matrix form as given by Eq. (31) except that there exists an equation of this type for each n = 1, ---, ∞.

b. Uniformly Spaced Stiffeners

Equations (31, 38) and (44) can be further reduced into additional subsets of coupled ordinary differential equations with periodic coefficients. This occurs in the case of uniform stiffener size, material properties, spacing and uniform in-plane edge loadings on both the ribs and stringers respectively. The condition of uniform stiffener spacing allows η_i and ζ_k to be written in the form

$$\eta_i = \frac{c_i}{N}\,, \quad \zeta_K = \frac{d_K}{L} \qquad \text{---------- (50)}$$

in which N is the number of bays in the y-direction and L is the number of bays in the x-direction, see Fig. 2. The summation limits R and P must now be replaced by N-1 and L-1 respectively. In addition, the condition of uniform in-plane edge loadings on the ribs and stringers implies that

$$\bar{V}_{ri} = \bar{V}_r\,, \quad \bar{V}_{sK} = \bar{V}_s \qquad \text{---------- (51)}$$

and

$$V'_{ri} = V'_r\,, \quad V'_{sK} = V'_s \qquad \text{---------- (52)}$$

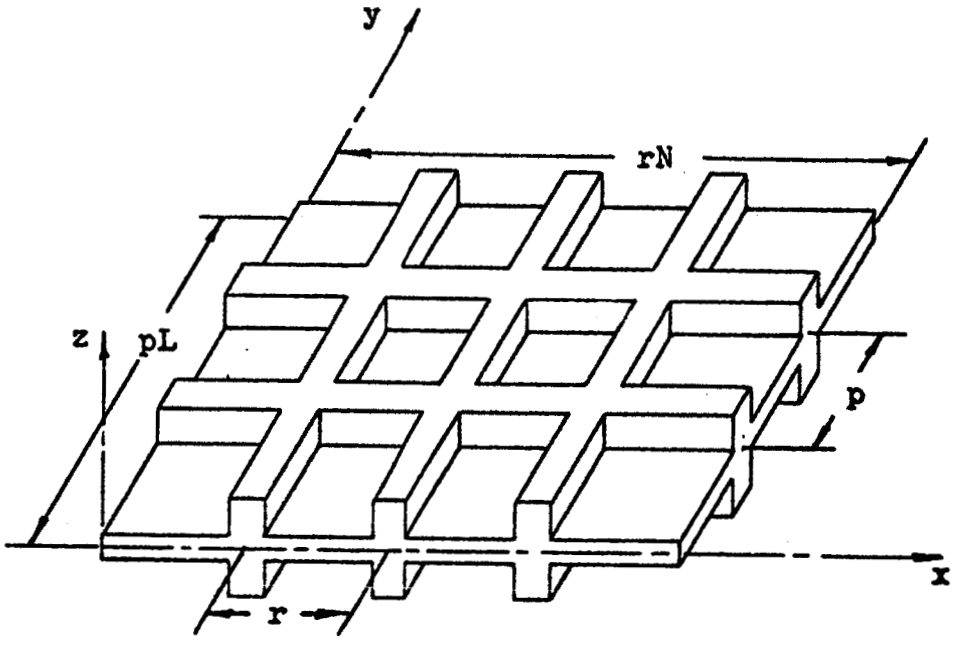

Fig. 2 Uniformly Spaced Stiffeners

If the ribs and stringers of a stiffened plate are made from the same material as the plate, then $\rho_{sk} = \rho_{ri} = \rho_p$ and $E_{ri} = E_{sk} = E$. Also, stiffened plates are usually designed so that the ribs and stringers are of a uniform size respectively, that is $A_{sk} = A_s$, $A_{ri} = A_r$, $I_{sk} = I_s$, and $I_{ri} = I_r$. Under these conditions the parameters introduced by Eqs. (23) through (26) and Eq. (19) reduce to

$$\lambda_{ri} = \lambda_r = \frac{A_r}{bh} \qquad (53)$$

$$\lambda_{sk} = \lambda_s = \frac{A_s}{ah} \qquad (54)$$

$$J_{ri} = J_r = \frac{EI_r}{bD} \qquad (55)$$

$$I_{sk} = J_s = \frac{EI_s}{aD} \qquad (56)$$

and

$$\epsilon_{ri} = 1.0\,, \quad \epsilon_{sk} = 1.0 \qquad (57)$$

The substitution of Eqs. (50) through (52) and Eqs. (53) through (57) into Eq. (21) and the corresponding interchange of finite and infinite summations yields

$$M\Big[\frac{1}{\beta}\ddot{q}_{mn}(t) + \frac{2\lambda_r}{\beta}\sum_{u=1}^{\infty}\ddot{q}_{mu}(t)\sum_{c=1}^{N-1}\sin\frac{n\pi c}{N}\sin\frac{u\pi c}{N} + \frac{2\lambda_s}{\beta}\sum_{v=1}^{\infty}\ddot{q}_{vn}(t)\cdot$$

$$\cdot\sum_{d=1}^{L-1}\sin\frac{m\pi d}{L}\sin\frac{v\pi d}{L}\Big] + \frac{1}{4\beta}\left[m^2+n^2\beta^2\right]q_{mn}(t) + \frac{m^4 J_r}{2\beta}\sum_{u=1}^{\infty}q_{mu}(t)\cdot$$

$$\cdot\sum_{c=1}^{N-1}\sin\frac{n\pi c}{N}\sin\frac{u\pi c}{N} + \frac{n^4 J_s \beta^3}{2}\sum_{v=1}^{\infty}q_{vn}(t)\sum_{d=1}^{L-1}\sin\frac{m\pi d}{L}\sin\frac{v\pi d}{L} -$$

$$-\left[\frac{\beta m^2}{4} + \frac{\beta^3 n^2 \bar{u}}{4}\right]\bar{\alpha}\,q_{mn}(t) - \left[\frac{\beta m^2}{4} + \frac{\beta^3 n^2 u'}{4}\right]\alpha'\cos\theta t\, q_{mn}(t) -$$

$$-\frac{\beta m^2}{2}\lambda_r\left(\bar{v}_r\bar{\alpha} + v_r'\alpha'\cos\theta t\right)\sum_{u=1}^{\infty}q_{mu}(t)\sum_{c=1}^{N-1}\sin\frac{n\pi c}{N}\sin\frac{u\pi c}{N} -$$

$$-\frac{\beta^3 n^2}{2}\lambda_s\left(\bar{v}_s\bar{u}\bar{\alpha} + v_s' u'\alpha'\cos\theta t\right)\sum_{v=1}^{\infty}q_{vn}(t)\sum_{d=1}^{L-1}\sin\frac{m\pi d}{L}\cdot$$

$$\cdot\sin\frac{v\pi d}{L} = 0 \qquad (58)$$

for m, n = 1, ----, ∞. Budiansky, Seide, and Weinberger (93) showed that series of the type

$$\sum_{c=1}^{N-1} \sin\frac{n\pi c}{N} \sin\frac{u\pi c}{N} \quad - - - - - - - - - - \tag{59}$$

and

$$\sum_{d=1}^{L-1} \sin\frac{m\pi d}{L} \sin\frac{v\pi d}{L} \quad - - - - - - - - - - \tag{60}$$

can be expressed in a closed form. The values given by the above series are summarized in Table 1 for Eq. (59) and in Table 2 for Eq. (60). In addition, the condition that will apply for each value of u for a given value on n is indicated in Table 1 where p and 1 are positive integers such that p + 1 is even, and k_1 and k_2 are positive or negative integer values that yield positive values of u. For a given value of m, the conditions that will apply for each value of v is indicated in Table 2 where g and f are positive integers such that g + f is even, and k_1 and k_2 are positive or negative values that yield positive values of N.

When m/L and n/N are both integers Eqs. (59) and (60) are both equal to zero. Thus, Eq. (58) reduces to

$$\frac{M}{\beta}\ddot{q}_{(gL)(pN)}(t)+\frac{1}{4\beta}\left[(gL)^2+\beta^2(pN)^2\right]q_{(gL)(pN)}(t)-\bar{\alpha}\left[\frac{\beta(gL)^2}{4}+\frac{\beta^3\bar{u}(pN)^2}{4}\right]\cdot$$

$$\cdot q_{(gL)(pN)}(t)-\alpha'\left[\frac{\beta(gL)^2}{4}+\frac{\beta^3\mu'(pN)^2}{4}\right]\cos\theta t\, q_{(gL)(pN)}(t)=0 \quad - - - \tag{61}$$

in which the following replacements are made

$$\begin{aligned} m &= gL \qquad (g = 1,2,\text{----}, \infty) \\ n &= pN \qquad (p = 1,2,\text{----}, \infty) \end{aligned} \quad - - - - - - - - - - - - - - - - \tag{62}$$

Equation (61) is uncoupled and a single equation exists for each set of g and p. The rearrangement of Eq. (61) gives

$$\ddot{q}_{(gL)(pN)}(t)+\Omega^2_{(gL)(pN)}\left[1-2\mu_{(gL)(pN)}\cos\theta t\right]q_{(gL)(pN)}(t) \quad - - - - - \tag{63}$$

in which

$$\Omega^2_{(gL)(pN)}=\frac{\left[(gL)^2+\beta^2(pN)^2\right]-\bar{\alpha}\left[\beta^2(gL)^2+\beta^4\bar{u}(pN)^2\right]}{4M} \quad - - - - - \tag{64}$$

and

$$\mu_{(gL)(pN)}=\frac{\alpha'\left[\beta^2(gL)^2+\beta^4u'(pN)^2\right]}{2\left[(gL)^2+\beta^2(pN)^2\right]^2-2\bar{\alpha}\left[\beta^2(gL)^2+\beta^4\bar{u}(pN)^2\right]} \quad - - - - - \tag{65}$$

TABLE 1

Conditions		$n = pN$	$n \neq pN$	$\sum_{c=1}^{N-1} \sin \frac{n\pi c}{N} \sin \frac{u\pi c}{N}$
$\frac{u+n}{2N}$	$\frac{u-n}{2N}$			
Not Integer	Not Integer	$u \neq 1N$	$u \neq 2K_1N - n$ $u \neq 2K_2N + n$	0
Integer	Integer	$u = 1N$	Never	0
Integer	Not Integer	Never	$u = 2K_1N - n$ $u \neq 2K_2N - n$	$-\frac{N}{2}$
Not Integer	Integer	Never	$u \neq 2K_1N - n$ $u = 2K_2N - n$	$\frac{N}{2}$

TABLE 2

Conditions		$m = gL$	$m \neq gL$	$\sum_{d=1}^{L-1} \sin \frac{m\pi d}{L} \sin \frac{v\pi d}{L}$
$\frac{v+m}{2L}$	$\frac{v-m}{2L}$			
Not Integer	Not Integer	$v \neq fL$	$v \neq 2K_1L - m$ $v \neq 2K_2L + m$	0
Integer	Integer	$v = fL$	Never	0
Integer	Not Integer	Never	$v = 2K_1L - m$ $v \neq 2K_2L + m$	$-\frac{L}{2}$
Not Integer	Integer	Never	$v \neq 2K_1L - m$ $v = 2K_2L + m$	$\frac{L}{2}$

Since the form of Eq. (63) is identical for all (gL) and (pN) the indices can be omitted, hence

$$\ddot{q}(t)+\Omega^2(1-2\mu\cos\theta t)\,q(t)=0 \qquad (66)$$

This equation is the well known Mathieu's equation. Physically, Eq. (66) represents the case where only the panels of the stiffened plate undergo motion but not the ribs and stringers.

When m/L is an integer but n/N is not an integer then the series given by Eq. (60) is equal to zero. Table 1 evaluates the series given by Eq. (59) for certain relationships between n and u. The application of this information to Eq. (58) yields

$$M\left\{\frac{1}{\beta}\ddot{q}_{(gL)n}(t)+\frac{\lambda_r N}{\beta}\left[\sum_{k_2}\ddot{q}_{(gL)(2k_2N+n)}(t)-\sum_{k_1}\ddot{q}_{(gL)(2k_1N-n)}(t)\right]\right\}+\frac{1}{4\beta}\left[(gL)^2+\right.$$

$$\left.+n^2\beta^2\right]^2 q_{(gL)n}(t)+\frac{J_r(gL)^2N}{4\beta}\left[\sum_{k_2}q_{(gL)(2k_2N+n)}(t)-\sum_{k_1}q_{(gL)(2k_1N-n)}(t)\right]-$$

$$-\left[\frac{\beta(gL)^2}{4}+\frac{\beta^3n^2\bar{u}}{4}\right]\bar{\alpha}\,q_{(gL)n}(t)-\left[\frac{\beta(gL)^2}{4}+\frac{\beta^3n^2u'}{4}\right]\alpha'\cos\theta t\,q_{(gL)n}(t)-$$

$$-\frac{\beta(gL)^2\lambda_r N(\bar{v}_r\bar{\alpha}+v_r'\alpha'\cos\theta t)}{4}\left[\sum_{k_2}q_{(gL)(2k_2N+n)}(t)-\right.$$

$$\left.-\sum_{k_1}q_{(gL)(2k_1N-n)}(t)\right]=0 \qquad (67)$$

for g = 1,2,---, ∞ and $n \neq pN$. Expansion and examination of Eq. (67) shows that it may be further subdivided into N-1 independent equations. These sets of equations correspond to the first N-1 values of the integer n. If $u_1 = 2k_2N + n$ then for a particular n equal to z the q's appearing in the summations of Eqs. (67) will have the subscripts

$$u_1 = 2N-z\ ,\ 4N-z\ ,\ 6N-z,\ \text{----} \qquad (68)$$

and

$$u_2 = z,\ 2N+z\ ,\ 4N+z\ ,\ 6N+z,\ \text{----} \qquad (69)$$

If Eqs. (67) are written for n equal to these preceding values, then only q's having the same subscripts will appear in the summations. Thus, if

$$n = z,\ 2N+z,\ 4N+z,\ 6N+z,\ \text{----}$$

then

$$u_1 = 2N-z,\ 4N-z,\ 6N-z,\ ------$$

and

$$u_2 = z,\ 2N+z,\ 4N+z,\ 6N+z,\ ------$$

If

$$n = 2N-z,\ 4N-z,\ 6N-z$$

then

$$u_1 = z,\ 2N+z,\ 4N+z,\ 6N+z,\ ------$$

and

$$u_2 = 2N-z,\ 4N-z,\ 6N-z,\ ------$$

Thus, it is evident from the above considerations that Eqs. (67) reduce to the following N-1 independent subsets of equations, which are given by the following two groups of equations;

$$M\left\{\frac{1}{\beta}\ddot{q}_{(qL)(2hN+z)}(t)+\frac{\lambda_c N}{\beta}\sum_{j=0}^{\infty}\left[\ddot{q}_{(qL)(2jN+z)}(t)-\ddot{q}_{(qL)(2(j+1)N-z)}(t)\right]\right\}+$$

$$+\frac{1}{4\beta}\left[(qL)^2+\beta^2(2hN+z)^2\right]^2 q_{(qL)(2hN+z)}(t)+\frac{J_r(qL)^4 N}{4\beta}\sum_{j=0}^{\infty}\left[q_{(qL)(2jN+z)}(t)-\right.$$

$$\left.-q_{(qL)(2(j+1)N-z)}(t)\right]-\left[\frac{\beta(qL)^2}{4}+\frac{\beta^3(2hN+z)^2\bar{\mu}}{4}\right]\alpha q_{(qL)(2hN+z)}(t)-$$

$$-\left[\frac{\beta(qL)^2}{4}+\frac{\beta^3(2hN+z)^2\bar{\mu}}{4}\right]\alpha'\cos\theta t\, q_{(qL)(2hN+z)}(t)-\frac{\beta(qL)^2\lambda_r N}{4}\cdot$$

$$\cdot(\bar{V}_r\bar{\alpha}+V_r'\alpha'\cos\theta t)\sum_{j=0}^{\infty}\left[q_{(qL)(2jN+z)}(t)-q_{(qL)(2(j+1)N-z)}(t)\right]=0\ ----\qquad(70)$$

and

$$M\left\{\frac{1}{\beta}\ddot{q}_{(gL)(2(h+1)N-z)}(t)-\frac{\lambda_r N}{\beta}\sum_{j=0}^{\infty}\left[\ddot{q}_{(gL)(2jN+z)}(t)-\ddot{q}_{(gL)(z(j+1)N+z)}(t)\right]\right\}+$$

$$+\frac{1}{4\beta}\left[(gL)^2+\beta^2(2(h+1)N-z)^2\right]^2 q_{(gL)(2(j+1)N-z)}(t)-\frac{J_r(gL)^4N}{4\beta}\sum_{j=0}^{\infty}\left[q_{(gL)(2jN+z)}(t)-\right.$$

$$\left.-q_{(gL)(2(j+1)N-z)}(t)\right]-\left[\frac{\beta(gL)^2}{4}+\frac{\beta^3(2(h+1)N-z)^2\bar{\mu}}{4}\right]\bar{\alpha}\,q_{(gL)(2(h+1)N-z)}(t)-$$

$$-\left[\frac{\beta(gL)^2}{4}+\frac{\beta^3(2(h+1)N-z)^2\mu'}{4}\right]\alpha'\cos\theta t\,q_{(gL)(2(h+1)N-z)}(t)+\frac{\beta(gL)^2\lambda_r N}{4}\cdot$$

$$\cdot(\bar{v}_r\bar{\alpha}+v_r'\alpha'\cos\theta t)\sum_{j=0}^{\infty}\left[q_{(gL)(2jN+z)}(t)-q_{(gL)(z(j+1)N-z)}(t)\right]=0 \quad ----- \quad (71)$$

in which g = 1,2,---, ∞ and h = 0,1,2,----, ∞ . The set of N-1 equations is given by Eqs. (70) and (71) for a particular value of z = 1,2,---,N-1. The required equations in a given subset are generated by expanding Eq. (70) and then Eq. (71) for a particular value of h.

Equations (70) and (71) can be expressed by a single matrix equation, by employing a procedure similar to that used in the last section. The resulting matrix equation is

$$M[V]\{\ddot{Q}\}+\left[[K]-\bar{\alpha}[S]-\alpha'\cos\theta t[T]\right]\{Q\}=0 \quad ---------- \quad (72)$$

in which

$$\{Q\}=\begin{Bmatrix} q_{(gL)(z)} \\ q_{(gL)(2N-z)} \\ q_{(gL)(2N+z)} \\ q_{(gL)(4N-z)} \\ \vdots \\ q_{(gL)(zjN+z)} \\ q_{(gL)(2(j+1)N-z)} \end{Bmatrix} \quad ---------- \quad (73)$$

$$[V] = v_{mn,vu} = \left\{ \begin{array}{ll} \frac{1}{\beta} + \frac{\delta_{un}\lambda_r N}{\beta}, & \begin{array}{l} m=v \\ n=u \end{array} \\ \frac{\delta_{un}\lambda_r N}{\beta}, & \begin{array}{l} m=v \\ n\neq u \end{array} \end{array} \right\} \text{---------} \quad (74)$$

$$[K] = K_{mn,vu} = \left\{ \begin{array}{ll} \frac{1}{4\beta}\left[m^2+\beta^2 n^2\right]^2 + \frac{\delta_{un} J_r m^4 N}{4\beta}, & \begin{array}{l} m=v \\ n=u \end{array} \\ \frac{\delta_{un} J_r m^4 N}{4\beta}, & \begin{array}{l} m=v \\ n\neq u \end{array} \end{array} \right\} \text{---} \quad (75)$$

$$[S] = S_{mn,vu} = \left\{ \begin{array}{ll} \left[\frac{\beta m^2}{4} + \frac{\beta^3 n^2 \bar{u}}{4}\right] + \frac{\delta_{un}\bar{v}_r m^2 \lambda_r \beta}{4}, & \begin{array}{l} m=v \\ n=u \end{array} \\ \frac{\delta_{un} v_r m^2 \lambda_r \beta}{4}, & \begin{array}{l} m=v \\ n\neq u \end{array} \end{array} \right\} \text{---} \quad (76)$$

$$[T] = t_{mn,vu} = \left\{ \begin{array}{ll} \left[\frac{\beta m^2}{4} + \frac{\beta^3 n^2 u'}{4}\right] + \frac{\delta_{un} v_r' m^2 \lambda_r \beta}{4}, & \begin{array}{l} m=v \\ n=u \end{array} \\ \frac{\delta_{un} v_r' m^2 \lambda_r \beta}{4}, & \begin{array}{l} m=v \\ n\neq u \end{array} \end{array} \right\} \text{---} \quad (77)$$

and

$$\delta_{un} = \left\{ \begin{array}{l} -1 \text{ for } (u+n)/2N = \text{Integer} \\ +1 \text{ for } (u-n)/2N = \text{Integer} \end{array} \right\} \text{------} \quad (78)$$

In Eq. (76) both (u+n)/2N and (u-n)/2N cannot be integers for the same values of u and n because of the nature of the relationship between u and n. The column matrix $\{Q\}$, Eq. (73), is composed of certain elements from a row, which corresponds to a multiple of the panel number L, of the general matrix $\{Q\}$ given by Eq. (29). The required elements from this row are determined from alternate use of first (2jN + Z) and then (2(j+1) N-z), beginning with j equal to zero and then increasing j by integer values after each alternation. The subscripts of the representative matrix $v_{mn,vu}$ have the same restrictions as the subscripts of $\{Q\}$. The subscript of m of $v_{mn,vu}$ has a constant value equal to some multiple of L. The subscript n is constant for any particular row of $v_{mn,vu}$, but varies alternately from first (2hN+Z) and then (2(h+1)N-z), beginning with h equal to zero and then increasing by integer values after each alternation until the required number of rows are generated. The subscript v takes on the corresponding value of the subscript m. The subscript u takes an alternate

values for first (2jN+z) and then (2(j+1)N-z), beginning with j equal to zero and then increasing j by integer values after each alternation until the required number of columns for the matrix v_{mn}, v_{u} are generated.

Physically, Eq. (72) represents the case where only the panels and ribs of the stiffened plate undergo motion but not the stringers.

When n/N is an integer but m/L is not an integer then the series given by Eq. (59) is equal to zero. Table 2 gives the evaluation of the series stated by Eq. (60) for certain relationships between m and v. The application of this information to Eq. (58) gives

$$M\left\{\frac{1}{\beta}\ddot{q}_{m(pN)}(t)+\frac{\lambda_s L}{\beta}\left[\sum_{k_2}\ddot{q}_{(2k_2L+m)(pN)}(t)-\sum_{k_1}\ddot{q}_{(2k_1L-m)(pN)}(t)\right]\right\}+$$

$$+\frac{1}{4}\left[m^2+\beta^2(pN)^2\right]^2 q_{m(pN)}(t)+\frac{J_s(pN)^4L\beta^3}{4}\left[\sum_{k_2}q_{(2k_2L+m)(pN)}(t)-\right.$$

$$\left.-\sum_{k_1}q_{(2k_1L-m)(pN)}(t)\right]-\left[\frac{\beta m^2}{4}+\frac{\beta^3(pN)^2\bar{\mu}}{4}\right]\bar{\alpha}\,q_{m(pN)}(t)-\left[\frac{\beta m^2}{4}+\right.$$

$$\left.+\frac{\beta^3(pN)^2\mu'}{4}\right]\alpha'\cos\theta t\,q_{m(pN)}(t)-\frac{\beta^3(pN)^2\lambda_s L}{4}\left(\bar{v}_s\bar{\mu}\bar{\alpha}+v_s'\mu'\alpha'\right.\cdot$$

$$\left.\cdot\cos\theta t\left[\sum_{k_2}q_{(2k_2L+m)(pN)}(t)-\sum_{k_1}q_{(2k_1L-m)(pN)}(t)\right]=0\quad\text{------}\right. \tag{79}$$

for p = 1,2,---, ∞ and $m \neq gL$. The integers k_1 and k_2 in the above equation can have either a positive or negative value or both. Expansion and examination of Eq. (79) shows that it can be further subdivided into L-1 independent sets of equations. These sets of equations correspond to the first L-1 values of the integer m. If $v_1 = 2k_1L-m$ and $v_2 = 2k_2L+m$ then for a particular m equal to e the q's appearing in the summation of Eq. (79) will have the subscripts

$$v_1 = 2L-e,\ 4L-e,\ 6L-e,\ \text{----------} \tag{80}$$

and

$$v_2 = e,\ 2L+e,\ 4L+e,\ 6L+e,\ \text{----------} \tag{81}$$

If Eq. (79) is written for m equal to these preceding values, then only q's having the same subscripts will appear in the summations, thus, if

$$m = e,\ 2L+e,\ 4L+e,\ 6L+e,\ \text{------}$$

then

$$V_1 = 2L-e\,,\ 4L-e,\ 6L-e,\ \text{------}$$

and

$$V_2 = e,\ 2L+e,\ 4L+e,\ 6L+e,\ \text{-----}$$

If

$$m = 2L-e,\ 4L-e,\ 6L-e,\ \text{------}$$

then

$$V_1 = e,\ 2L+e,\ 4L+e,\ 6L+e,\ \text{----}$$

and

$$V_2 = 2L-e\,,\ 4L-e,\ 6L-e,\ \text{------}$$

Thus, Eq. (79) reduces to the following L-1 independent subsets of equations, which are given by the fol owing two groups of equations;

$$M\left\{\frac{1}{\beta}\ddot{q}_{(2cL+e)(pN)}(t)+\frac{\lambda_s L}{\beta}\sum_{K=0}^{\infty}\left[\ddot{q}_{(2kL+e)(pN)}(t)-\ddot{q}_{(2(K+1)L-e)(pN)}(t)\right]\right\}+$$

$$+\frac{1}{4\beta}\left[(2cL+e)^2+\beta^2(pN)^2\right]^2 q_{(2cL+e)(pN)}(t)+\frac{J_s(pN)^4L\beta^3}{4}\sum_{K=0}^{\infty}\left[q_{(2kL+e)(pN)}(t)-\right.$$

$$\left.-q_{(2(K+1)L-e)(pN)}(t)\right]-\left[\frac{\beta(2cL+e)^2}{4}+\frac{\beta^3(pN)^2\bar{\mu}}{4}\right]\bar{\alpha}\,q_{(2cL+e)(pN)}(t)-$$

$$-\frac{\beta(2cL+e)^2}{4}+\frac{\beta^3(pN)^2\mu'}{4}\Big]\alpha'\cos\theta t\,q_{(2cL+e)(pN)}(t)-\frac{\beta^3\lambda_s L(pN)^2}{4}\cdot$$

$$\cdot(\bar{v}_s\bar{\mu}\bar{\alpha}+v_s'\mu'\alpha'\cos\theta t)\sum_{K=0}^{\infty}\left[q_{(2kL+e)(pN)}(t)-q_{(2(K+1)L-e)(pN)}(t)\right]=0 \quad (82)$$

and

$$M\left\{\frac{1}{\beta}\ddot{q}_{(2(c+1)L-e)(pN)}(t)-\frac{\lambda_s L}{\beta}\sum_{K=0}^{\infty}\left[\ddot{q}_{(2KL+e)(pN)}(t)-\ddot{q}_{(2(K+1)L-e)(pN)}(t)\right]\right\}+$$

$$+\frac{1}{4\beta}\left[(2(c+1)L-e)^2+\beta^2(pN)^2\right]^2 q_{(2(c+1)L-e)(pN)}(t)-\frac{J_s(pN)^4L\beta^3}{4}\cdot$$

$$\cdot\sum_{k=0}^{\infty}\left[q_{(2kL+e)(pN)}(t)-q_{(2(k+1)L-e)(pN)}(t)\right]-\left[\frac{\beta(2(c+1)L-e)^2}{4}+\right.$$

$$\left.+\frac{\beta^3(pN)^2\bar{\mu}}{4}\right]\bar{\alpha}\,q_{(2(c+1)L-e)(pN)}(t)-\left[\frac{\beta(2(c+1)(L-e)^2}{4}+\frac{\beta^3(pN)^2\mu'}{4}\right]\cdot$$

$$\cdot\alpha\cos\theta t\,q_{(2(c+1)L-e)(pN)}(t)+\frac{\beta^3\lambda_s L(pN)^2}{4}\left(\bar{v}_s\bar{\mu}\bar{\alpha}+v_s'\mu'\alpha'\cos\theta t\right)\cdot$$

$$\cdot\sum_{k=0}^{\infty}\left[q_{(2kL+e)(pN)}(t)-q_{(2(k+1)L-e)(pN)}(t)\right]=0 \qquad (83)$$

in which p = 1,2,3,---, ∞ and c = 1,2,----, ∞. The set of L-1 equations is given by Eqs. (84) and (83) for a particular value of e = 1,2,---, L-1. The required equations in a given subset are generated by expanding Eq. (82) and then Eq. (83) for a particular value of c.

Equations (82) and (83) can be expressed by a single matrix equation, by employing a procedure similar to the one used in the previous section. The resulting matrix equation is

$$M[V]\{\ddot{Q}\}+\left[[K]-\bar{\alpha}[S]-\alpha'\cos\theta t[T]\right]\{Q\}=0 \qquad (84)$$

in which

$$\{Q\}=\begin{Bmatrix} q_{e(pN)} \\ q_{(2L-e)(pN)} \\ q_{(2L+e)(pN)} \\ q_{(4L-e)(pN)} \\ \vdots \\ q_{(2kL+e)(pN)} \\ q_{(2(k+1)L-e)(pN)} \end{Bmatrix} \qquad (85)$$

$$[V]=V_{mn,vu}=\begin{Bmatrix} \frac{1}{\beta}+\frac{\delta_{vm}\lambda_s L}{\beta}, & \begin{matrix} m=v \\ n=u \end{matrix} \\ \frac{\delta_{vm}\lambda_s L}{\beta}, & \begin{matrix} m\neq v \\ n=u \end{matrix} \end{Bmatrix} \qquad (86)$$

$$[K] = K_{mn,vu} = \begin{cases} \frac{1}{4\beta}\left[m^2+\beta^2 n^2\right]^2 + \frac{\delta_{vm} J_s n^4 L \beta^3}{4}, & \begin{matrix} m=v \\ n=u \end{matrix} \\ \frac{\delta_{vm} J_s n^4 L \beta^3}{4}, & \begin{matrix} m\neq v \\ n=u \end{matrix} \end{cases} \quad \text{---} \quad (87)$$

$$[S] = S_{mn,vu} = \begin{cases} \left[\frac{\beta m^2}{4} + \frac{\beta^3 n^2 \bar{u}}{4}\right] + \frac{\delta_{vm} \bar{v}_s \bar{u} n^2 \lambda_s L \beta^3}{4}, & \begin{matrix} m=v \\ n=u \end{matrix} \\ \frac{\delta_{vm} \bar{v}_s \bar{u} n^2 \lambda_s L \beta^3}{4}, & \begin{matrix} m\neq v \\ n=u \end{matrix} \end{cases} \quad \text{---} \quad (88)$$

$$[T] = t_{mn,vu} = \begin{cases} \left[\frac{\beta m^2}{4} + \frac{\beta^3 n^2 u'}{4}\right] + \frac{\delta_{vm} v_s' u' n^2 \lambda_s L \beta^3}{4}, & \begin{matrix} m=v \\ n=u \end{matrix} \\ \frac{\delta_{vm} v_s' u' n^2 \lambda_s L \beta^3}{4}, & \begin{matrix} m\neq v \\ n=u \end{matrix} \end{cases} \quad \text{---} \quad (89)$$

and

$$\delta_{vm} = \left\{ \begin{matrix} -1 \text{ for } (v+m)/2L = \text{Integer} \\ +1 \text{ for } (v-m)/2L = \text{Integer} \end{matrix} \right\} \quad \text{----------} \quad (90)$$

In Eq. (90) both (v+m)/2L and (v-m)/2L cannot be integers for the same values of v and m because of the nature of the relationships between v and m. The column matrix $\{Q\}$, Eq. (85), is composed of certain elements from a column, which corresponds to a multiple of the panel number N, of the general matrix $\{Q\}$ given by Eq. (29). The required elements from this column are determined from alternate use of first (2kL+e) and then (2(k+1)L-e), beginning with k equal to zero and then increasing k by integer values after each alternation. The subscripts of the representative matrix $v_{mn,vu}$ have the same restrictions as the subscripts of $\{Q\}$. The subscript m is a constant value for any given row of $v_{mn,vu}$, but it varies alternately from first (2cL+e) and the (2(c+1)L-e), beginning with c equal to zero and then increasing c by integer values after each alternation. The subscript n has a constant value equal to some multiple of N. The subscript v takes an alternate values of (2kL+e) and then (2(k+1)L-e) beginning with k equal to zero and then increasing k by integer values after each alternation until the required number of columns for the matrix $v_{mn,vu}$ are generated. The subscript u takes on the corresponding value of the subscript n.

Physically, Eq. (84) represents the case where only the panels and stringers of the stiffened plate undergo motion but not the ribs.

The only case that remains to be considered is when both m/L and n/N are not integers. The application of the information contained in tables 1 and 2 to Eq. (58), when both m/L and n/N are not integers, yields

$$M\Big\{\frac{1}{\beta}\ddot{q}_{mn}(t)+\frac{\lambda_r N}{\beta}\Big[\sum_{k_2}\ddot{q}_{m(2k_2N+n)}(t)-\sum_{k_1}\ddot{q}_{m(2k_1N-n)}(t)\Big]+\frac{\lambda_s L}{\beta}\cdot$$

$$\cdot\Big[\sum_{k_2}\ddot{q}_{(2k_2L+m)n}(t)-\sum_{k_1}\ddot{q}_{(2k_1L-m)n}(t)\Big]\Big\}+\frac{1}{4\beta}\Big[m^2+\beta^2n^2\Big]^2 q_{mn}(t)+$$

$$+\frac{m^4 J_r N}{4\beta}\Big[\sum_{k_2}q_{m(2k_2N+n)}(t)-\sum_{k_1}q_{m(2k_1N-n)}(t)\Big]+\frac{n^4 J_s L\beta^3}{4}\Big[\sum_{k_2}q_{(2k_2L+m)n}(t)-$$

$$-\sum_{k_1}q_{(2k_1L-m)n}(t)\Big]-\Big[\frac{\beta m^2}{4}+\frac{\beta^3 n^2\bar{u}}{4}\Big]\bar{\alpha}\,q_{mn}(t)-\Big[\frac{\beta m^2}{4}+\frac{\beta^3 n^2 u'}{4}\Big]\alpha'\cdot$$

$$\cdot\cos\theta t\,q_{mn}(t)-\frac{\beta m^2\lambda_r N}{4}\left(\bar{V}_r\bar{\alpha}+V_r'\alpha'\cos\theta t\right)\Big[\sum_{k_2}q_{m(2k_2N+n)}(t)-$$

$$-\sum_{k_1}q_{m(2k_1N-n)}(t)\Big]-\frac{\beta^3 n^2\lambda_s L}{4}\left(\bar{V}_s\bar{u}\bar{\alpha}+V_s'u'\alpha'\cos\theta t\right)\cdot$$

$$\cdot\Big[\sum_{k_2}q_{(2k_2L+m)n}(t)-\sum q_{(2k_1L-m)n}(t)\Big]=0 \qquad \text{---------} \qquad (91)$$

The integers k_1 and k_2 in the above equation can have either positive or negative values. Expansion and examination of Eq. (91) shows that it can be further subdivided into (L-1) x (N-1) independent sets of equations. These sets of equations correspond to all combinations of the first L-1 values of the integer m with the first N-1 values of the integer n. The subscripts of Eq. (91) behave in a manner similar to that of the subscripts of Eqs. (67) and (79). Thus, the subscripts u_1 and u_2 take on the values given by Eqs. (68) and (69) respectively with the subscript n restricted to the same set of values as u_1 and u_2 for a given set of equation. The subscripts v_1 and v_2 take on the values given by Eqs. (80) and (81) respectively with the subscript n restricted to the same set of values as v_1 and v_2 a given set of equations. Hence, Eqs. (91) reduce to (L-1) x (N-1) independent subsets of equations, which are given by the following four groups of equations;

$$M\Big\{\frac{1}{\beta}\ddot{q}_{(2cL+e)(2hN+z)}(t)+\frac{\lambda_r N}{\beta}\sum_{j=0}^{\infty}\Big[\ddot{q}_{(2cL+e)(2jN+z)}(t)-q_{(2cL+e)(2(j+1)N+z)}(t)\Big]+$$

$$+\frac{\lambda_s L}{\beta}\sum_{K=0}^{\infty}\Big[\ddot{q}_{(2kL+e)(2hN+z)}(t)-q_{(2(K+1)L-e)(2hN+z)}(t)\Big]\Big\}+\frac{1}{4\beta}\Big[(2cL+e)^2+$$

$$+\beta^2(2hN+z)^2\Big]^2 q_{(2cL+e)(2hN+z)}(t)+\frac{J_r(2cL+e)^4 N}{4\beta}\sum_{j=0}^{\infty}\Big[q_{(2cL+e)(2jN+z)}(t)-$$

$$-q_{(2cL+e)(2(j+1)N-z)}(t)\Big]\frac{J_s(2hN+z)^4 L\beta^3}{4}\sum_{K=0}^{\infty}\Big[q_{(2kL+e)(2hN+z)}(t)-$$

$$-q_{(2(K+1)L-e)(2hN+z)}(t)\Big]-\Big[\frac{\beta(2cL+e)^2}{4}+\frac{\beta^3(2hN+z)^2\bar{u}}{4}\Big]\bar{\alpha}\cdot$$

$$\cdot q_{(2cL+e)(2hN+z)}(t)-\left[\frac{\beta(2cL+e)^2}{4}+\frac{\beta^3(2hN+z)^2u'}{4}\right]\alpha'\cos\theta t\cdot$$

$$\cdot q_{(2cL+e)(2hN+z)}(t)-\frac{\beta(2cL+e)^2\lambda_r N}{4}(\bar{v}_r\bar{\alpha}+v_r'\alpha'\cos\theta t)\cdot$$

$$\cdot\sum_{j=0}^{\infty}\left[q_{(2cL+e)(2jN+z)}(t)-q_{(2cL+e)(2(j+1)N-z)}(t)\right]-\frac{\beta^3\lambda_s L(2hN+z)^2}{4}\cdot$$

$$\cdot(\bar{v}_s\bar{u}\bar{\alpha}+v_s'u'\alpha'\cos\theta t)\sum_{K=0}^{\infty}\left[q_{(2kL+e)(2hN+z)}(t)-\right.$$

$$\left.-q_{(2(K+1)L-e)(2hN+z)}(t)\right]=0 \qquad \text{(92)}$$

$$M\left\{\frac{1}{\beta}\ddot{q}_{(2cL+e)(2(h+1)N-z)}(t)-\frac{\lambda_r N}{\beta}\sum_{j=0}^{\infty}\left[\ddot{q}_{(2cL+e)(2jN+z)}(t)-\right.\right.$$

$$-\ddot{q}_{(2cL+e)(2(j+1)N-z)}(t)+\frac{\lambda_s L}{\beta}\sum_{K=0}^{\infty}\left[\ddot{q}_{(2kL+e)(2(h+1)N-z)}(t)-\right.$$

$$\left.\left.-\ddot{q}_{(2(K+1)L-e)(2(h+1)N-z)}(t)\right]\right\}+\frac{1}{4\beta}\left[(2cL+e)^2+\beta^2(2(h+1)N-z)^2\right]^2\cdot$$

$$\cdot q_{(2cL+e)(2(h+1)N-z)}(t)-\frac{J_r(2cL+e)^4N}{4\beta}\sum_{j=0}^{\infty}\left[q_{(2cL+e)(2jN+z)}(t)-\right.$$

$$\left.-q_{(2cL+e)(2(j+1)N-z)}(t)\right]+\frac{J_s(2(h+1)N-z)^4L\beta^3}{4}\sum_{K=0}^{\infty}\left[q_{(2kL+e)(2(h+1)N-z)}(t)-\right.$$

$$\left.-q_{(2(K+1)L-e)(2(h+1)N-z)}(t)\right]-\left[\frac{\beta(2cL+e)^2}{4}+\frac{\beta^3(2(h+1)N-z)^2\bar{u}}{4}\right]\bar{\alpha}\cdot$$

$$\cdot q_{(2cL+e)(2(h+1)N-z)}(t)-\left[\frac{\beta(2cL+e)^2}{4}+\frac{\beta^3(2(h+1)N-z)^2u'}{4}\right]\alpha'\cos\theta t\cdot$$

$$\cdot q_{(2cL+e)(2(h+1)N-z)}(t)+\frac{\beta(2cL+e)^2\lambda_r N}{4}(\bar{v}_r\bar{\alpha}+v_r'\alpha'\cos\theta t)\cdot$$

$$\cdot\sum_{j=0}^{\infty}\left[q_{(2cL+e)(2jN+z)}(t)-q_{(2cL+e)(2(j+1)N-z)}(t)\right]-\frac{\beta^3\lambda_s L(2(h+1)N-z)^2}{4}\cdot$$

$$\cdot(\bar{v}_s\bar{u}\bar{\alpha}+v_s'u'\alpha'\cos\theta t)\sum_{K=0}^{\infty}\left[q_{(2kL+e)(2(h+1)N-z)}(t)-\right.$$

$$\left.-q_{(2(k+1)L-e)(2(h+1)N-z)}(t)\right]=0 \qquad \text{(93)}$$

$$\frac{M}{\beta}\Big[\ddot{q}_{(2(c+1)L-e)(2hN+z)}(t)+\lambda_r N\sum_{j=0}^{\infty}\big[\ddot{q}_{(2(c+1)L-e)(2jN+z)}(t)-$$

$$-\ddot{q}_{(2(c+1)L-e)(2(j+1)N-z)}(t)\big]-\lambda_s L\sum_{K=0}^{\infty}\big[\ddot{q}_{(2kL+e)(2hN+z)}(t)-$$

$$-\ddot{q}_{(2(k+1)L-e)(2hN+z)}(t)\big]\Big\}+\frac{1}{4\beta}\Big[(2(c+1)L-e)^2+\beta^2(2hN+z)^2\Big]^2\cdot$$

$$\cdot q_{(2(c+1)L-e)(2hN+z)}(t)+\frac{J_r(2(c+1)L-e)^4N}{4\beta}\sum_{j=0}^{\infty}\big[q_{(2(c+1)L-e)(2jN+z)}(t)-$$

$$-q_{(2(c+1)L-e)(2(j+1)N-z)}(t)\big]-\frac{J_s(2hN+z)^4L\beta^3}{4}\sum_{K=0}^{\infty}\big[q_{(2kL+e)(2hN+z)}(t)-$$

$$-q_{(2(k+1)L-e)(2hN+z)}(t)\big]-\Big[\frac{\beta(2(c+1)L-e)^2}{4}+\frac{\beta^3(2hN+z)^2\bar{u}}{4}\Big]\bar{\alpha}\cdot$$

$$\cdot q_{(2(c+1)L-e)(2hN+z)}(t)-\Big[\frac{\beta(2(c+1)L-e)^2}{4}+\frac{\beta^3(2hN+z)^2u'}{4}\Big]\alpha'\cos\theta t\cdot$$

$$\cdot q_{(2(c+1)L-e)(2hN+z)}(t)-\frac{\beta(2(c+1)L-e)^2\lambda_r N}{4}(\bar{v}_r\bar{\alpha}+v_r'\alpha'\cos\theta t)\cdot$$

$$\cdot\sum_{j=0}^{\infty}\big[q_{(2(c+1)L-e)(2jN+z)}(t)-q_{(2(c+1)L-e)(2(j+1)N-z)}(t)\big]+\frac{\beta^3\lambda_s L(2hN+z)^2}{4}\cdot$$

$$\cdot(\bar{v}_s\bar{u}\bar{\alpha}+v_s'u'\alpha'\cos\theta t)\sum_{K=0}^{\infty}\big[q_{(2kL+e)(2hN+z)}(t)-$$

$$-q_{(2(k+1)L-e)(2hN+z)}(t)=0 \qquad (94)$$

and

$$M\Big\{\frac{1}{\beta}\ddot{q}_{(2(c+1)L-e)(2(h+1)N-z)}(t)-\frac{\lambda_r N}{\beta}\sum_{j=0}^{\infty}\big[\ddot{q}_{(2(c+1)L-e)(2jN+z)}(t)-$$

$$-\ddot{q}_{(2(c+1)L-e)(2(j+1)N-z)}(t)\big]-\frac{\lambda_s L}{\beta}\sum_{K=0}^{\infty}\big[\ddot{q}_{(2kL+e)(2(h+1)N-z)}(t)-$$

$$-\ddot{q}_{(2(k+1)L-e)(2(h+1)N-z)}(t)\big]\Big\}+\frac{1}{4\beta}\Big[(2(c+1)L-e)^2+\beta^2(2(h+1)N-z)^2\Big]^2\cdot$$

$$\cdot q_{(2(c+1)L-e)(2(h+1)N-z)}(t)-\frac{J_r(2(c+1)L-e)^4N}{4\beta}\sum_{j=0}^{\infty}\big[q_{(2(c+1)L-e)(2jN+z)}(t$$

$$-q_{(2(c+1)L-e)(2(j+1)N-z)}(t)\big]-\frac{J_s(2(h+1)N-z)^4L\beta^3}{4}\sum_{K=0}^{\infty}\big[q_{(2kL+e)(2(h+1)N-z)}(t,$$

$$-q_{(2(K+1)L-e)(2(h+1)N-z)}(t)\Big]-\Big[\frac{\beta(2(c+1)L-e)^2}{4}+\frac{\beta^3(2(h+1)N-z)^2\bar{u}}{4}\Big]\bar{\alpha}\cdot$$

$$\cdot q_{(2(c+1)L-e)(2(h+1)N-z)}(t)-\Big[\beta(2(c+1)L-e)^2+\beta^3(2(h+1)N-z)^2u'\Big]\alpha'\cdot$$

$$\cdot\cos\theta t\, q_{(2(c+1)L-e)(2(j+1)N-z)}(t)+\frac{\beta(2(c+1)L-e)^2\lambda_r N}{4}(\bar{v}_r\bar{\alpha}+$$

$$+v_r'\alpha'\cos\theta t)\sum_{j=0}^{\infty}\Big[q_{(2(c+1)L-e)(2jN+z)}(t)-q_{(2(c+1)L-e)(2(j+1)N-z)}(t)\Big]+$$

$$+\frac{\beta^3\lambda_s L(2(h+1)N-z)^2}{4}(\bar{v}_s\bar{u}\bar{\alpha}+v_s'u'\alpha'\cos\theta t)\sum_{K=0}^{\infty}\Big[q_{(2KL+e)(2(h+1)N-z)}(t)-$$

$$-q_{(2(K+1)L-e)(2(h+1)N-z)}(t)\Big]=0 \quad ---------- \quad (95)$$

in which c = 1,2,----, ∞ and h = 1,2,----, ∞ . The set of (L-1) x (N-1) equations corresponds to Eqs. (92) through (95) for all combinations of the integers e = 1,2,----, L-1 and z = 1,2,---,N-1. The required equations of a given set are generated by expanding Eqs (92) through (95) for all combinations of the integers s, c and h.

Equations (92) through (95) can be expressed by a single matrix equation, by employing a procedure similar to that used in the previous section.

$$M[V]\{\ddot{Q}\}+\big[[K]-\bar{\alpha}[S]-\alpha'\cos\theta t[T]\big]\{Q\}=0 \quad ------- \quad (96)$$

in which

$$\{Q\}=\left\{\begin{array}{l} q_{ez} \\ \vdots \\ q_{(2KL+e)z} \\ q_{(2(K+1)L-e)z} \\ q_{e(2N-z)} \\ \vdots \\ q_{(2KL+e)(2(j+1)N-z)} \\ q_{(2(K+1)L-e)(2(j+1)N-z)} \end{array}\right\} \quad ------- \quad (97)$$

$$[V] = V_{mn,vu} = \begin{cases} \frac{1}{\beta} + \frac{\delta_{un}\lambda_r N}{\beta} + \frac{\delta_{vm}\lambda_s L}{\beta}, & m=v \\ & n=u \\ \frac{\delta_{un}\lambda_r N}{\beta}, & m=v \\ & n\neq u \\ \frac{\delta_{vm}\lambda_s L}{\beta}, & m\neq v \\ & n=u \\ 0, & m\neq v \\ & n\neq u \end{cases} \quad \text{-------} \qquad (98)$$

$$[K] = K_{mn,vu} = \begin{cases} \frac{1}{4\beta}\left[m^2+\beta^2 n^2\right]^2 + \frac{\delta_{un} J_r m^4 N}{4\beta} + \\ + \frac{\delta_{vm} J_s n^4 L \beta^3}{4}, & m=v \\ & n=u \\ \frac{\delta_{un} J_r m^4 N}{4\beta}, & m=v \\ & n\neq u \\ \frac{\delta_{vm} J_s n^4 L \beta^3}{4}, & m\neq v \\ & n=u \\ 0, & m\neq v \\ & n\neq u \end{cases} \quad \text{---} \qquad (99)$$

$$[S] = S_{mn,vu} = \begin{cases} \left[\frac{\beta m^2}{4} + \frac{\beta^3 n^2 u'}{4}\right] + \frac{\delta_{un} V_r' m^2 \lambda_r N \beta}{4} + \\ + \frac{\delta_{vm} V_s' u' n^2 \lambda_s L \beta^3}{4}, & m=v \\ & n=u \\ \frac{\delta_{un} V_r' m^2 \lambda_r N \beta}{4}, & m=v \\ & n\neq u \\ \frac{\delta_{vm} V_s' u' n^2 \lambda_s L \beta^3}{4}, & m\neq v \\ & n=u \\ 0, & m\neq v \\ & n\neq u \end{cases} \quad \text{---} \qquad (100)$$

$$[T]=t_{mn,v\bar{u}}=\begin{cases}\left[\frac{\beta m^2}{4}+\frac{\beta^3 n^2 u'}{4}\right]+\frac{\delta_{un}V_r' m^2\lambda_r N\beta}{4}+ & \\ +\frac{\delta_{vm}V_s' u' n^2\lambda_2 L\beta^3}{4}, & m=v,\ n=u \\ \frac{\delta_{un}V_r' m^2\lambda_r N\beta}{4}, & m=v,\ n\neq u \\ \frac{\delta_{vm}V_s' u' n^2\lambda_s L\beta^3}{4}, & m\neq v,\ n=u \\ 0, & m\neq v,\ n\neq u \end{cases}\text{---} \quad (101)$$

$$\delta_{un}=\begin{cases}-1 \text{ for } (u+n)/2N=\text{Integer} \\ +1 \text{ for } (u-n)/2N=\text{Integer}\end{cases}\text{---} \quad (102)$$

and

$$\delta_{vm}=\begin{cases}-1 \text{ for } (v+m)/2L=\text{Integer} \\ +1 \text{ for } (v-m)/2L=\text{Integer}\end{cases}\text{---------} \quad (103)$$

In Eq. (102) both (u+n)/2N and (u-n)/2N cannot be integers for the same value of u and n because of the nature of the relationships between u and n. Also, in Eq. (103) both (v+m)/2L and (v-m)/2L cannot be integers for the same value of v and m because of the nature of the relationships between v and m. The column matrix $\{Q\}$, Eq. (97), is composed of certain elements from the general square matrix $\{Q\}$ given by Eq. (29). The columns from which the elements are taken are determined from alternate use of first (2kL+e) and then (2(k+1)L-e), beginning with k equal to zero and then increasing k by integer values after each alternation. The required elements from each of the columns are determined from alternate use of first (2jN+z) and then (2(j+1)N-z), beginning with j equal to zero and then increasing k by integer values after each alternation. Since $\{Q\}$ is restricted in form then matrices which are multiplied by $\{Q\}$, the matrix

[V] being representative, are also restricted. An examination of Eqs. (98) through (101) reveals the following requirements for the generation of the subscripts of the representive matrix $v_{mn,vu}$. The generation of first m rows of $v_{mn,vu}$ requires that the subscript n = (2hN+z) in which h= 0. For these first m rows the subscript m takes on alternate values of first (2cL + e) and then (2(c+1)L-e) beginning with c equal to zero and then increasing c by integer values after each alternation. The generation of the second m rows of $v_{mn,vu}$ requires that the subscript n = (2(h+1)N-z) in which h = 0. The subscript m is determined the same way as given above with c beginning with zero. The third set of m rows requires that the subscript n return to the form n = (2hN+z) in which h = 1. Thus the subscript n alternates between first (2hN + z) and then (2(h+1)N-z), beginning with h equal to zero and then increasing h by integer values after each 2m rows until the m x n rows of the matrix $v_{mn,vu}$ are generated.

The subscripts v and u are generated as follows for each row of $v_{mn,vu}$. The subscript u alternates between u = (2jN+z) for the first columns and then u = (2(j+1)N-z) for the second n columns, beginning with j equal to zero and then increasing j by integer values after each 2n columns until the m x n columns are generated. The subscript v takes on alternate values of first (2kL-e) and then (2(k+1)L-e), beginning with k equal to zero and then increasing k by integer values after each alternation until n columns are generated. At the beginning of each n columns the integer k reverts back to zero.

Physically, Eq. (96) represents the case where the panels and both the ribs and stringers undergo motion. The independence of the sets of equations corresponds to different modes of motion.

2.6 Solution of the System of Differential Equations

a. The General Equation

The problem of parametric stability of stiffened plates reduces to six specific cases involving stiffener size, material properties, and spacing. The governing expression for the six cases is given by

$$M[V]_i\{\ddot{Q}\}_i+\left[[K]_i-\bar{\alpha}[S]_i-\alpha' Cos\,\theta t\,[T]_i\right]\{Q\}_i=0 \quad ----- \qquad (104)$$

in which the subscript i refers to the specific matrix that corresponds to a particular case. For convenience, Table 3 gives the equation number for each matrix of Eq. (104) for all of the six cases studied.

It has been shown that the determination of the regions of instability reduces to seeking conditions under which Eq. (104) has periodic solutions with period T and 2T.(33). Since the required solutions are periodic, they can be expressed in terms of a Fourier series, thus for a region of 2T

$$\{Q\}_{i1}=\{a\}_{io}+\sum_{K=2,4}^{\infty}\left[\{Q\}_{ik}Cos\frac{k\theta t}{2}+\{b\}_{ik}Sin\frac{k\theta t}{2}\right] \quad ------ \qquad (105)$$

represents the solutions with period T and

$$\{Q\}_{i2}=\sum_{K=1,3}^{\infty}\left[\{c\}_{ik}Cos\frac{k\theta t}{2}+\{d\}_{ik}Sin\frac{k\theta t}{2}\right] \quad --------- \qquad (106)$$

represents the solutions with period 2T.

Table 3

Equation Numbers for Matrices Given in Eq. (104)

Case No.	Equation Number				
	$\{Q\}_i$	$[V]_i$	$[K]_i$	$[S]_i$	$[T]_i$
1	(30)	(32)	(33)	(34)	(35)
2	(39)	(40)	(41)	(42)	(43)
3	(45)	(46)	(47)	(48)	(49)
4	(73)	(74)	(75)	(76)	(77)
5	(85)	(86)	(87)	(88)	(89)
6	(97)	(98)	(99)	(100)	(101)

The substitution of Eq. (105) into Eq. (104) and combining like terms of 1, $\cos\frac{k\theta t}{2}$ and $\sin\frac{k\theta t}{2}$ yields

$$\frac{1}{2}[K]_i\{a\}_{i0}-\frac{\alpha}{2}[S]_i\{a\}_{i0}-\frac{\alpha'}{2}[T]_i\{a\}_{i0}\cos\theta t+\sum_{k=2,4}^{\infty}\Big\{\Big[-[V]_i\{a\}_{ik}\cdot k^2M\theta^2+[K]_i\{a\}_{ik}-\alpha[S]_i\{a\}_{ik}\Big]\cos\frac{k\theta t}{2}+\Big[-[V]_i\{b\}_{ik}\frac{k^2M\theta^2}{4}+$$

$$+[K]_i\{b\}_{ik}-\alpha[S]_i\{b\}_{ik}\Big]\sin\frac{k\theta t}{2}-\alpha'[T]_i\{a\}_{ik}\cos\theta t\cos\frac{k\theta t}{2}-$$

$$-\alpha|T|_i\{b\}_{ik}\cos\theta t\sin\frac{k\theta t}{2}=0 \quad \text{---------} \qquad (107)$$

However,

$$\{a\}_k\cos\theta t\cos\frac{k\theta t}{2}=\left\{\begin{array}{ll}\frac{\{a\}_{i2}}{2} & ,\ k=0\\ \frac{1}{2}\{a\}_{i4}\cos\theta t & ,\ k=2\\ \frac{1}{2}\cos\frac{k\theta t}{2}(\{a\}_{i(k+2)}+ & \\ +\{a\}_{i(k-2)}) & ,\ k=4,6,--\end{array}\right\}--- \qquad (108)$$

and

$$\{b\}_k\cos\theta t\sin\frac{k\theta t}{2}=\left\{\begin{array}{ll}\frac{1}{2}\{b\}_{i4}\sin\theta t & ,\ k=2\\ \frac{1}{2}\sin\frac{k\theta t}{2}(\{b\}_{i(k+2)}+ & \\ +\{b\}_{i(k-2)}) & ,\ k=4,6,--\end{array}\right\}--- \qquad (109)$$

The substitution of Eqs. (108) and (109) into Eq. (107) yields

$$\Big[\frac{1}{2}[K]_i-\frac{\alpha}{2}[S]_i\Big]\{a\}_{i0}-\frac{\alpha'}{2}[T]_i\{a\}_{i2}+\sum_{k=2,4}^{\infty}\Big\{-\frac{\alpha'}{2}[T]_i\{a\}_{i(k-2)}+$$
$$+\Big[-[V]_i\frac{k^2M\theta^2}{4}+[K]_i-\alpha[S]_i\Big]\{a\}_{ik}-\frac{\alpha'}{2}[T]_i\{a\}_{i(k+2)}\Big\}\cos\frac{k\theta t}{2}+$$
$$+\Big\{\Big[-[V]_iM\theta^2+[K]_i-\alpha[S]_i\Big]\{b\}_{i2}-\frac{\alpha'}{2}[T]_i\{b\}_{i4}\Big\}\sin\theta t+$$

$$+\sum_{k=4,6}^{\infty}\left\{-\frac{\alpha'}{2}[T]_i\{b\}_{i(k-2)}+\left[-[V]_i\frac{k^2M\theta^2}{4}+[K]_i-\bar{\alpha}[S]_i\right]\{b\}_{ik}-\right.$$

$$\left.-\frac{\alpha'}{2}[T]_i\{b\}_{i(k+2)}\right\}\sin\frac{k\theta t}{2}=0 \quad \text{----------} \qquad (110)$$

If φ_i is a linearly independent set of functions, then the condition

$$\sum_{i=1}^{\infty} r_i\varphi_i=0 \quad \text{----------} \qquad (111)$$

requires that the r_i 's be equal to zero. Equation (110) has the same form as Eq. (111) and the functions 1, cos $\frac{k\theta t}{2}$ and sin $\frac{k\theta t}{2}$ form a linearly independent set of functions. Thus, the coefficients of Eq. (110) are equal to zero, which implies that

$$\left[\frac{1}{2}[K]_i-\bar{\alpha}[S]_i\right]\{a\}_{i0}-\frac{\alpha'}{2}[T]_i\{a\}_{i2}=0 \quad \text{----------} \qquad (112)$$

$$-\frac{\alpha'}{2}[T]_i\{a\}_{i(k-2)}+\left[-[V]_i\frac{k^2M\theta^2}{4}+[K]_i-\bar{\alpha}[S]_i\right]\{a\}_{ik}-$$

$$-\frac{\alpha'}{2}[T]_i\{a\}_{i(k+2)}=0,\ k=2,4,6, \quad \text{----------} \qquad (113)$$

$$\left[-[V]_iM\theta^2+[K]_i-\bar{\alpha}[S]_i\right]\{b\}_{i2}+\frac{\alpha'}{2}[T]_i\{b\}_{i4}=0 \quad \text{----} \qquad (114)$$

and

$$-\frac{\alpha'}{2}[T]_i\{b\}_{i(k-2)}+\left[-[V]_i\frac{k^2M\theta^2}{4}+[K]_i-\alpha[S]_i\right]\{b\}_{ik}-$$

$$-\frac{\alpha'}{2}[T]_i\{b\}_{i(k+2)}=0,\ k=2,4,6, \quad \text{----------} \qquad (115)$$

The premultiplication of Eq. (112) by $2[V]^{-1}$ and the corresponding pre-multiplication of Eq. (113) by $\frac{4}{k^2}[V]^{-1}$ yields

$$[F]_i\{a\}_{i0}-\alpha'[G]_i\{a\}_{i2}=0 \quad \text{------} \qquad (116)$$

$$-\frac{\alpha'}{2}[G]_i\{a\}_{i0}+\left[[F]_i-\delta[I]\right]\{a\}_{i2}-\frac{\alpha'}{2}[G]_i\{a\}_{i4}=0 \quad \text{--} \qquad (117)$$

and

$$-\frac{2\alpha'}{k^2}[G]_i\{a\}_{i(k-2)}+\left[\frac{4}{k^2}[F]_i-\delta[I]\right]\{a\}_k-$$

$$-\frac{2\alpha'}{k^2}[G]_i\{a\}_{i(k+2)}=0\ ,\ k=2,4,6,\text{-----} \qquad (118)$$

The premultiplication of Eq. (116) by $[F]_1^{-1}$ yields

$$\{a\}_{i0}=\alpha'[F]_i^{-1}[G]_i\{a\}_{i2} \qquad (119)$$

The substitution of Eq. (119) into Eq. (117) gives

$$\left[[W]_i-\delta[I]\right]\{a\}_{i2}-\frac{\alpha'}{2}[G]_i\{a\}_{i4}=0 \qquad (120)$$

in which

$$[W]_i=[F]_i-\frac{\alpha'}{2}[G]_i[F]_i^{-1}[G]_i \qquad (121)$$

The premultiplication of Eq. (114) by $[V]^{-1}$ and the corresponding premultiplication of Eq. (115) by $\frac{4}{k^2}[V]^{-1}$ yields

$$\left[[F]_i-\delta[I]\right]\{b\}_{i2}-\frac{\alpha'}{2}[G]_i\{b\}_{i4}=0 \qquad (122)$$

and

$$-\frac{2\alpha'}{k^2}[G]_i\{b\}_{i(k-2)}+\left[\frac{4}{k^2}[F]_i-\delta[I]\right]\{b\}_{ik}-$$

$$-\frac{2\alpha'}{k^2}[G]_i\{b\}_{i(k+2)}=0\ ,\ k=4,6,8 \qquad (123)$$

The first system of equations, Eqs. (118) and (120) contains only $\{a\}_{ik}$ coefficients and the second system of equations, Eqs. (122) and (123), contains only $\{b\}_{ik}$ coefficients. The existence of non-trival solutions for the above two systems of homogeneous equations requires that $\{a\}_{ik}$ and $\{b\}_{ik}$ be non-zero. This condition requires that the determinant of the coefficients of each of the two systems be equal to zero. Hence, the condition for the existence of periodic solutions with period $2\pi/\theta$ has the form

$$\det.([A]_i-\delta[E])=0 \qquad (124)$$

and

$$\det([A]_2 - \delta[E]) = 0 \qquad (125)$$

in which

$$[A]_1 = \begin{bmatrix} [W]_i & -\frac{\alpha'}{2}[G]_i & [0] \\ -\frac{\alpha'}{8}[G]_i & \frac{1}{4}[F]_i & -\frac{\alpha'}{8}[G]_i \\ [0] & -\frac{\alpha'}{18}[G]_i & \frac{1}{9}[F]_i \end{bmatrix} \qquad (126)$$

and

$$[A]_2 = \begin{bmatrix} [F]_i & -\frac{\alpha'}{2}[G]_i & [0] \\ -\frac{\alpha'}{8}[G]_i & \frac{1}{4}[F]_i & -\frac{\alpha'}{8}[G]_i \\ [0] & -\frac{\alpha'}{18}[G]_i & \frac{1}{9}[F]_i \end{bmatrix} \qquad (127)$$

and

$$[E] = \begin{bmatrix} [I] & [0] & [0] \\ [0] & [I] & [0] \\ [0] & [0] & [I] \end{bmatrix} \qquad (128)$$

The matrix [O] is the null matrix. Thus the problem is reduced to an eigenvalue problem.

Similarily the substitution of Eq. (106) into Eq. (104) yields the condition for the existence of periodic solutions with a period $4\pi/\theta$ which is

$$\det([A]_3 - \delta[E]) = 0 \qquad (129)$$

and

$$\det([A]_4 - \delta[E]) = 0 \qquad (130)$$

in which

$$[A]_3 = \begin{bmatrix} 4[P]_i & -2\alpha'[G]_i & [0] \\ -\frac{2\alpha'}{9}[G]_i & \frac{4}{9}[F]_i & -\frac{2\alpha'}{9}[G]_i \\ [0] & -\frac{2\alpha'}{25}[G]_i & \frac{4}{25}[F]_i \end{bmatrix} \qquad (131)$$

$$[A]_4 = \begin{bmatrix} 4[R]_i & -2\alpha'[G]_i & [0] \\ -\frac{2\alpha'}{9}[G]_i & \frac{4}{9}[F]_i & -\frac{2\alpha'}{9}[G]_i \\ [0] & -\frac{2\alpha'}{25}[G]_i & \frac{4}{25}[F]_i \end{bmatrix} \qquad (132)$$

$$[G]_i = \alpha'[V]_i^{-1}[T]_i \qquad (133)$$

$$[F]_i = [V]_i^{-1}[K]_i - \alpha[V]_i^{-1}[S]_i \qquad (134)$$

and

$$[P]_i = [F]_i - \frac{\alpha'}{2}[G]_i \qquad (135)$$

b. Mathieu's Equation

All of the equations considered in the preceeding section belonged to a system of equations. However, Eq. (66) is a single equation and is known as Mathieu's equation. If each of the matrices in Eq. (104) contains only one element then Eq. (104) is the same as Eq. (66). The conditions for the existence of periodic solutions of Eq. (66) can be found by employing procedures similar to those used in the previous section except that the matrix notation is replaced with the single scalar notation. Thus, the conditions for the existence of periodic solutions with period $4\pi/\theta$ have the form

$$\det.([B]_1 - \delta'[I]) = 0 \qquad (136)$$

and

$$\det.([B]_2 - \delta'[I]) = 0 \qquad (137)$$

in which

$$\delta' = \frac{\theta^2}{4\Omega^2} \qquad (138)$$

$$[B]_1 \begin{bmatrix} 1-\mu & -\mu & 0 \\ -\frac{\mu}{9} & \frac{1}{9} & -\frac{\mu}{9} \\ 0 & -\frac{\mu}{25} & \frac{1}{25} \end{bmatrix} \qquad (139)$$

and

$$[B]_2 \begin{bmatrix} 1+\mu & -\mu & 0 \\ -\frac{\mu}{9} & \frac{1}{9} & -\frac{\mu}{9} \\ 0 & -\frac{\mu}{25} & \frac{1}{25} \end{bmatrix} \qquad (140)$$

The parameters Ω and μ are given by Eqs.(64) and (65) respectively. These conditions are similar to those expressed by Eqs. (129) through (132). The conditions for the existence of periodic solutions with period $2\pi/\theta$ have the form

$$\det.([B]_3 - \delta'[I]) = 0 \qquad (141)$$

and

$$\det([B]_4 - \delta'[I]) = 0 \qquad (142)$$

in which

$$[B]_3 = \begin{bmatrix} \left(-\frac{\mu^2}{2}+\frac{1}{4}\right) & -\frac{\mu}{4} & 0 \\ -\frac{\mu}{16} & \frac{1}{16} & -\frac{\mu}{16} \\ 0 & -\frac{\mu}{36} & \frac{1}{36} \end{bmatrix} \quad \text{(143)}$$

and

$$[B]_4 = \begin{bmatrix} \frac{1}{4} & -\frac{\mu}{4} & 0 \\ -\frac{\mu}{16} & \frac{1}{16} & -\frac{\mu}{16} \\ 0 & -\frac{\mu}{36} & \frac{1}{36} \end{bmatrix} \quad \text{(144)}$$

These conditions are similar to those expressed by Eqs. (124) through (128).

The eigenvalues, δ', which are necessary for the existence of periodic solutions of Eq. (66) are determined numerically from Eqs. (136) (137), (141), and (142).

2.7 Special Cases

a. Natural Vibration Case

It can be shown that the natural frequencies of a stiffened plate subjected to static in-plane boundary loading can be found from the previous results. If $\bar{\alpha}$ is specified and α' is taken to be equal to zero, then Eq. (104) reduces to the form

$$M[V]_i\{\ddot{Q}\}_i + \left[[K]_i - \bar{\alpha}[S]_i\right]\{Q\}_i = 0 \quad \text{(145)}$$

The premultiplication of Eq. (145) by $[V]_i^{-1}$ yields

$$M\{\ddot{Q}\}_i + [F]_i\{Q\}_i = 0 \quad \text{(146)}$$

in which $[F]_i$ is given by Eq. (134). A solution to Eq. (146) can be sought in the form

$$\{Q\}_i = \cos\Omega t\,\{D\}_i \quad \text{(147)}$$

in which $[D]_i$ is a constant column matrix and Ω is the natural frequency of the stiffened plate. The substitution of Eq (147) into Eq. (146) gives

$$\left[[F]_i - \delta[I]\right]\{D\}_i = 0 \quad \text{- - - - - - - - - - -} \tag{148}$$

in which

$$\bar{\delta} = M\Omega^2 \quad \text{- - - - - - -} \tag{149}$$

The condition for the existence of a non-trival solution requires

$$\det.\left([F]_i - \bar{\delta}[I]\right) = 0 \quad \text{- - - - - - - - -} \tag{150}$$

The matrix $[F]_i$ is known for any given stiffened plate since $\bar{\alpha}$ is specified. Thus, the determination of the eigenvalues of Eq. (50) gives the natural frequency when static inplane boundary loading is present.

b. Parametric Stability Near α' Equal to Zero

An important result can be obtained for the parametric stability case from the information given by Eq. (150). For the case $\bar{\alpha}$ specified and α' equal to zero Eqs. (116), (117), and (118) reduce to the following equations

$$[F]_i\{a\}_{i0} = \{0\} \quad \text{- - - - - - - - - - -} \tag{151}$$

$$\left[[F]_i - \delta[I]\right]\{a\}_{i2} = \{0\} \quad \text{- - - - - - - - - -} \tag{152}$$

and

$$\left[\frac{4}{k^2}[F]_i - \delta[I]\right]\{a\}_{ik} = \{0\}, \quad k = 4, 6, 8, \text{- - -} \tag{153}$$

Each of the above equations is independent of the other. Since $\bar{\alpha}$ is specified, the matrix $[F]_i$ is completely known for a given stiffened plate. The requirements for the existence of a non-trivial solution for Eqs. (151) through (153) yields the conditions

$$\{a\}_{i0} = \{0\} \quad \text{- - - - - - - - - -} \tag{154}$$

and

$$\det.\left([F]_i - \frac{k^2\delta}{4}[I]\right) = 0, \quad k = 2, 4, 6, \text{- - - -} \tag{155}$$

If the above procedure is applied to Eqs. (122) and (123) an equation which is the same Eq. (155) is obtained. An equation which is similar to Eq. (155) can be found for odd values of k which is

$$\det\left(|F|_i - \frac{k^2\delta}{4}|I|\right) = 0\,, \quad k = 1,3,5, \quad \text{- - - - - - - -} \tag{156}$$

Equations (155) and (156) are the same as Eq. (150). This fact yields the result that for $\alpha' \to 0$ there exist periodic solutions with period 2T in the vicinity of

$$\theta = \frac{2\Omega}{k}\,, \quad k = 1,3,5, \quad \text{- - - - - - - - - - - -} \tag{157}$$

and periodic solutions with period T in the vicinity of

$$\theta = \frac{2\Omega}{k}\,, \quad k = 2,4,6, \quad \text{- - - - - - - - - - - -} \tag{158}$$

Equations (157) and (158) give a relationship between the frequency of the in-plane boundary forces and the frequencies of the free vibrations of the stiffened plate, near which the formation of unboundedly increasing vibrations is possible. Thus, these relationships define the vicinity of the regions of parametric instability for a stiffened plate. Also these equations indicate that there exists an infinite number of regions associated with each Ω. Sommerset (20) calls the mode associated with a particular value of Ω as the spatial mode and each mode associated with Eqs. (157) and (158) for a given spatial mode is called a temporal mode. This nomenclature is adopted in this investigation.

c. Static Stability Case

The static stability of a stiffened plate corresponds to the conditions that $\bar{\alpha}$ is not specified and that α' is equal to zero. Also, the system is not time dependent. Subject to these conditions Eq. (104) takes the form

$$\left[[K]_i - \bar{\alpha}[S]\right]\{Q\}_o = \{0\} \quad \text{- - - - - - - - - -} \tag{159}$$

in which $\{Q\}_o$ is an unknown constant column matrix. The premultiplication of Eq. (159) by $[S]_i$ yields

$$\left[[H]_i - \bar{\alpha}[I]\right]\{Q\}_o = \{0\} \quad \text{- - - - - - - - - -} \tag{160}$$

in which

$$[H]_i = [S]_i^{-1}[K]_i \quad \text{- - - - - - - - - - - -} \tag{161}$$

The condition for the existence of a non-trival solution of Eq. (161) yields

$$\det([H]_i - \bar{\alpha}[I]) = 0 \quad \text{- - - - - - - - - -} \tag{162}$$

The eigenvalues of Eq. (162) give the critical stability parameter α_{cr}. However, in this investigation only the lowest eigenvalue is of interest.

3. EXPERIMENTAL INVESTIGATION

The purpose of the experimental portion of this investigation is to verify some of the theoretical results. For this purpose two cases are selected. The first case represents a stiffened plate with a single centrally located stiffener transverse to the in-plane boundary force of the form $P(t) = P_o + P_t \cos \Theta t$. The size of the stiffener which is located on both sides of the stiffener which is located on both sides of the plate is selected so that the lowest critical instability mode is the first mode, see Fig. 3. The second case is the same as the first except that the size of the stiffener is selected so that the lowest critical instability mode is the second mode, see Fig. 4.

The experimental apparatus is designed so that the edges of the stiffened plate rest on knife-edge supports (simple supports) and that the load parameters P_o, P_t, and Θ are independent variables. These parameters are varied within the limits of the experimental equipment so that the boundaries (onset) of the temporal mode regions of parametric instability of the spatial mode which corresponds to the lowest value of the natural frequencies can be measured.

3.1 The Apparatus

The test apparatus is shown in Figs. 5 and 6. A Calidyne model 44 electromagnetic shaker [2] is bolted to the test frame as shown in Fig. 5. The variable component of the applied force is transmitted from the shaker to a lower load bar [3] by means of a two force member [4]. The magnitude of the variable component, P_t, of the load is controlled by a power rheostat located on the front panel of the shaker control unit [5] shown in Fig. 6. The frequency of the variable load component, , is regulated by two rheostats also located on the front panel of the shaker control unit.

The static component of the applied force, P_o, is transmitted to the lower load bar by means of two steel rods [6] which are connected between the lower load bar and the top of the test frame. The static load is applied by tightening a nut at the test frame end of each of the rods. Two Baldwin-Lima-Hampliton U-1 [8] load cells are used to record the total load applied to the stiffened plate.

The simple supports for the stiffened plate are constructed by means of two rigid rectangular support frames [9] which have edges on one side which are beveled, so as to achieve knife-edge supports.

The material of the test plates and stiffeners is aluminum for the purpose of reducing the magnitude of the critical buckling force and also the natural frequencies so that they are within the limits of the test equipment. The modulus of elasticity of the aluminium is taken as 10×10^6 psi.

The actual stringer parameters for the test plate (first mode static buckling) are $J_s = 0.984$ and $\lambda_s = 0.045$. The lowest theoretical critical buckling force for this test plate is 880 lbs. The configuration and dimensions of this plate are given in Fig. 8.

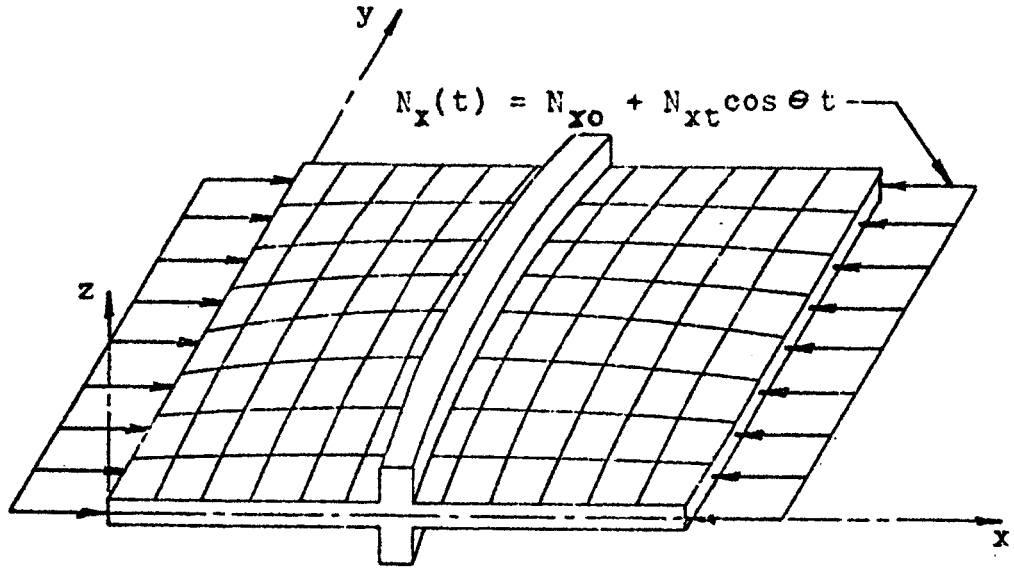

Fig. 3 First Static Instability Mode

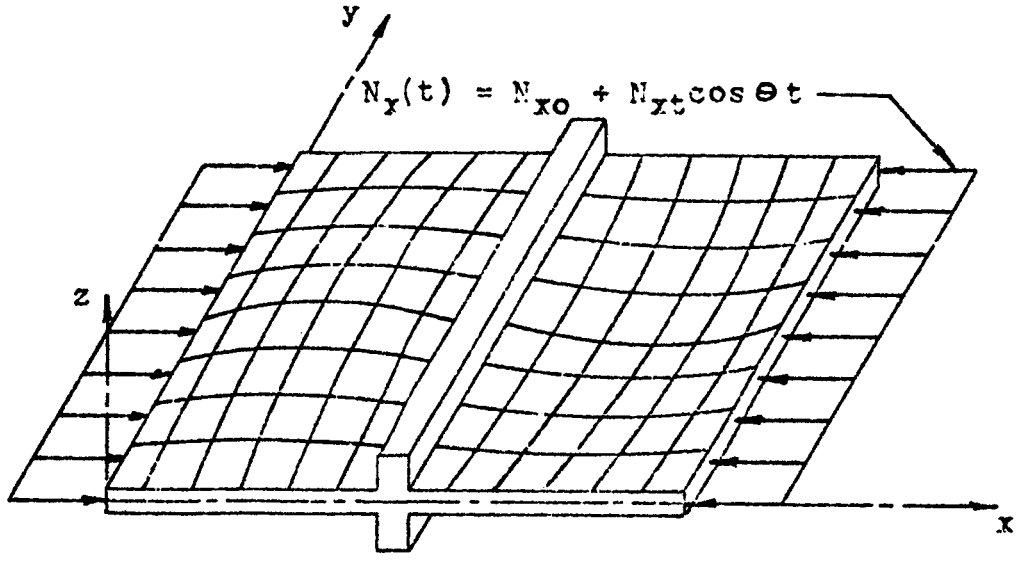

Fig. 4 Second Static Instability Mode

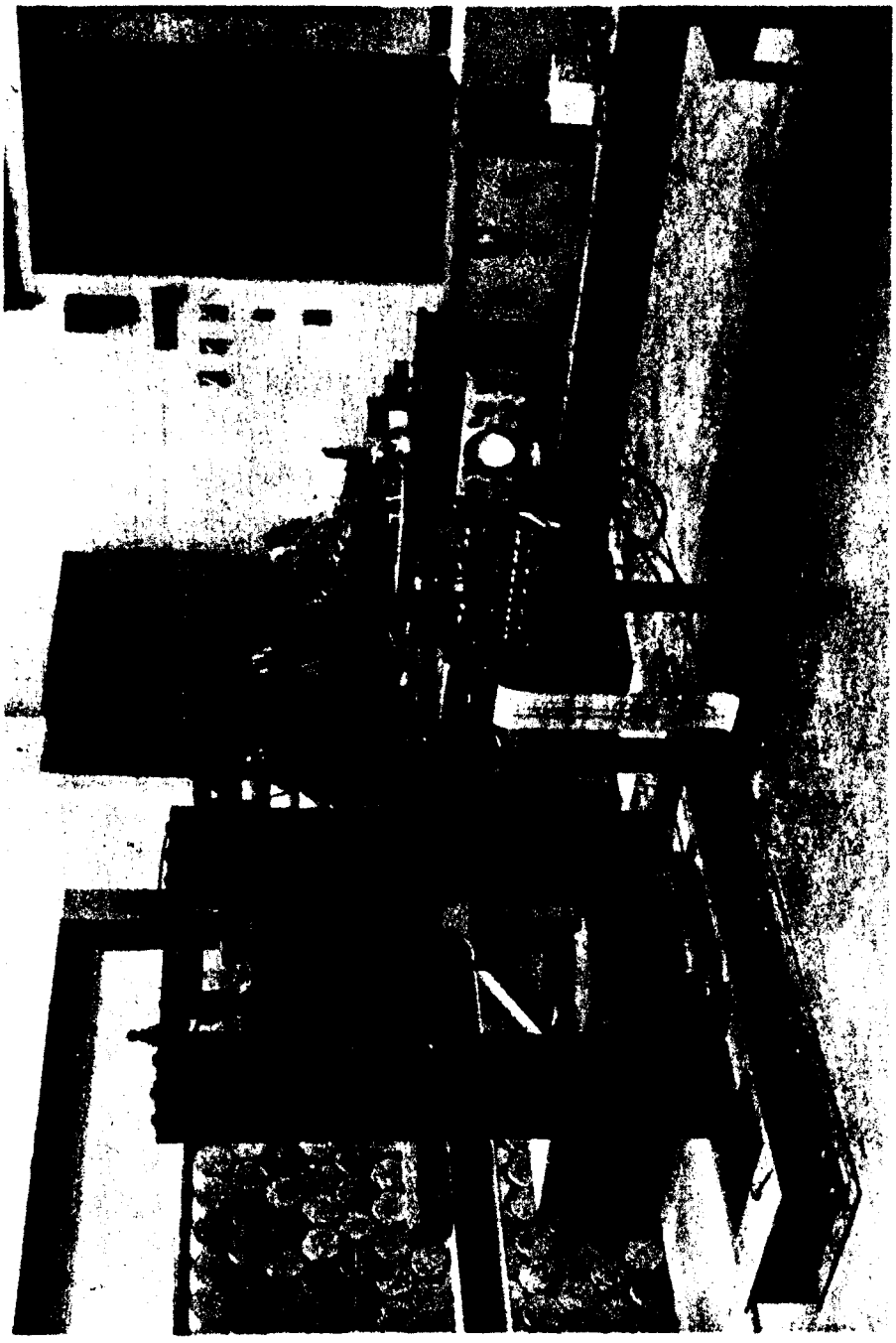

Fig. 5

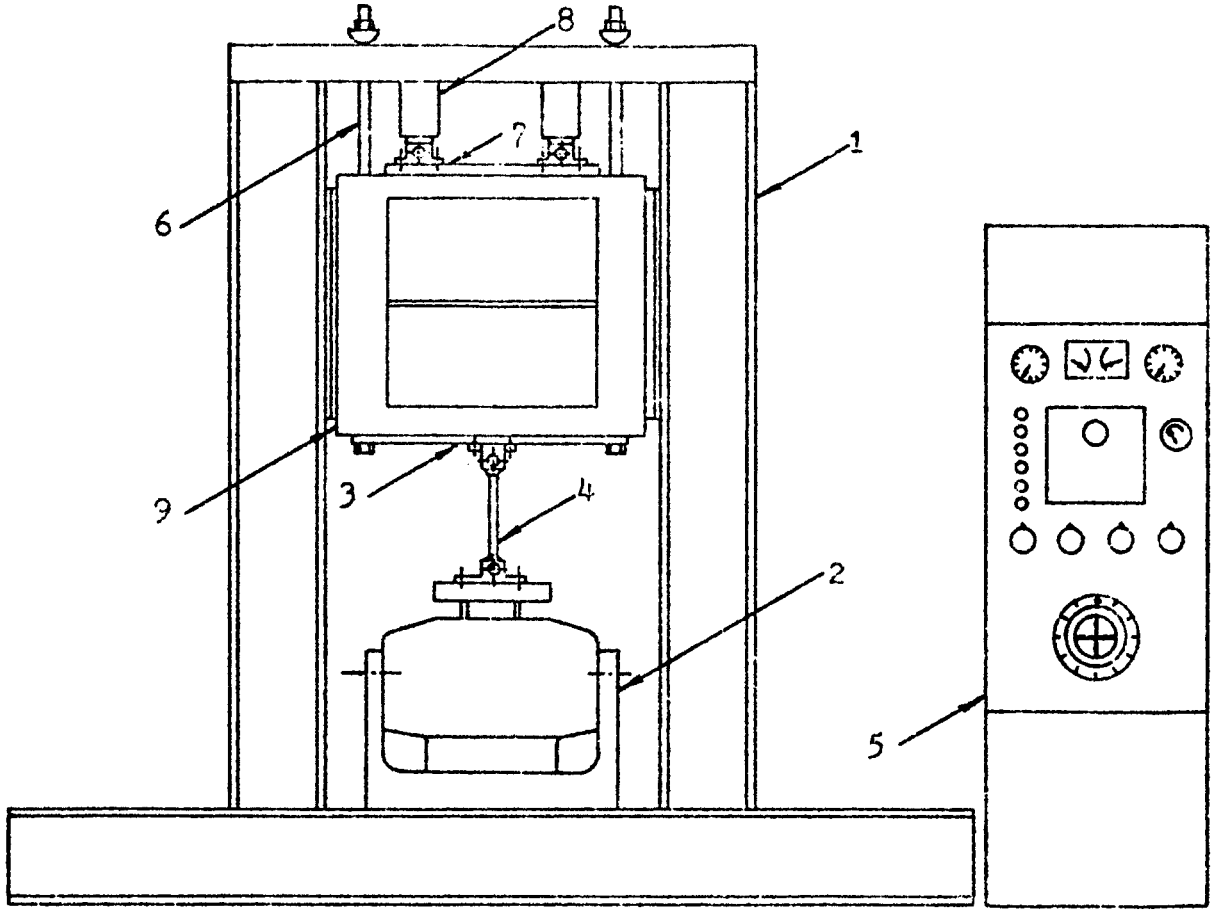

1. Test Frame
2. Electrodynamic Shaker
3. Lower Load Bar
4. Two Force Member
5. Control Console
6. Steel Rod
7. Upper Load Bar
8. Load Cell
9. Support Frame

Fig. 6 Line Drawing - Test Apparatus

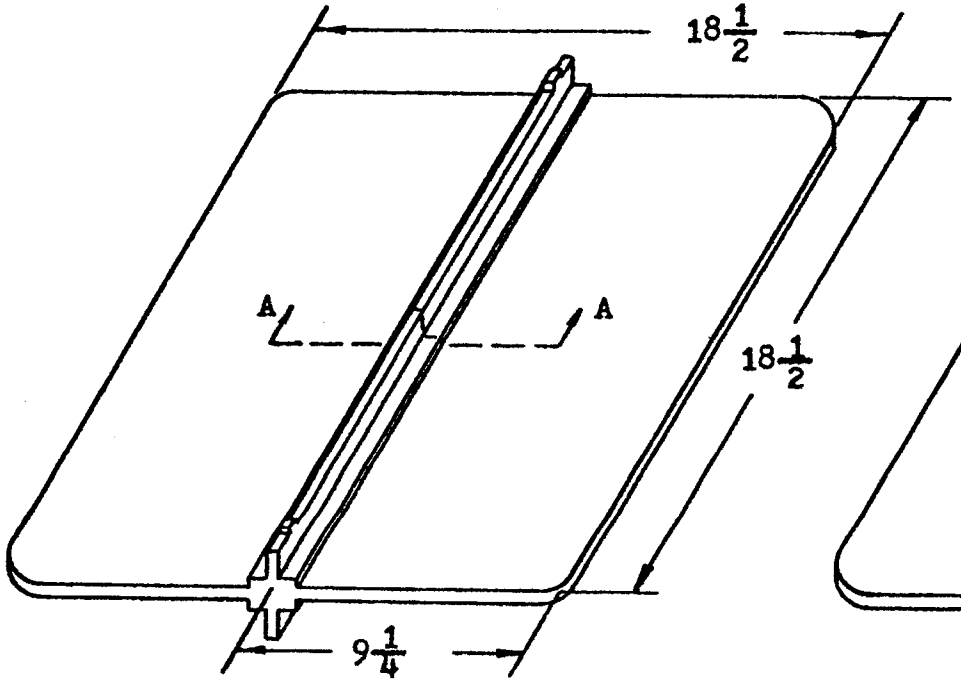

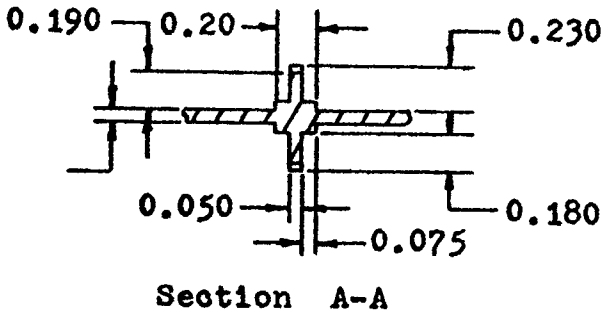

Fig. 7 First Test Specimen

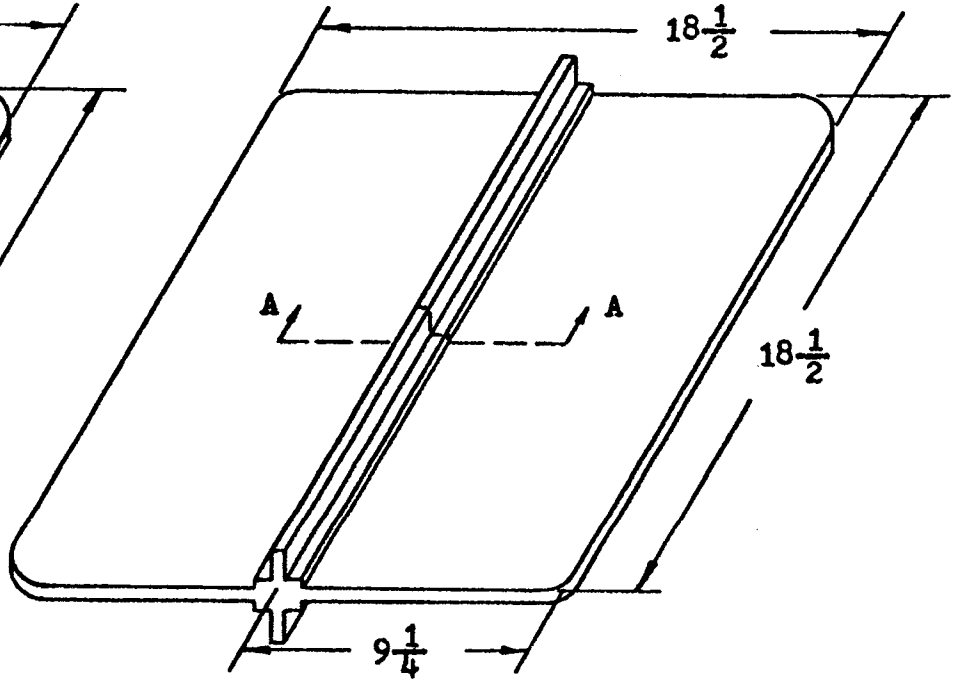

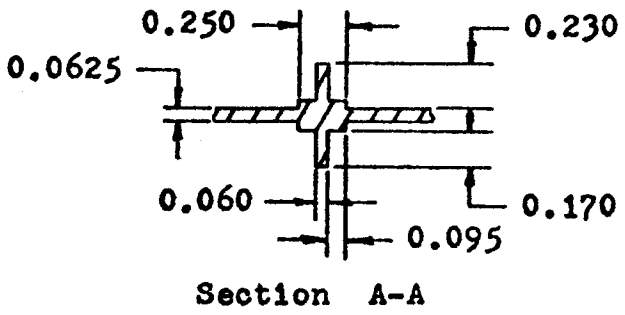

Fig. 8 Second Test Specimen

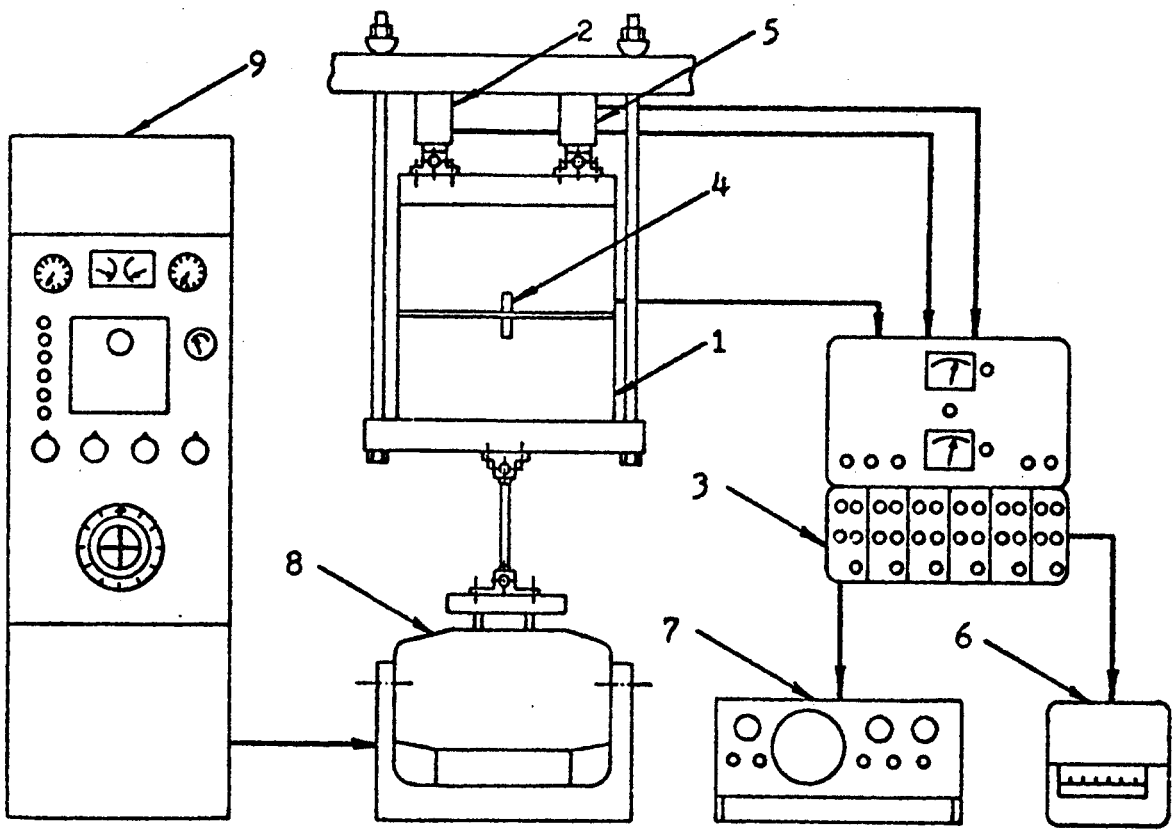

1. Stiffened Plate Specimen
2. Load Cell
3. Power Supply and Carrier Amplifiers
4. Strain Gages
5. Load Transducer Gages
6. Viscorder
7. Oscilloscope
8. Electrodynamic Shaker
9. Control Console

Fig. 9 Schematic of Experimental Arrangement.

The size of both test plates over the simple-supports is eighteen inches in both directions. The tee-shaped stiffener shown in Figs. 7 and 8 are attached permanently to the plates with Armstrong Epoxy cement.

Four SR-4 A-7 strain gages are mounted to each of the test plates with two gages on each side of the plate. The four strain gages are connected together to form a Wheatstone bridge circuit. The four strain gages are so located in the circuit that only the curvature (bending strain) of the stiffened plate is measured.

The data monitoring and recording equipment used in the experimental investigation is shown in Fig. 9.

3.2 Experimental Procedure

The boundaries of the principal region of parametric instability is considered first since it is slightly different from the procedure used to determine the boundaries of the higher order regions of parametric instability. At the beginning of each test series the stiffened plate was loaded with a static load, P_o, equal to one-half the theoretical critical buckling load. This level of static load was chosen so as to agree with the value of P_o selected for the theoretical case. For each test run the power rheostat which controls the magnitude of the variable component of the load, P_t, was set at a particular value. The load frequency at the start of each test run was set at a value lower than the frequencies for the lower boundary of the region of parametric instability. The load frequency was then increased, with the stiffened plate oscillating at an idling vibration, until the plate became unstable. The instability was characterized by an increase in the amplitude of the lateral oscillation and a change in the vibration frequency of the stiffened plate, that is, the oscillation frequency of the plate reduced to half that of the load frequency. With the stiffened plate oscillating in the instability region the Viscorder was turned on and the load frequency was then decreased until the stiffened plate again became stable. The stable oscillation was characterized by a idling lateral oscillation of the stiffened plate at a frequency equal to that of the load frequency. This procedure was repeated for various settings of the power rheostat.

The determination of the location of the upper boundaries for the principal region of parametric instability was much more difficult. The upper boundary could not be determined by increasing the load frequency from a value within the instability region to a value greater than those on the upper boundary (33). The location of the upper boundary was determined by starting at a load frequency greater than those of the upper boundary and then decreasing the load frequency with the Viscorder on until the stiffened plate became unstable; again denoted by a change of the amplitude and frequency of the lateral oscillation of the plate.

Experimental verification of the existence of higher order instability regions was found only for the second region of parametric instability. The location of the lower boundary for the second region of parametric instability was determined by setting the power rheostat at a particular value for each test run and then increasing the load frequency until the stiffened plate exhibited an instability. The instability

for the second region was characterized only by an increase in the lateral oscillation of the plate. At this point the Viscorder was turned on and the load frequency was decreased until the stiffened plate again stabilized. The second instability region did not exhibit an instability characteristic similar to that of the principal instability region. For this region the stiffened plate became stable as the load frequency passed beyond the frequencies associated with the upper boundary of the region. The location of the upper boundary of the second region of parametric instability was found in a manner similar to that used for the location of the lower region except that the load frequency was increased instead of decreased for the recording run.

4. EVALUATION OF RESULTS

4.1 Theoretical Results

The theory developed in Section two led to the determination of the eigenvalues of four matrices for each of the problems studied. The numerical procedure used to determine the eigenvalues of these matrices is based on the idea of reducing the original matrix to a similar matrix whose eigenvalues are much easier to determine.

The algorithm used in this investigation to reduce the matrices to similar matrices was developed by Francis (30,31,32) which he calls QR-Transformation. The computer subroutines based on this alogorithm are from the SHARE library program package 3006-01 and were written by Imad and VanNess (34).

Three cases of the theoretic study are presented in this section. The number of spatial modes considered for each case is limited to the three modes having the lowest load frequency range. For a given spatial mode, only the first four temporal modes are presented.

Case one represents a plate stiffened by a longitudinal rib subjected to a uniformly distributed edge load on both the plate and rib. The parameters for this system are given by Fig. 10. The results for this case are given by Figs. 11 through 13. A comparison of the instability regions which correspond to the first spatial mode, (Fig. 11), with the instability regions associated with Mathieu's equation, (Fig. 14), shows that the first four temporal modes are identical. This is to be expected since the governing equation of motion for the parametric response of a simply-supported column and plate is Mathieu's equation. Thus the first spatial mode of case one corresponds to the superposition of the individual column and plate problem. As a check on the superposition principle, case one is repeated so that superposition can not exist. This is accomplished by setting the variable component of the edge load on the rib equal to zero. This situation is denoted as case two, Fig. 15, and the results for the first three spatial modes are given by Figs. 16 through 18. A comparison of Fig. 16 with Figs. 14 and 11 shows that the boundaries of the instability regions for the first spatial mode of case two are not the same as the instability boundaries given by Mathieu's equation. This difference is indicated by the narrower widths of the temporal modes of case two. It is also seen that widths of the temporal modes for the higher order spatial modes are much narrower than for the corresponding temporal modes of the first spatial mode.

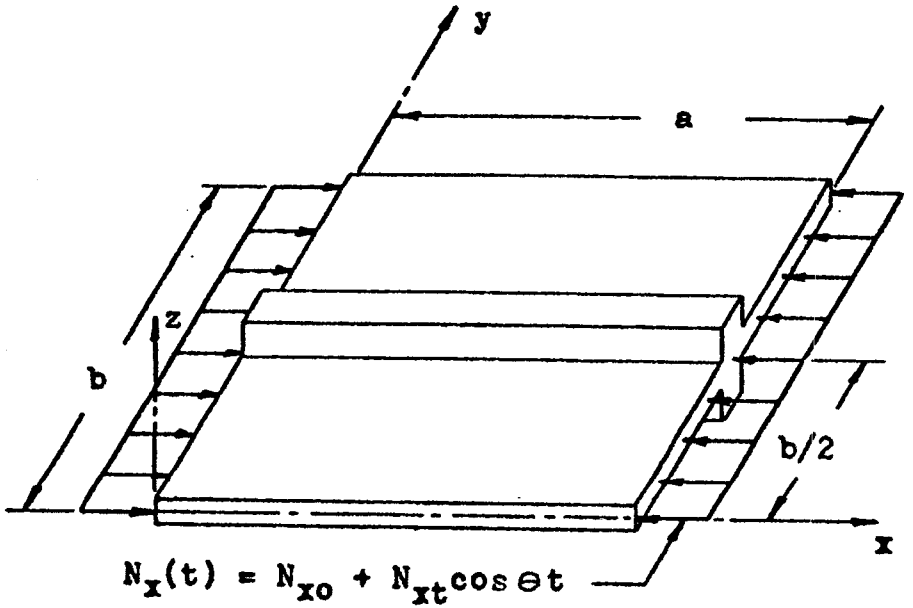

Beta = a/b = 1.0

$J_r = 2.5$

$\Lambda_r = 0.2$

$N_{xo}/N_{xcr} = 0.5$

Fig. 10 Stiffened Plate Configuration Representing Case One

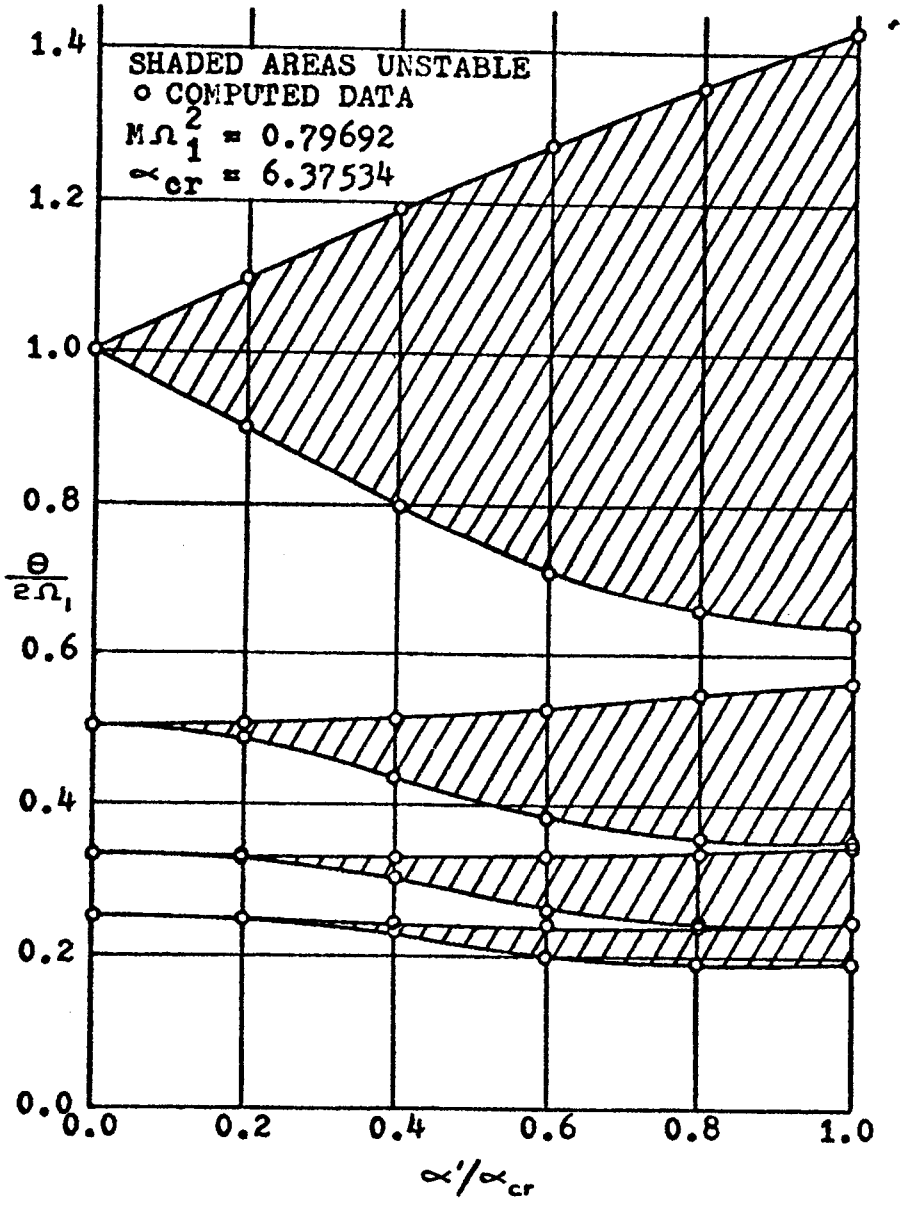

Fig. 11 Parametric Instability Regions Associated with the First Spatial Mode of Case One

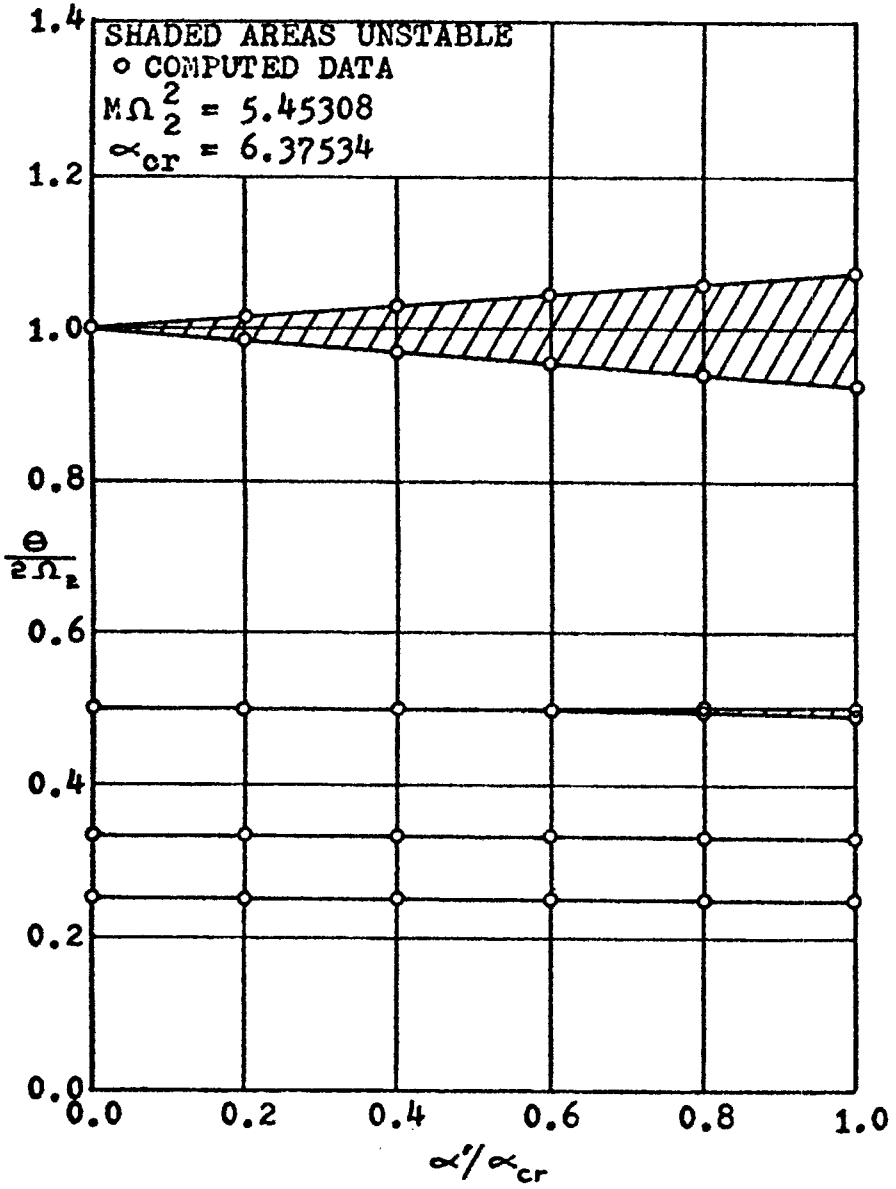

Fig. 12 Parametric Instability Regions Associated with the Second Spatial Mode of Case One

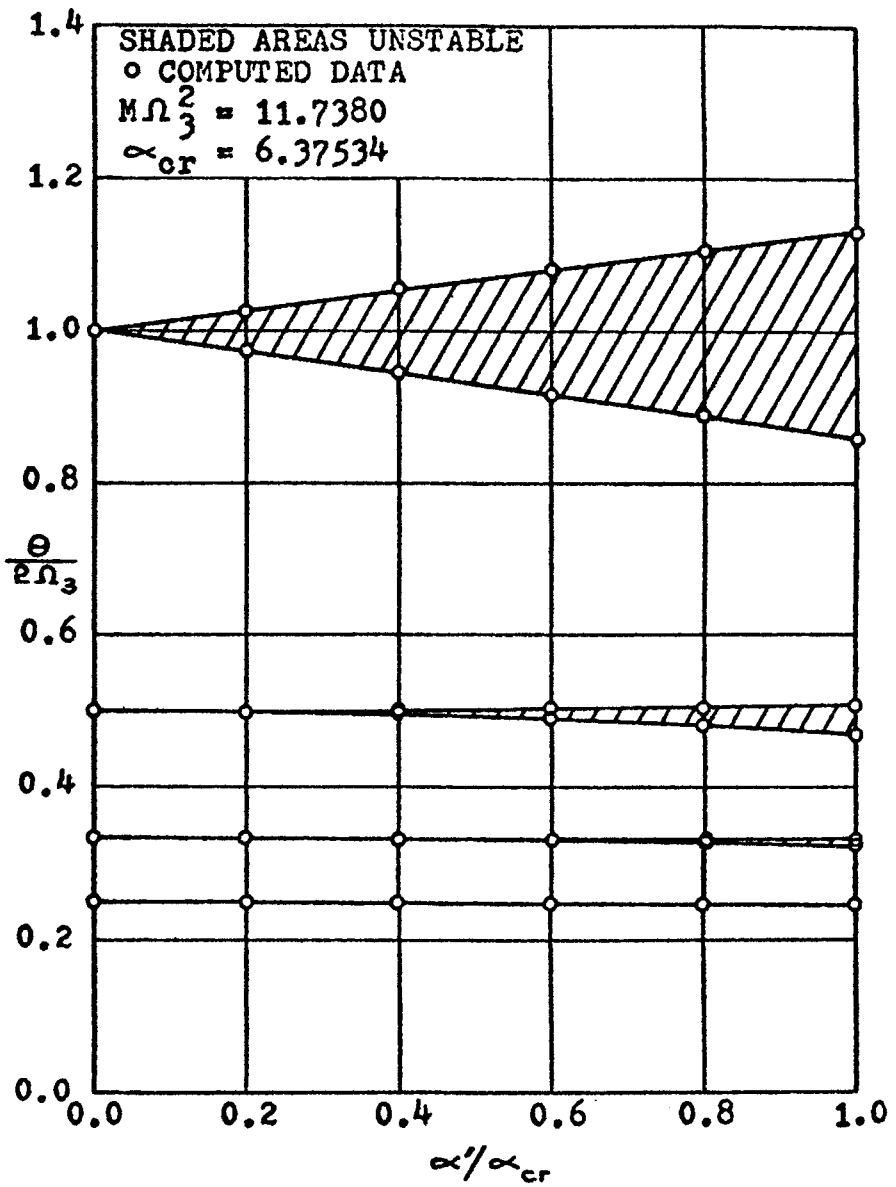

Fig. 13 Parametric Instability Regions Associated with the Third Spatial Mode of Case One

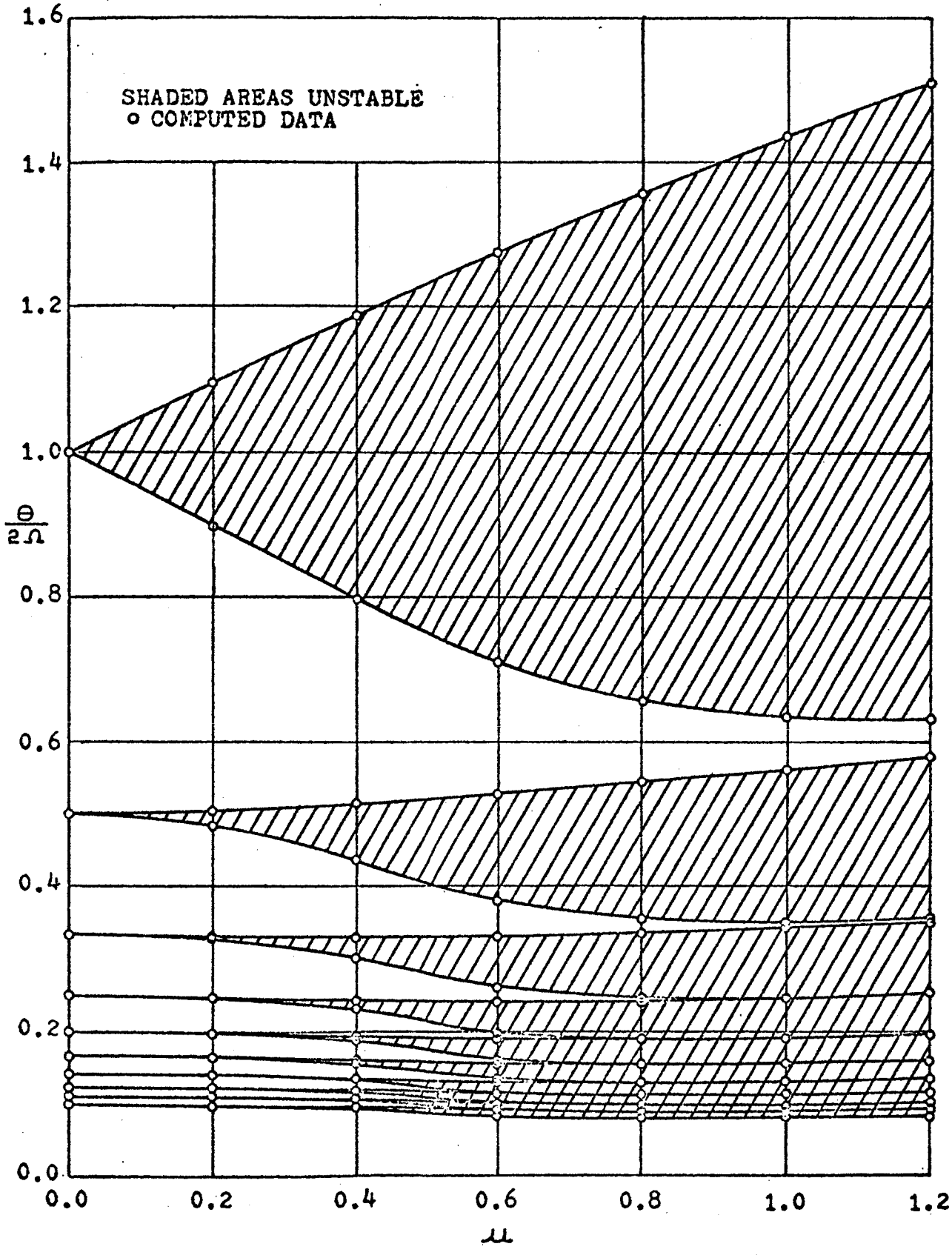

Fig. 14 Parametric Instability Regions Associated with the Orthotropic Model (Mathieu's Equation)

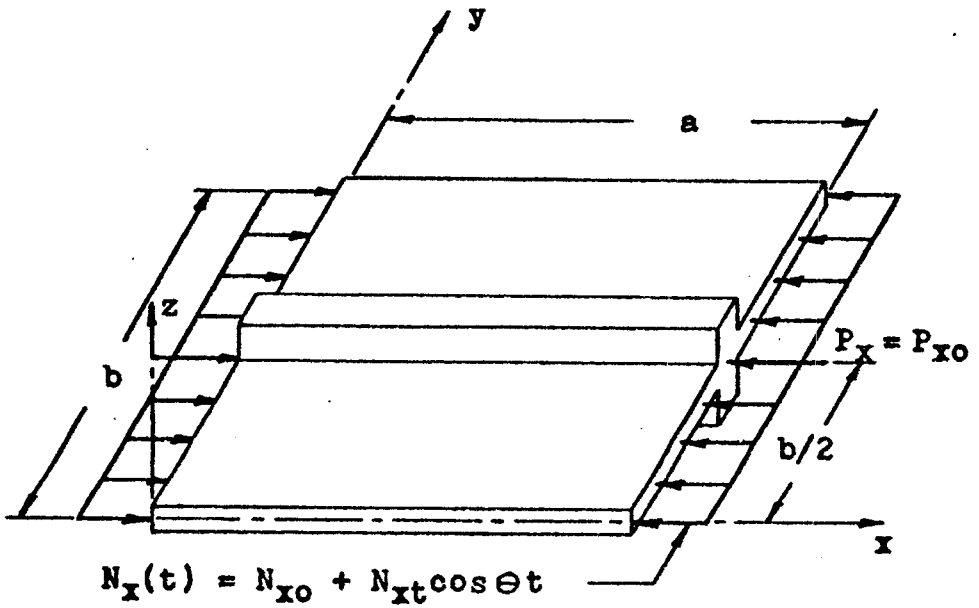

Beta = a/b = 1.0

$J_r = 2.5$

$\lambda_r = 0.2$

$N_{xo}/N_{xcr} = 0.5$

Fig. 15 Stiffened Plate Configuration Representing Case Two

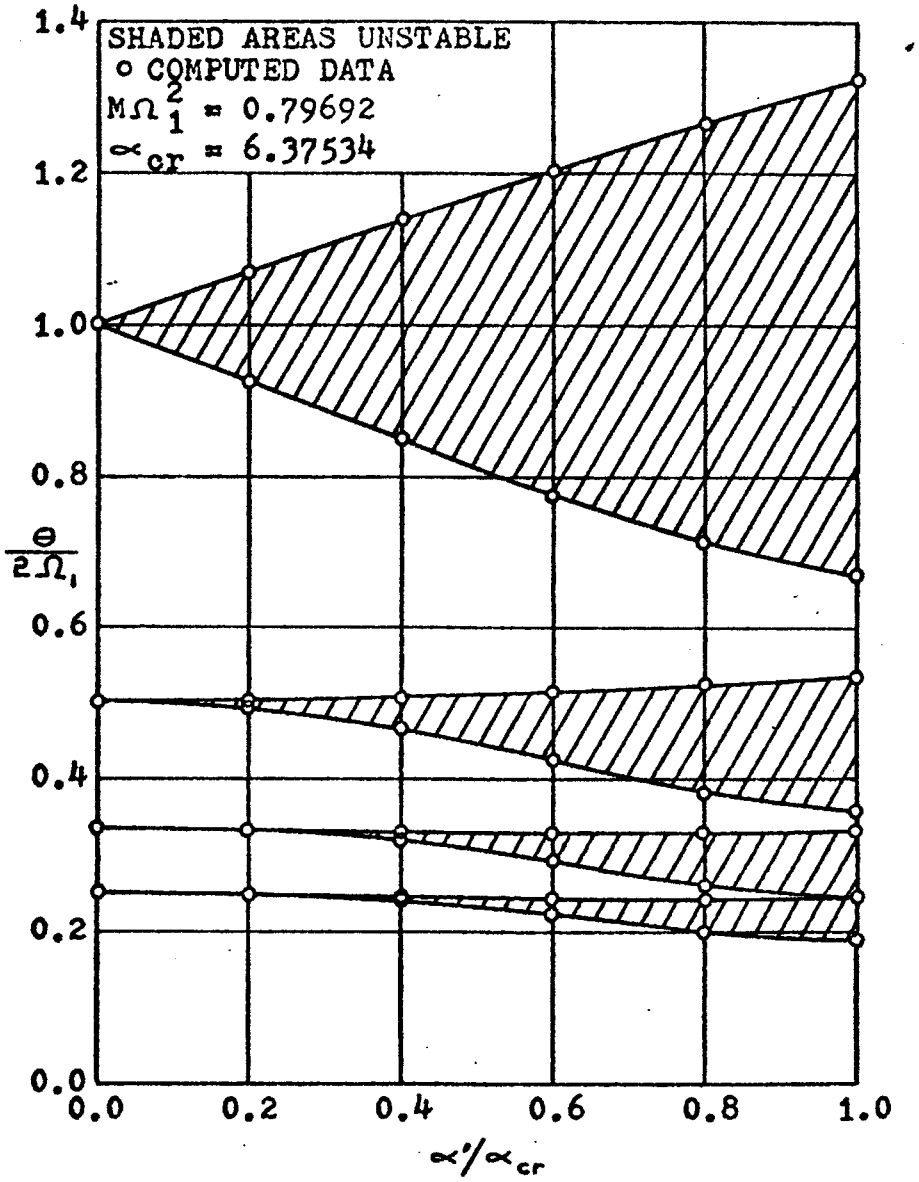

Fig. 16 Parametric Instability Regions Associated with the First Spatial Mode of Case Two

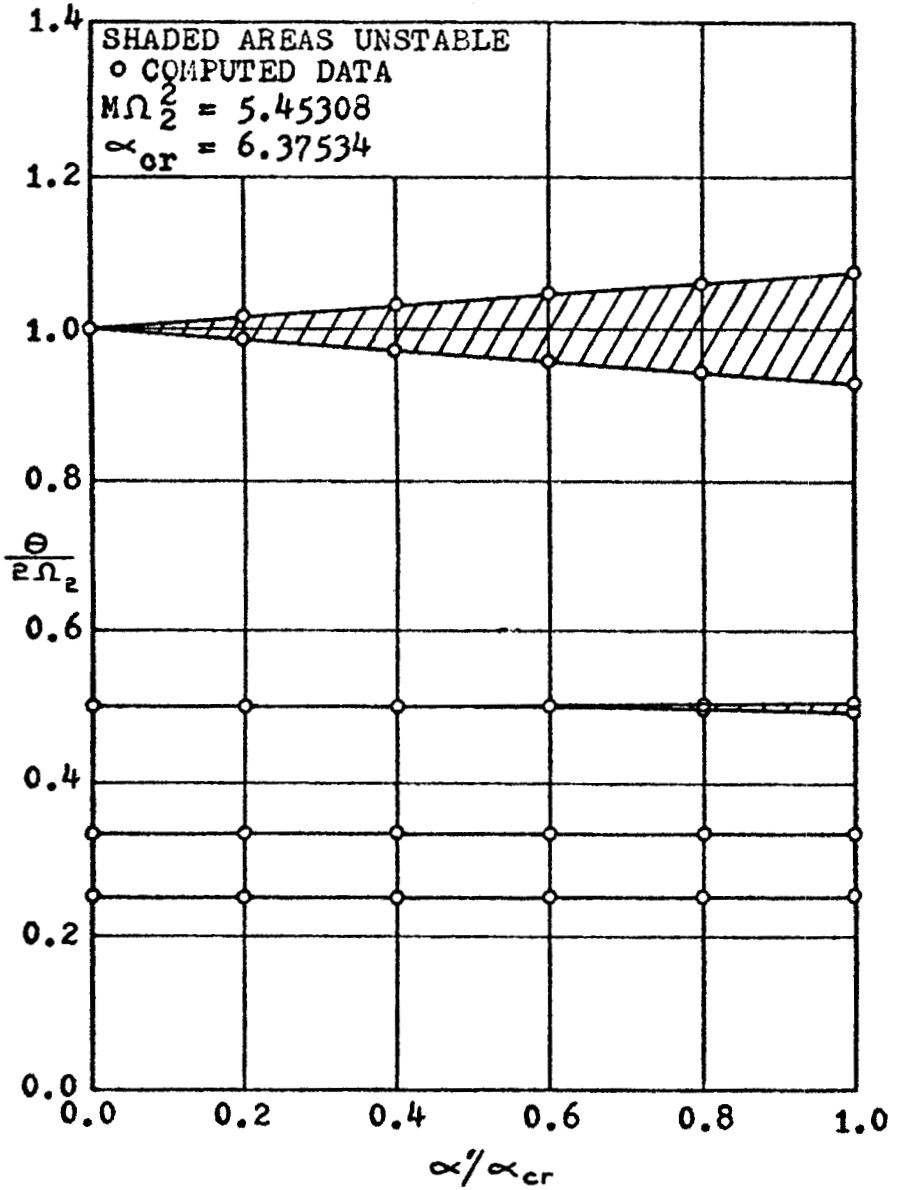

Fig. 17 Parametric Instability Regions Associated with the Second Spatial Mode of Case Two

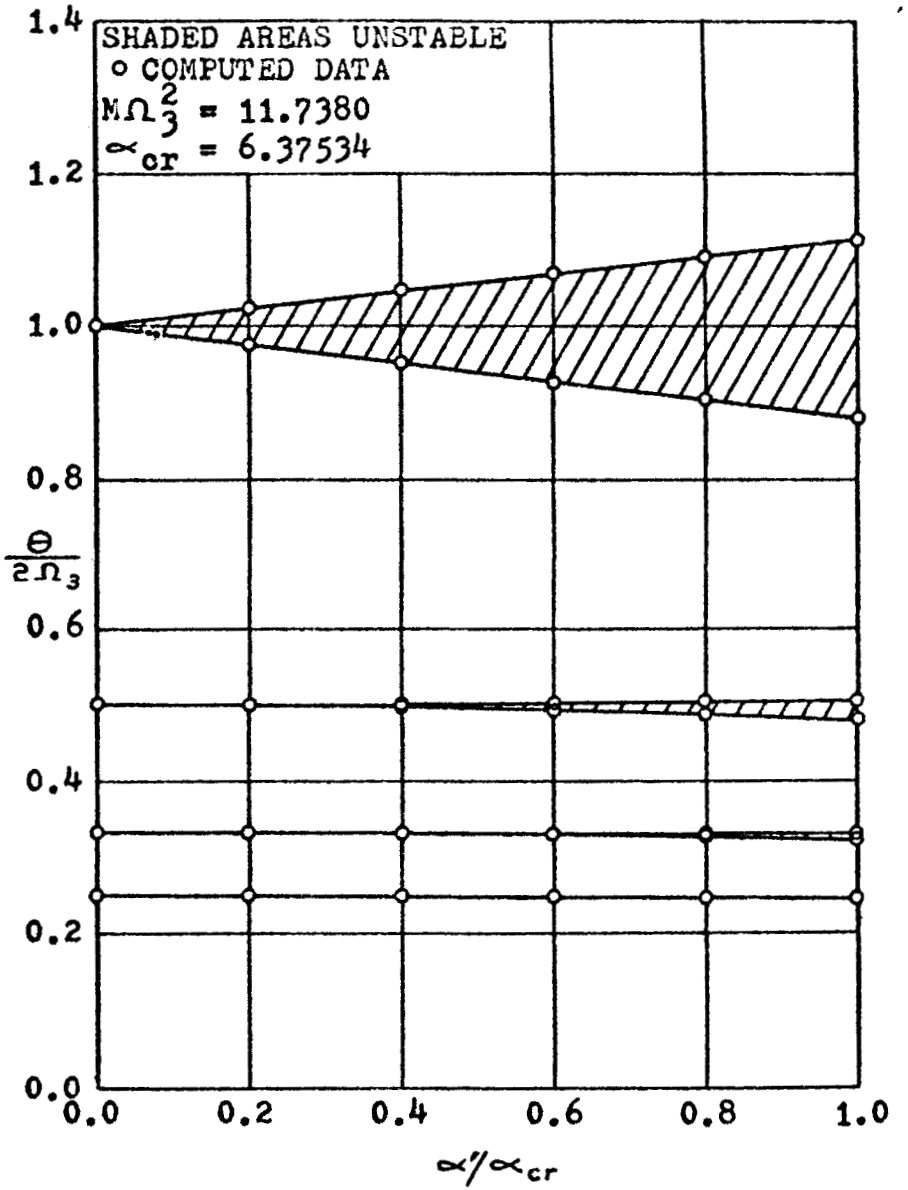

Fig. 18 Parametric Instability Regions Associated with the Second Spatial Mode of Case Two

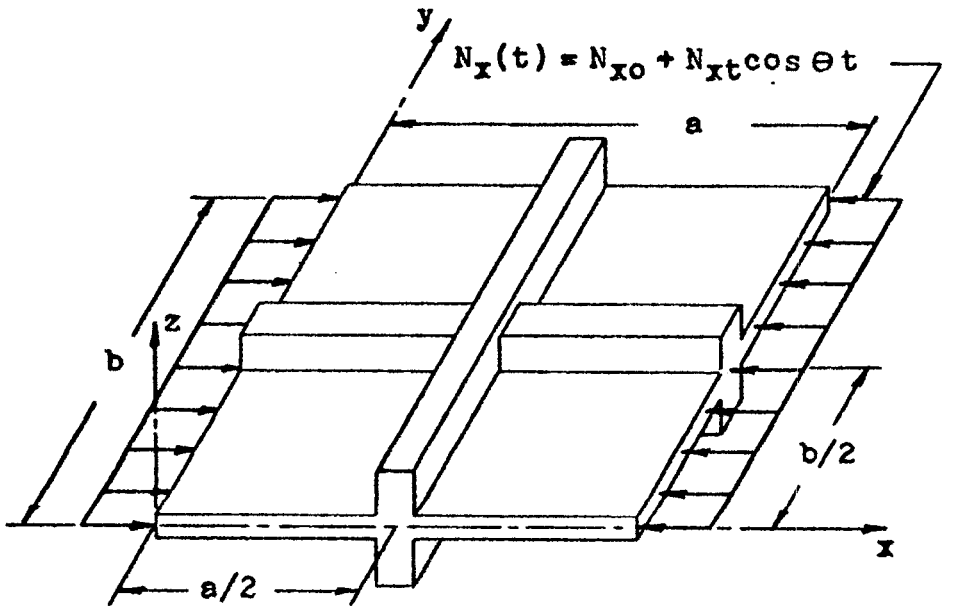

Beta = a/b = 1.0

$J_r = 2.5$

$J_s = 7.5$

$\lambda_r = \lambda_s = 0.2$

$N_{xo}/N_{xcr} = 0.5$

Fig. 19 Stiffened Plate Configuration Representing Case Three

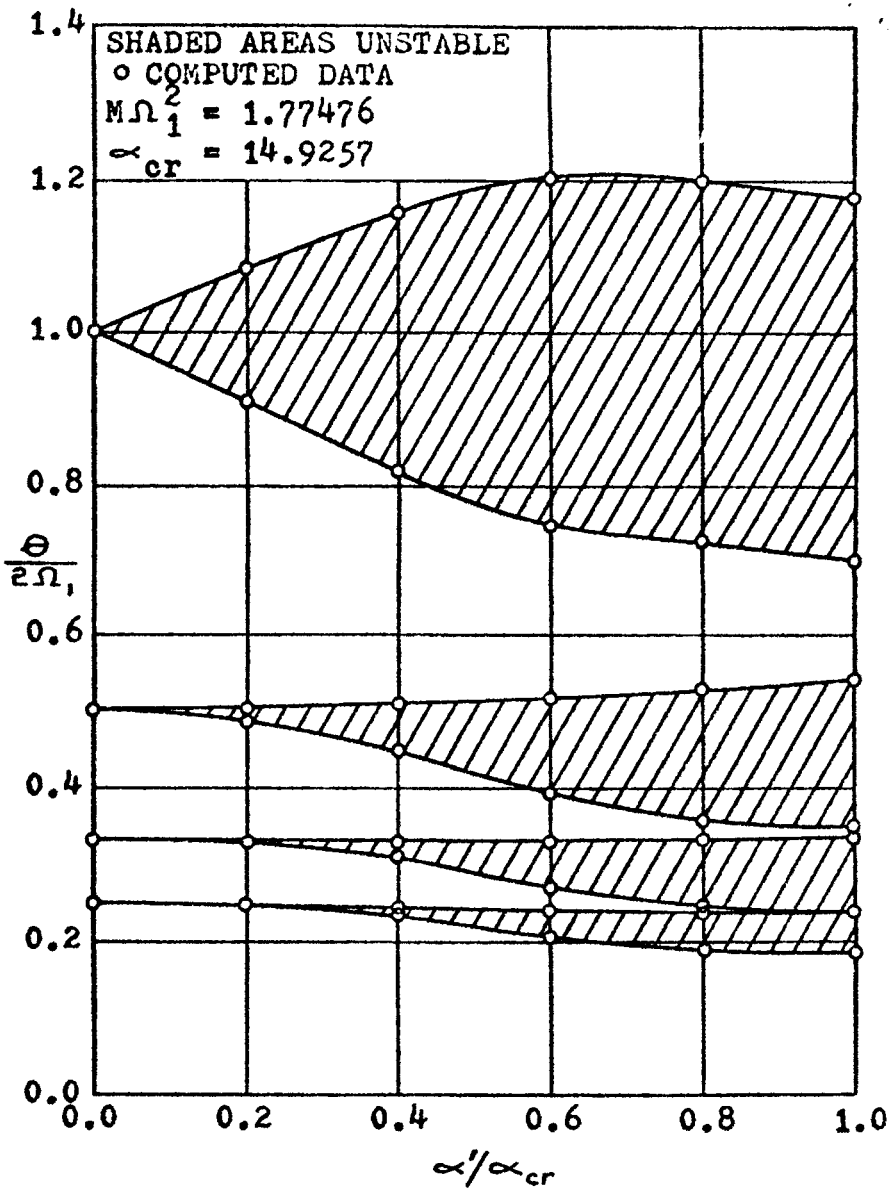

Fig. 20 Parametric Instability Regions Associated with the First Spatial Mode of Case Three

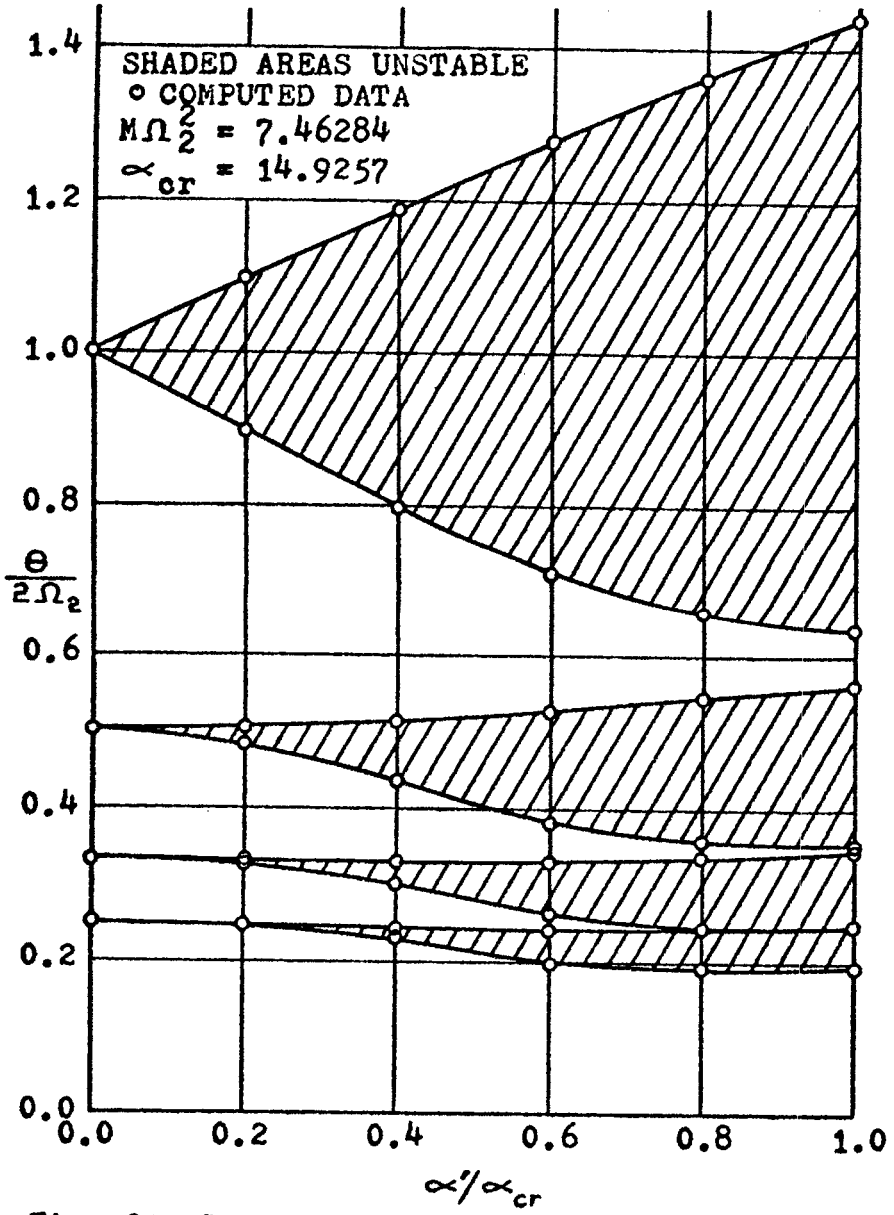

Fig. 21 Parametric Instability Regions Associated with the Second Spatial Mode of Case Three

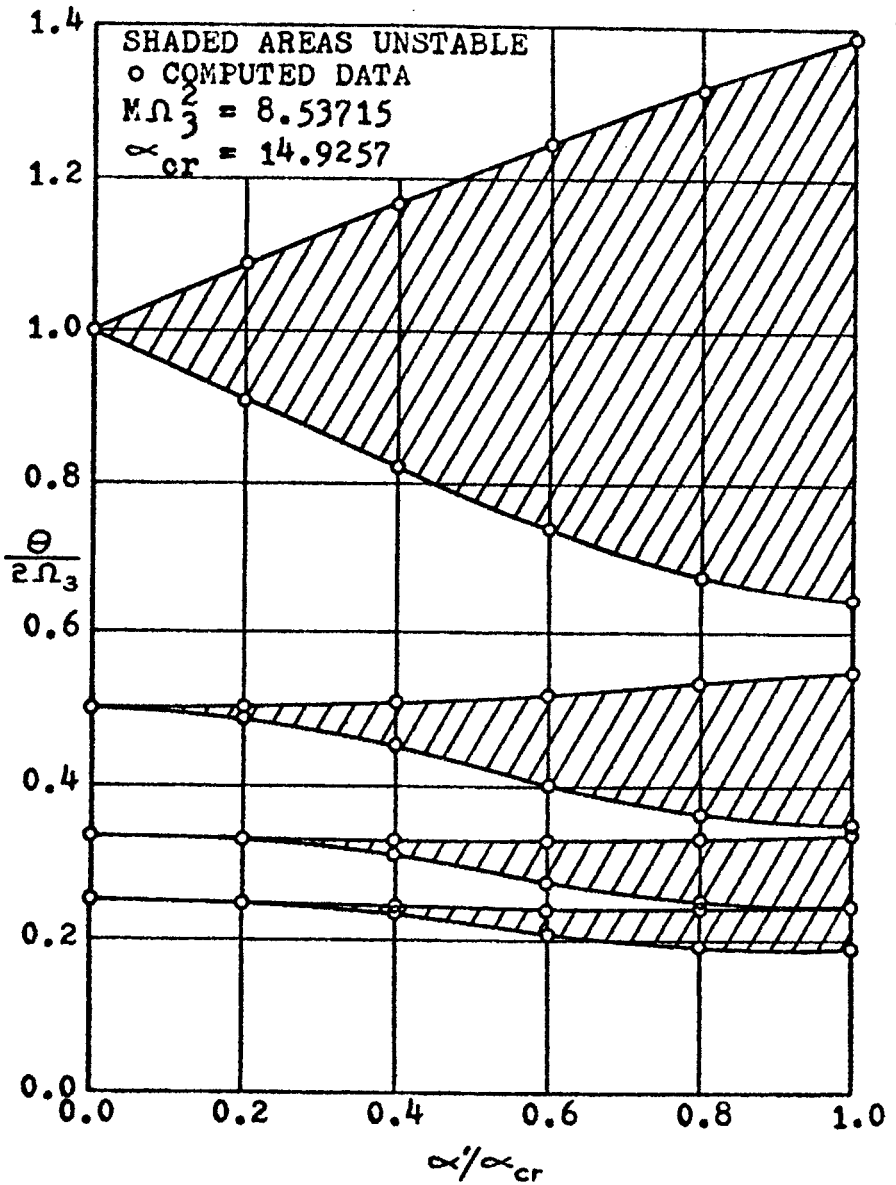

Fig. 22 Parametric Instability Regions Associated with the Third Spatial Mode of Case Three

The stiffened plate considered in case three is designed to buckle first in a mode which is represented by a full sine wave in the direction of the rib, that is, the bending rigidity of the stringer is such that it acts as a rigid beam. The parameters for this stiffened plate are shown in Fig. 19 while the instability regions are given by Figs. 20 through 22. Significantly the shape of the first temporal mode region is greatly changed by the very rigid stringer when compared with the same temporal mode region of case one. The width of this region is the narrowest and the boundaries are the most distorted of any principal region associated with the first spatial mode of previous studies. The greatest change in the location of the boundaries is for values of α'/α_{cr} greater than 0.5. The temporal mode regions of the second spatial mode coincide with those of Fig. 14. The lowest value of α_{cr} is associated with this spatial mode. The results for the second spatial mode of case three represent the superposition of the second spatial mode parametric response of the individual column and plate problems. The governing equation for the third spatial mode is Mathieu's equation and the widths of the corresponding temporal mode regions are greater than those of the first spatial mode. The parametric response of the second and third spatial modes does not involve the motion of the stringer. However, the parametric response of the first spatial mode, does involve motion of the stringer. The same can be shown to be true for the fourth and fifth spatial modes. Thus, like the first spatial mode, the results show that the rigid stringer does distort the boundaries of the fourth and fifth spatial modes.

4.2 Experimental Results

The experimental procedure used to verify the theory developed in this investigation was discussed in section three. The experimental results given at the end of this section are presented in the same ($\theta/2\Omega$, α'/α_{cr}) parameter space as are the theoretical results.

In order to present the experimental results in the form indicated above it was necessary to obtain values for the undamped natural frequency Ω for the various values of P_{xo}. The theory developed shows that the value of the load frequency, θ , for small values of α'/α_{cr} , associated with the second temporal mode region approximately equals the undamped natural frequency, Ω . This was confirmed by the experimental investigation. For experimental case one the value of θ , for small values of α'/α_{cr} , corresponded with those given by the theoretical Ω vs. P_{xo} curve. Thus, for experimental case one the theoretical curve for Ω vs. P_{xo} was used to obtain the magnitude of the undamped natural frequency for various values of P_{xo}. For experimental case two the values of the load frequency, θ , associated the second temporal mode, for small values of α'/α_{cr} , did not agree with either the theoretical or experimental values for the natural frequency. Thus, for this case the values of the load frequency, θ , associated with the second temporal mode, for small values of α'/α_{cr} , was used as the values of the undamped natural frequency for a given magnitude of the static load component.

During the experimental investigation the vibratory motion occuring within the loading mechanism caused the magnitude of the static component to decrease. This problem did not eliminate some of the data recorded since

in case one the theory was found to be approximately valid for values of α'/α_{cr} less than 0.4. However, for experimental case two this does not hold ture and therefore, the recorded data were limited to those which correspond to a value for P_{xo} close to the selected magnitude for P_{xo}.

Because a distance is involved in the determination of the load frequency, θ, errors result because of the difficulty of obtaining a real precise measurement of the distance. To minimize this error the distance measured was taken over several oscillations. Because of this problem, errors up to five per cent exist in the measured magnitude of the load frequency, θ. The magnitude of load frequency, θ, was measured at the point of transition from the idling vibration, due to initial imperfections, to the parametric resonant vibration. Additional error in the magnitude of the load frequency, θ, is introduced here because the transition point can not precisely be defined experimentally, see Fig. 25.

The experimental results obtained from the two test specimen are presented in Figs. 23 and 24 for experimental cases one and two respectively. These two figures represent the ($\theta/2\Omega$, α'/α_{cr}) parameter space for a value of $\bar{\alpha}/\alpha_{cr} = 0.5$. Equations (27) and (28) show that

$$\alpha'/\alpha_{cr} = P_{xt}/P_{cr} \qquad (163)$$

and

$$\bar{\alpha}/\alpha_{cr} = P_{xo}/P_{cr} \qquad (164)$$

in which P_{xt} is the magnitude of the total variable component of the in-plane force acting on the stiffened plate. The experimental investigation established the existence of some of the regions of instability predicted by the theory developed in section two. Figure 23 shows the location of experimentally determined points on the boundaries of the regions of instability associated with the first and second temporal mode of the first spatial mode. The experimental results for this case show good agreement with the theoretical boundaries shown in the same figure. Particularly important is the good agreement with the width or openness of the v-shaped instability region. The upper limit on the maximum value of α'/α_{cr} obtained experimentally was due to the power limitations of the shaker.

Figure 24 gives the same type of results for experimental case two. The experimental results for this case are limited only to those results which correspond to the first temporal mode associated with the first spatial mode. Again the agreement between the experimental and theoretical results is good. One of the important facts established by the results for experimental case two is that a stiffened plate will still possess parametric resonance in the first spatial mode when this mode is not associated with the fundamental static stability mode. An interesting observation for this case is that the stiffened plate would not always develop a parametric instability when it passed through the principal region of instability. This phenomenon did not occur for the test plate of experimental case one. Figures 25 through 30 represent actual strip charts which show behavior of the stiffened plate prior to and just after entering a region of instability.

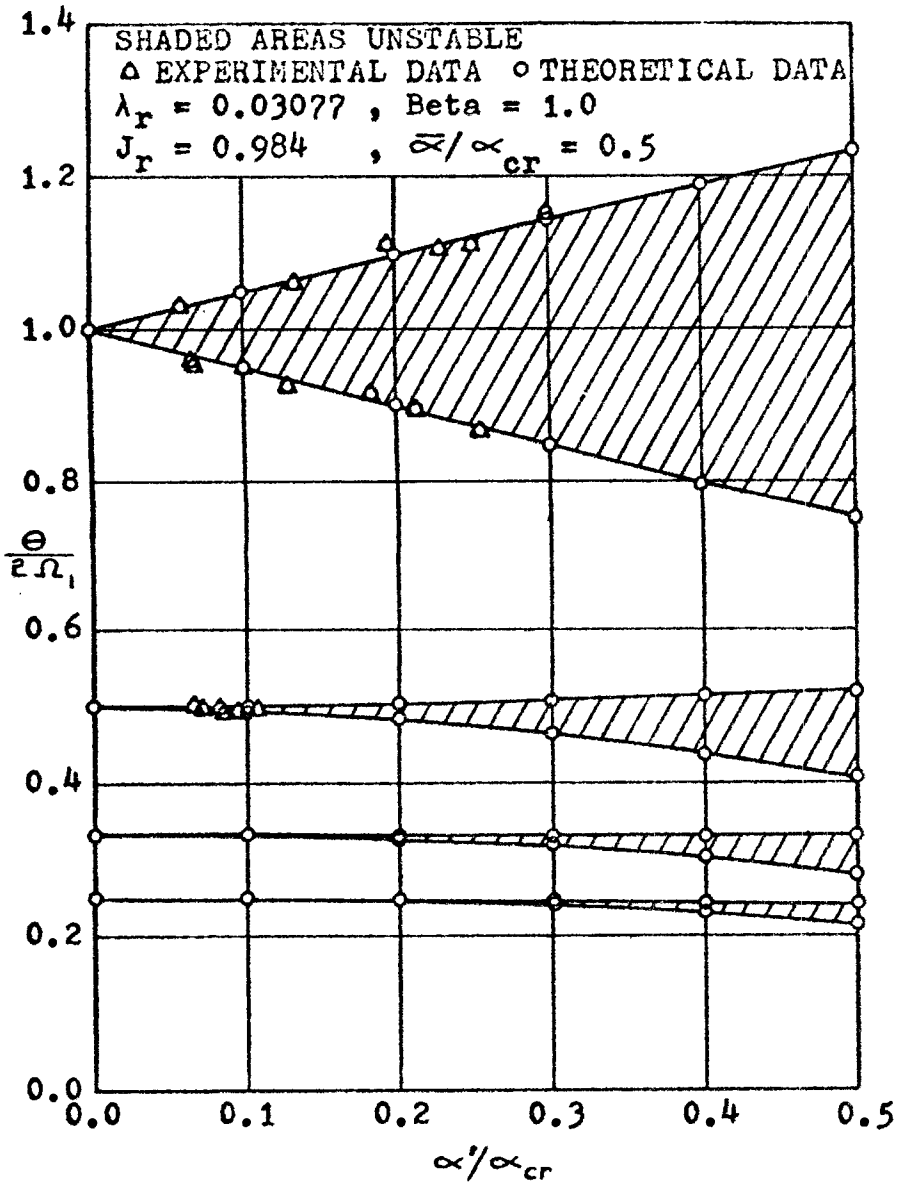

Fig. 23 Instability Regions Associated with the First Spatial Mode of Experimental Case One

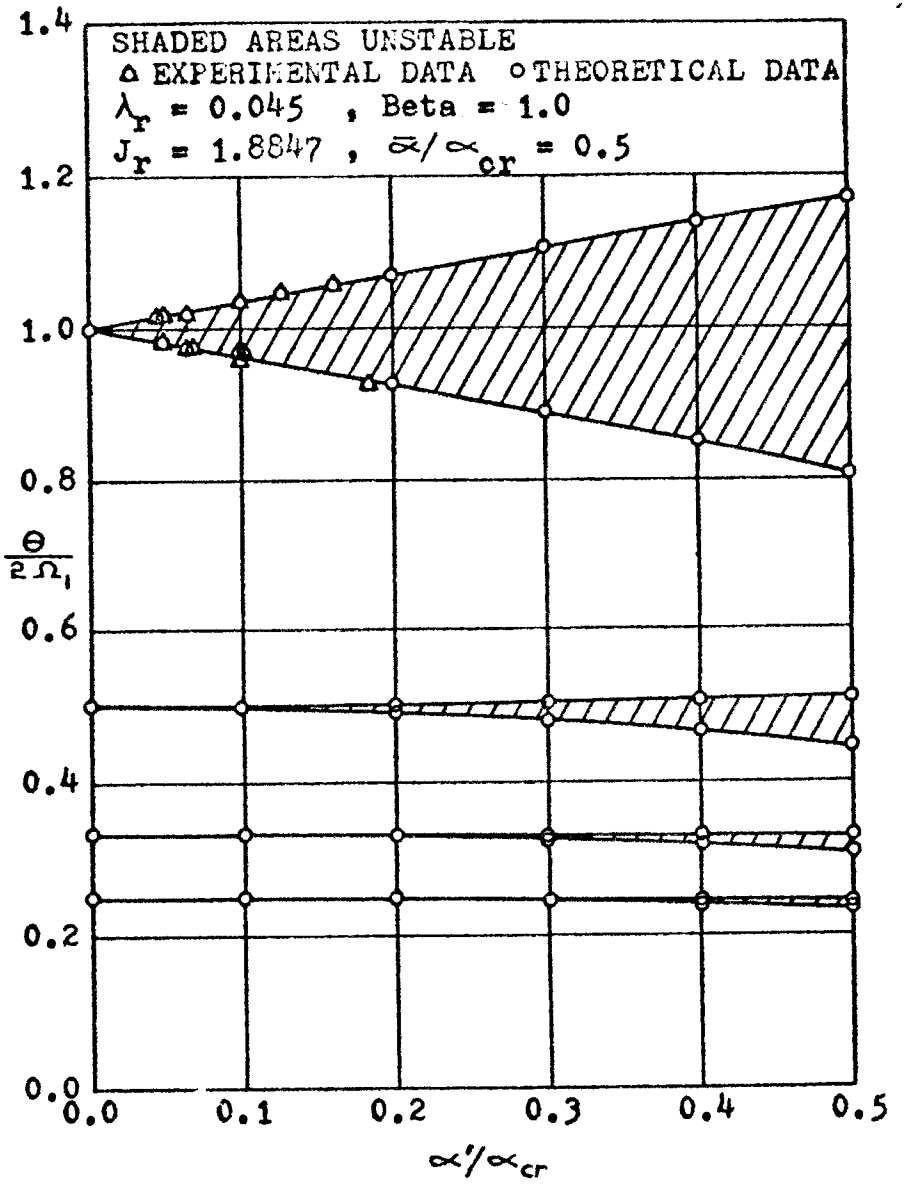

Fig. 24 Instability Regions Associated with the First Spatial Mode of Experimental Case Two

Figure 25 shows the behavior of the stiffened plate within the principal region of the first spatial mode and then the transient motion into the stable region denoted by the idling vibration. The transient motion crosses the lower boundary of the principal region of instability. This figure also shows that the period of vibration of the oscillatory motion within the principal region is twice that of the periodic in-plane load which is indicated by the vibratory record shown at the bottom of Fig. 25. This agrees with the predictions of the theory for this region. Also clearly shown on this figure is the transition point on the boundary between the stable and unstable region as indicated by the change of the period of oscillation of the stiffened plate.

The parametric response of the stiffened plate within the principal region of instability of the first spatial mode was characterized by a gradual increase in the amplitude of the plate as the load frequency increased. When the load frequency reached the theoretically predicted upper boundary, for values of α'/α_{cr} greater than 0.08 the stiffened plate did not drop back into the stable region, but continued to vibrate at a frequency twice that of the load frequency. The stiffened plate remained in the principal region of instability as the load frequency was increased to a value above that corresponding to the upper boundary. However, if the stiffened plate was disturbed the plate would change frequency to that of the load frequency and the transverse amplitude would be reduced to a level characteristic of the stable region. When the stiffened plate was in the stable region above the principal region and was struck hard transversely, the stiffened plate would snap back into the principal region of instability. This behavior is the same as that of the unstiffened flat plate which was discussed by Sommerset (20,21,22).

Because of the behavior of the stiffened plate discussed above for values of α'/α_{cr} greater than approximately 0.08, the upper boundary had to be determined by entering the principal region of instability from above. Figure 26 shows the transient motion of the plate from the stable region above the principal region of instability to within the principal region itself. Again the transition from the stable to the unstable region is indicated by the change of frequency of the plate to half that of the load frequency. Also indicated by Fig. 26 is a rapid increase of the transverse amplitude as the plate goes from the stable to the unstable region. Figure 26 also shows within the principal region of instability, the beat phenomenon of the transverse amplitude of the plate. This result has been predicted theoretically for a column by Bolotin (18) and has been obtained experimentally by others (15, 16). The transition from the stable region above the principal region of instability to within the unstable region itself is again illustrated in Fig. 27. However, this time the change of amplitude is not as rapid and the amplitude does not exhibit the beat phenomenon.

It was indicated above that the upper boundary of the principal region of instability could not be located when exiting from this region by way of the upper boundary for values of α'/α_{cr} greater than approximately 0.08. However, when the stiffened plate was allowed to completely transverse the principal region of instability for the first spatial mode for values of α'/α_{cr} less than approximately 0.08, the plate always became

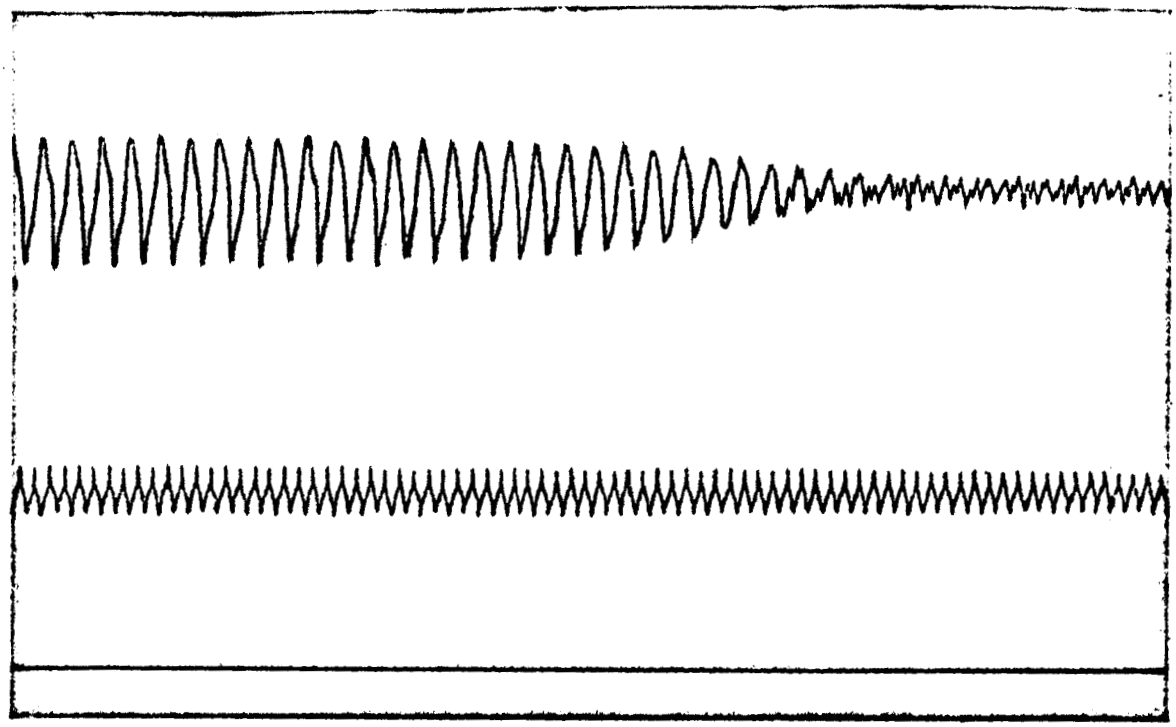

Fig. 25

Transient Motion from the Principal Region
of Instability to the Lower Stability Region

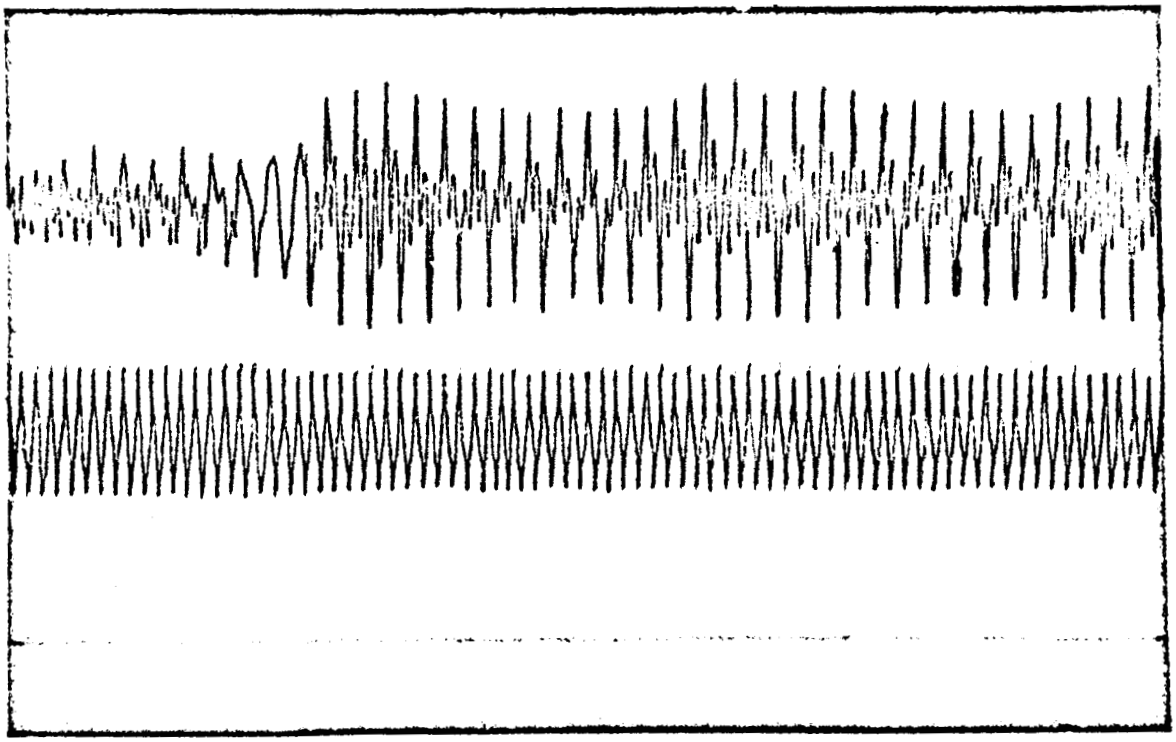

Fig. 26

Transient Motion from the Upper Stability Region
to the Principal Region of Instability (Beat)

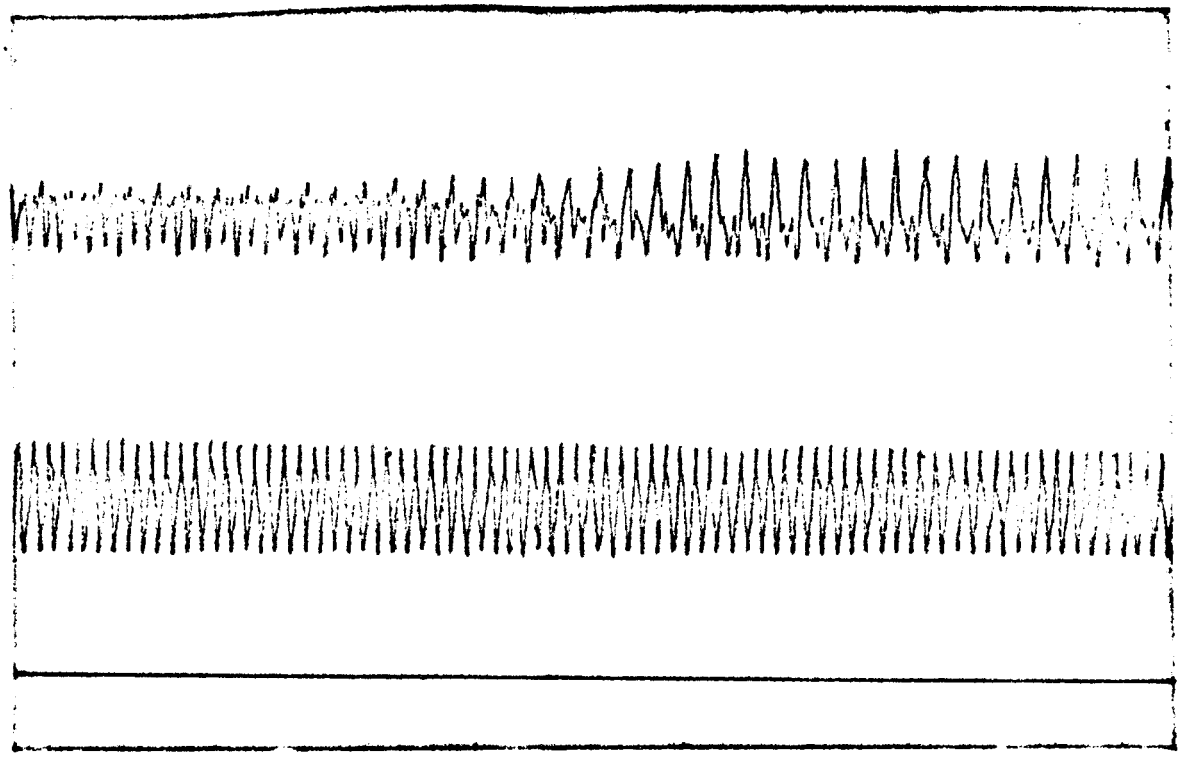

Fig. 27

Transient Motion from the Upper Stability Region
to the Principal Region of Instability

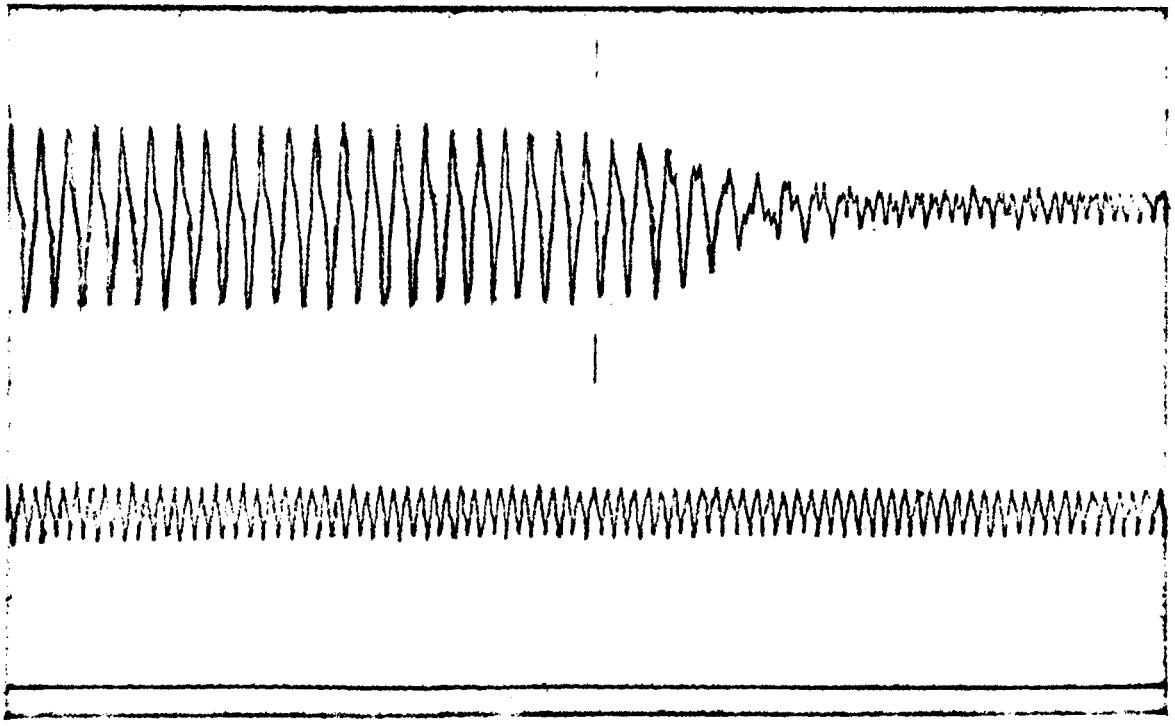

Fig. 28

Transient Motion from the Principal Region of
Instability to the Upper Stability Region

stable as the upper boundary was crossed from the unstable to the stable region as indicated in Fig. 28. This result was always obtained for both the test specimens and is contrary to the behavior predicted by the theory for the unstiffened flat plate for values of α'/α_{cr} less than approximately 0.08. Figure 28 again indicates clearly the transition between the unstable and stable region.

The parametric response of the stiffened plate as it makes the transient motion from the second temporal mode instability region corresponding to the first spatial mode into the surrounding stable regions is shown in Figs. 29 and 30. Figure 29 shows the behavior of the stiffened plate within the second temporal mode region and then the transient motion into the stable region lying below this unstable region. This figure also shows that the frequency of the oscillatory motion within the second temporal mode region is the same as that of the load frequency. The periodic in-plane load is indicated by the vibratory record at the bottom of Fig. 29. This result agrees with the predictions of the theory. Figure 30 shows the transient motion from within the second temporal mode region to the stable region lying above this unstable region. The behavior indicated by Fig. 30 is the same as for Fig. 29. The strip charts show that the buildup of amplitude in this region is not as great as the buildup of amplitude in the principal region of instability. Also the transient point on the boundaries of the second mode region is not as clearly defined as it is for the principal region. The parametric response of the stiffened plate within the second temporal mode region appears not to be the same as it is for the principal region of instability. The stiffened plate did not remain in the unstable configuration as the magnitude of the load frequency passes the corresponding value on the upper stability boundary. Instead, the stiffened plate became stable again, as indicated by Fig. 30. This was not the case for the principal region of instability.

The remaining higher order temporal mode instability regions associated with the first spatial mode were not detected during the experiments. There were some indications of the existence of the third temporal mode instability region but insufficient to obtain a detectable record.

4.3 Evaluation of Results

The theoretical results presented were limited to the first four temporal mode instability regions associated with the first three spatial mode regions. This restriction does not appear to be a severe limitation on the prediction of the parametric response for several reasons. The first of these reasons is the influence of damping. The effects of damping on the boundaries of typical instability regions is shown in Fig. 31 which represents the results given by Mathieu's function modified to include damping, see Bolotin (18). Figure 31 shows that damping causes the instability regions to withdraw from the $\Theta/2\Omega$ ordinate. The amount of withdrawal increases as the order of the temporal mode increases. In case of an undamped temporal mode region the portion of the instability region where the upper and lower boundaries coincide will disappear if a damping is present. Figure 31 also indicates that temporal mode instability regions of order greater than four would not exist in a practical range for α'/α_{cr}. This was confirmed by the experimental investigation. Figure 31 also shows why

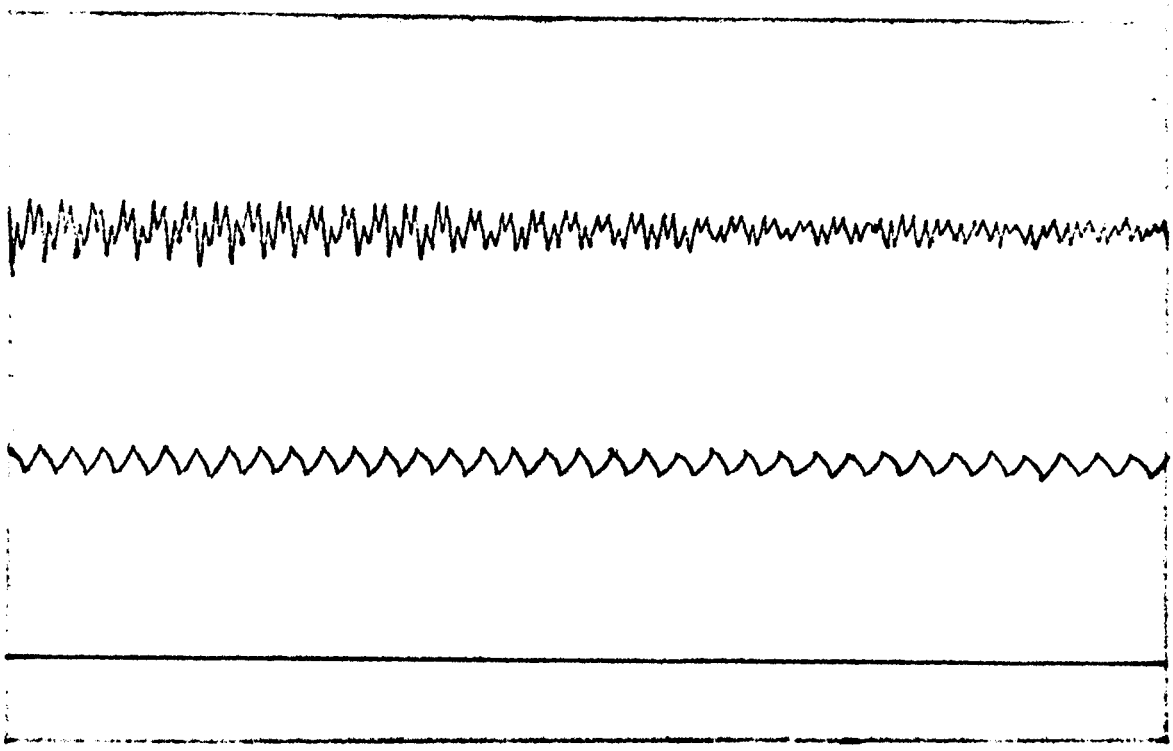

Fig. 29

Transient Motion from the Second Temporal Mode of Instability to the Lower Stability Region

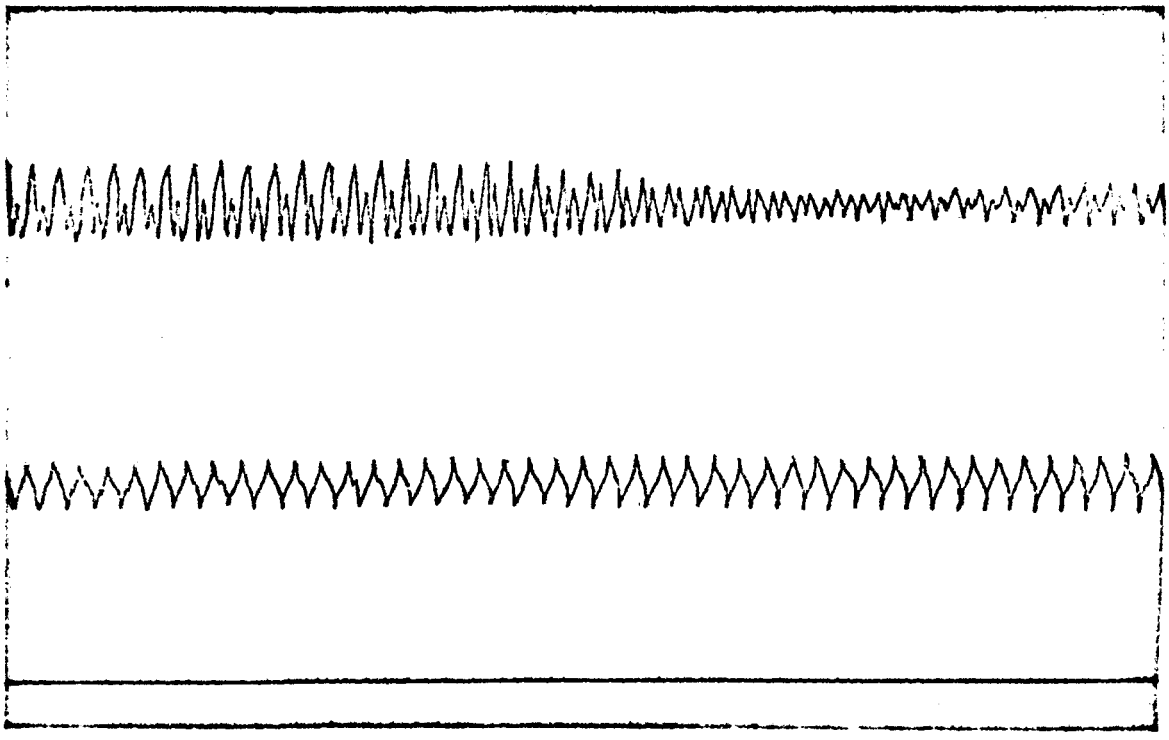

Fig. 30

Transient Motion from the Second Temporal Mode of Instability to the Upper Stability Region

the principal region of instability is considered to be the most critical as it exists for relatively small values of α'/α_{cr} even when damping is present. The widths of the temporal mode regions of instability of order greater then four are narrow in comparison with those of lesser order. The narrow width of these higher order regions implies that a small change in the load frequency, θ , would remove the system from these instability regions. Thus these regions are not as critical as the lower order ones. The experimental results also indicate that the higher the order the less the magnitude of the transverse amplitude. The build up of the transverse amplitude for these higher order modes does not appear to be sufficient to cause these regions to be of concern. However, this point does need further investigation.

The results obtained for the spatial mode regions of order greater than five, but not presented, shows that the widths of the temporal mode regions of instability decreased in an irregular manner as the order of the spatial mode increases. Generally, the widths of the temporal mode regions of instability degenerated to a line for the higher order spatial modes. When the widths of these regions degenerate to a line if damping is not considered, instability would probably not exist if damping was taken into account.

The general parametric response characteristics of the stiffened plate are for the most part similar to those of the unstiffened flat plate. It was reported in section 4.2 that the stiffened plate exhibited a dropout behavior as the system passed the upper boundary from the unstable to the stable region. This phenomenon occurred for the principal region of instability of the first spatial mode for values of α'/α_{cr} less than 0.08 and always for the second temporal mode region of the same spatial mode. The reason for this phenomenon may be due to the possible causes given below. Bolotin (18) studied a typical parametric response equation which included the effects of nonlinear inertia, nonlinear elasticity, and nonlinear damping. The effect of nonlinear elasticity on the build up of amplitude is illustrated by Fig. 32a and was shown by Somerset and Bolotin to be the principal effect on the build up of amplitude of the unstiffened flat plates. Figure 32b shows the effect of nonlinear damping on the build up of amplitude. Finally, Fig. 32c illustrates the effect on nonlinear inertia on the build-up of amplitude. These three results indicate that the drop-out effect may be due to an overriding influence of nonlinear damping or it may be due to a combined and near equal influence of nonlinear elasticity and nonlinear inertia.

The theoretical results were based on a nondimensional representation of the data which is standard practice. However, such representation can lead to misinterpretation of the results. Examination of the results given in section 4.1 could lead to the mistaken conclusion that the temporal mode instability regions associated with each of the spatial modes are separate from one another. Figure 33 represents experimental case two. It shows the first two temporal mode regions of instability for each of the first three spatial modes superimposed in the same (α'/α_{cr}, $\sqrt{M}\,\theta$) parameter space, in which $\sqrt{M}\,\theta$ is the square root of the eigenvalue for this problem. As can be seen the temporal mode regions of instability associated with the various spatial modes can overlap.

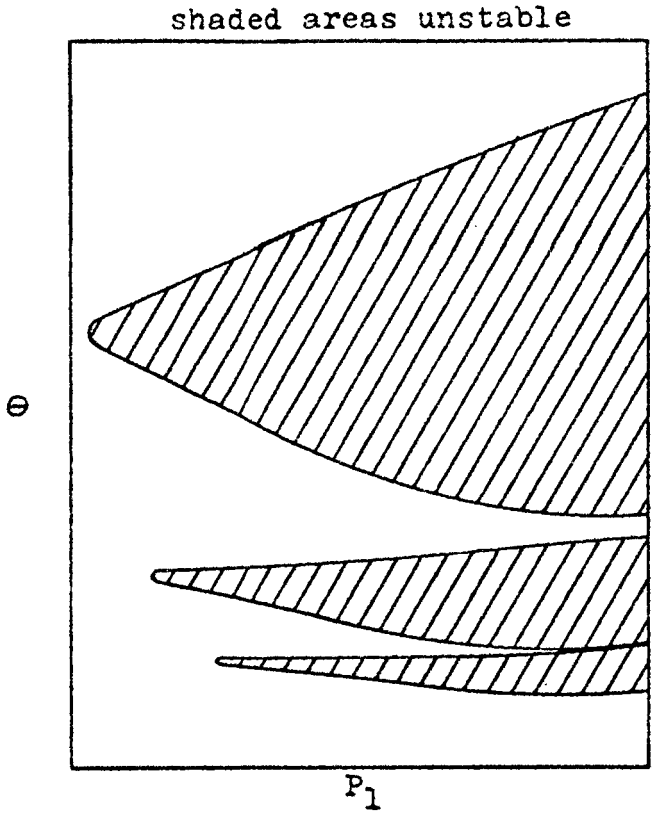

Fig. 31 Typical Instability Regions in the (P_1, Θ) Parameter Space (with damping)

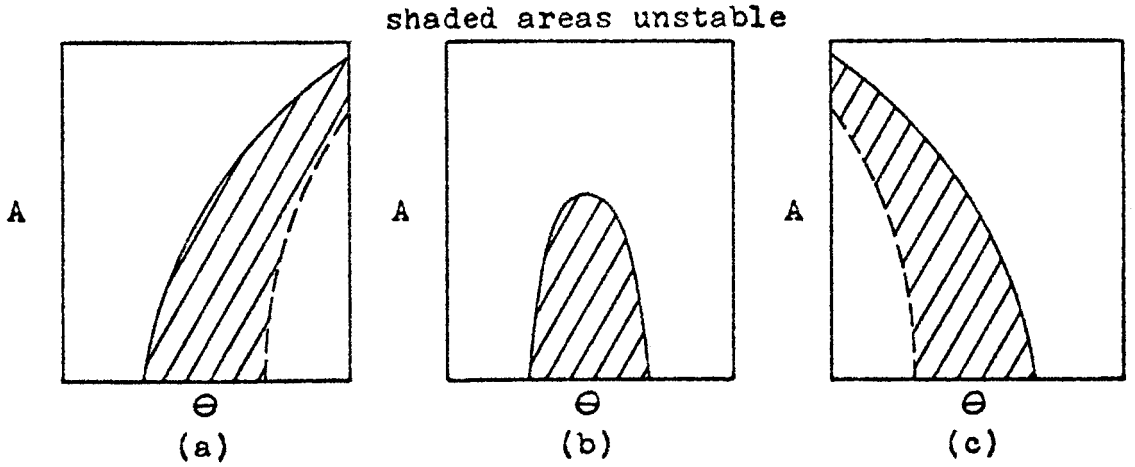

Fig. 32 Nonlinear Effects on the Instability Region, in the (Θ ,A) Parameter Space

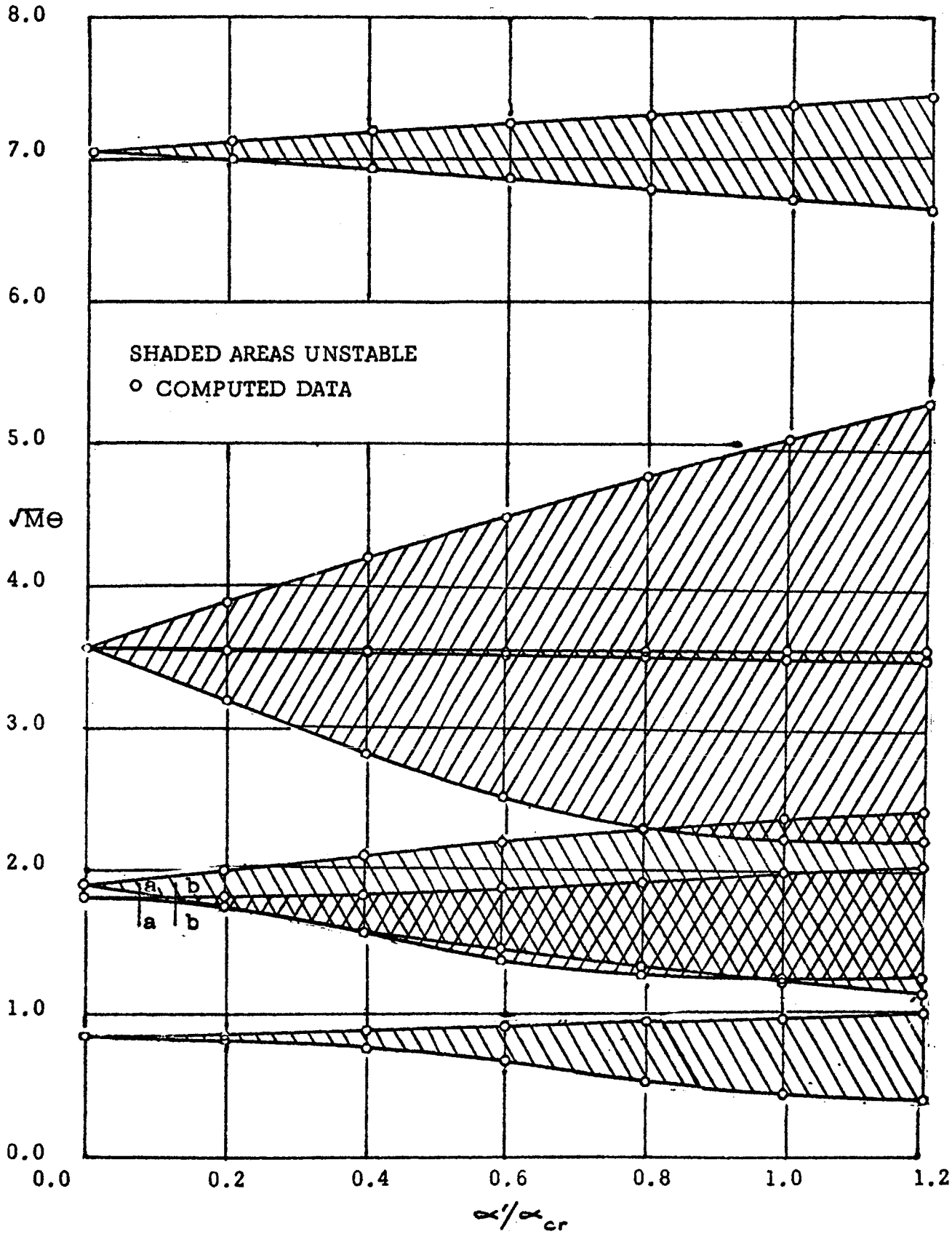

Fig. 33 Superposition of Spatial Modes, Case No. 2

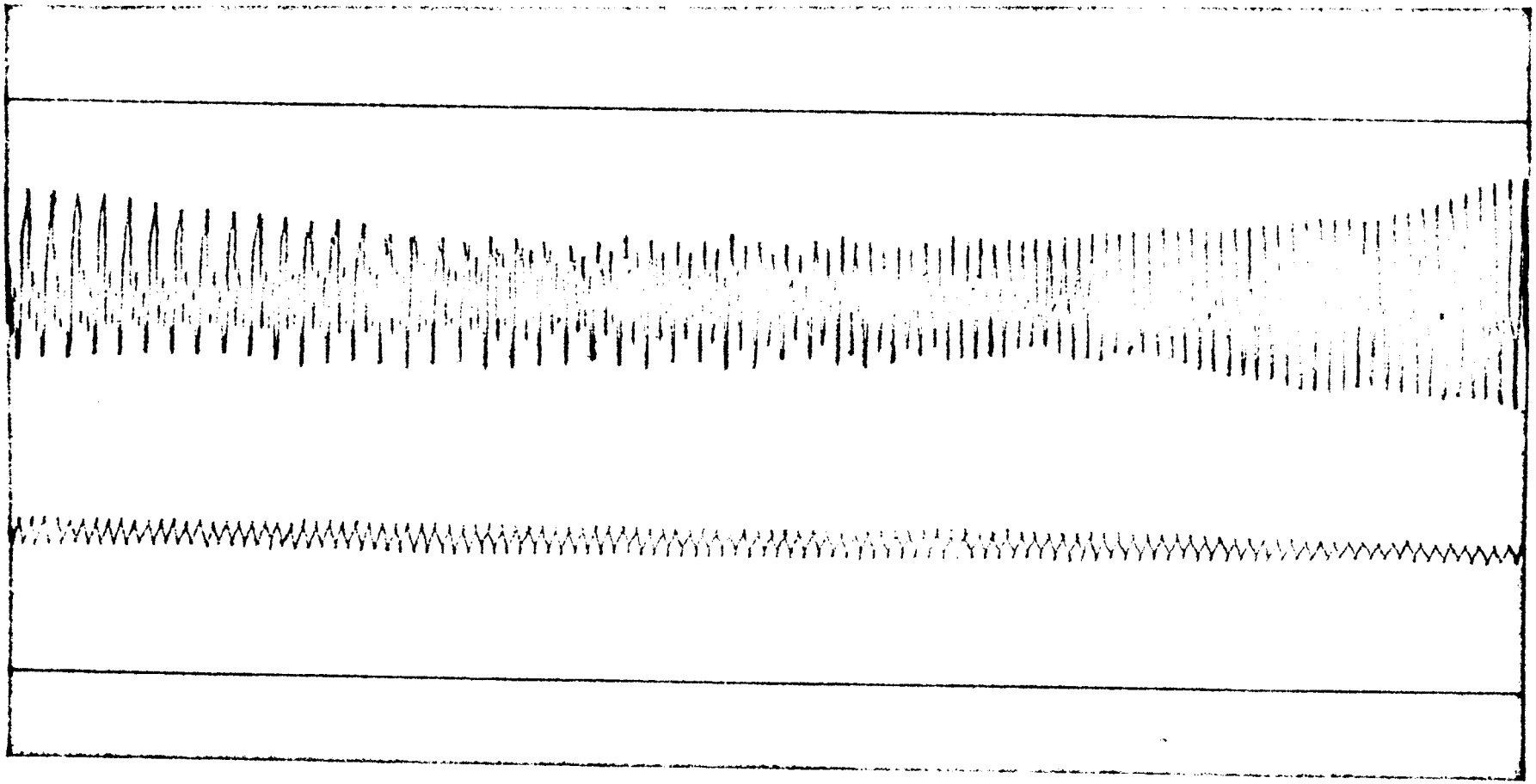

Fig. 34

Transient Motion from the Principal Mode of the First Spatial Mode to the Second Temporal Mode Region of the Second Spatial Mode

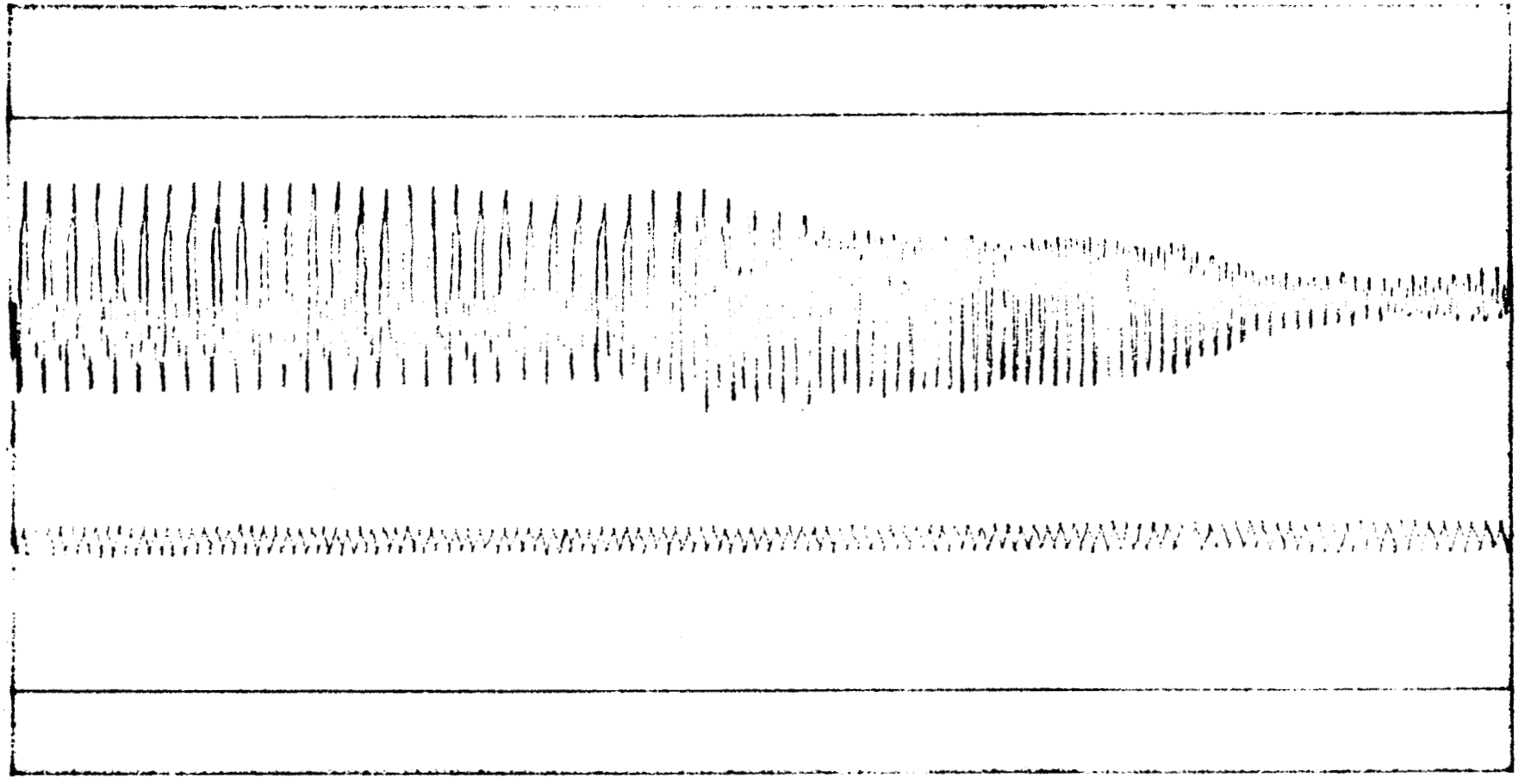

Fig. 35

Combined Motion Between the Principal Mode of the First Spatial Mode and the Second Temporal Mode Region of the Second Spatial Mode

Also it is seen that for large values of $\bar{\alpha}/\alpha_{cr}$ the second temporal mode region of instability associated with the second spatial mode lies partly below the principal region of instability associated with the first spatial mode for values of α'/α_{cr} less than 0.4. Figure 34 shows the result for experimental case two. It illustrates the transitional motion from the principal region associated with the first spatial mode by way of the lower boundary. This transitional motion transcends the second temporal mode region of instability associated with the second spatial mode and a stable region located between the two regions of instability under consideration. The build up and decrease of transverse amplitude associated with both the second temporal mode region and principal mode region can also be seen. It is significant that the build up of transverse amplitude for the second temporal region associated with the second spatial mode is greater than any experimentally indicated build up of amplitude for the corresponding region of the first spatial mode. Figure 35 represents a test run in the vicinity of line b-b of Fig. 33. This figure shows the transient motion of the stiffened plate from the principal region associated with the first spatial mode, by way of the lower boundary, into the second temporal mode region associated with the second spatial mode which overlaps the principal region at this point. Figure 35 also indicates an interaction between the two regions of instability where they overlap. Again the buildup of amplitude for the second temporal mode region is significant.

The experimental results presented in section 4.1 show that the theory developed in section two gives a correct prediction of the location of the boundaries of the regions of instability associated with the (α'/α_{cr}, $\theta/2\Omega$) parameter space. However, the experimental results also show that this theory does not give any information about the very important three dimensional regions of instability located in the (α'/α_{cr}, $\theta/2\Omega$, A) parameter space. The theory developed in this investigation also does not give a clear indication about the behavior of the stiffened plate in the vicinity of the upper boundary of the principal region of instability. The theory seems to imply that in crossing this upper boundary from the unstable to the stable region the stiffened plate will become stable again which is not the case for values of α'/α_{cr} greater than approximately 0.08. The linear theory presented in this investigation however does predict accurately the location of the boundaries of the regions of instability at which the onset of parametric response takes place. The knowledge of these boundary locations provides the designer with the necessary information so that a stiffened plate can be designed to operate within the stable regions.

The theoretical results presented in section 4.1 show that the advantages normally gained by stiffening a flat plate can be lost when the parametric response of the plate is considered. Stiffening of a flat plate can bring the magnitudes of the critical buckling load parameter, α_{cr}, associated with the various static stability modes closer together. For the stiffened plate this causes an increase in the width of the temporal mode regions of instability associated with the higher order spatial modes as compared with the unstiffened flat plate. This is dangerous since it causes a wider range of load frequencies, θ, over which the plate can be unstable.

5. CONCLUSIONS

Based on the results of this investigation the following conclusions can be drawn:

1. The theory developed for the stiffened plate treated as a discrete element model correctly predicts the location of the boundaries of the regions of instability as shown by good agreement with the experimental results.
2. The theory developed also completely predicts the parametric response, natural frequencies and static buckling values for any simply-supported rectangular stiffened plate and allows for an arbitrary choice in the size, location and number of ribs and stringers.
3. The location and size of the stiffeners can have a pronounced effect on the location of the boundaries of the instability regions when compared with those of a flat unstiffened plate.
4. The most dangerous region of instability, from the standpoint of width, is the first temporal mode associated with the spatial mode which is the closest to the fundamental static stability mode.
5. Variations in the loading arrangement on the stiffened plate can also cause changes in the location of the boundaries of the regions of instability.
6. The widths of the instability regions connected with the spatial modes, other than the one associated with the fundamental static stability mode, are also wide if the values of α_{cr} associated with these modes are close to the lowest value of α_{cr}.
7. For the cases studied, the greatest single effect on the location of the boundaries of the regions of instability is caused by the increase of the rigidity of either a rib or a stringer to the point that the lowest value of α_{cr} corresponds with a spatial mode other than the first spatial mode.
8. The theories developed in this investigation only predict the boundaries of the regions of instability and they do not give information about the behavior of the stiffened plate within a region of instability.

BIBLIOGRAPHY

1 Faraday, M. "On a Peculiar Class of Acoustical Figures, and on Certain Forms Assumed by a Group of Particles upon Vibrating Elastic Surfaces," Phil. Trans. Roy. Soc., London, Vol. 121 (1831), 299-318.

2 Melde, F. "Uber Erregung Stehender Wellen eines fadenformigen Korpers," Ann. der Physik u Chemic, Vol. 109, Ser. 2 (1859), 193-215.

3 Strutt, J. W. (Lord Rayleigh). "On the Crispations of Fluid Resting upon a Vibrating Support," Phil. Mag., Vol. 16 (1883), 50-53.

4 Strutt, J. W. (Lord Rayleigh). "On the Maintenance of Vibrations by Forces of Double Frequency and on the Propagation of Waves through a Medium Endowed with a Periodic Structure," Phil. Mag., Vol. 24, Ser. 5 (1883), 145-159.

5 Beilin, E. A., and Dzhanelidze, "Survey of Work on the Dynamic Stability of Elastic Systems," (in Russian), Prikl. Mat. i Mekhan., Vol. 16, No. 5 (1952), 635-648.

6 Evan-Iwanowski, R. M. "Parametric Instability of Elastic Systems," Developments in Theoretical and Applied Mechanics, Proceedings of the First Southeastern Conference on Theoretical and Applied Mechanics, Vol. I, Plenum Press, New York (1963), 100-109.

7 Evan-Iwanowski, R. M. "On the Parametric Response of Structures," Applied Mechanics Reviews, Vol. 18, No. 9 (1965), 699-702.

8 Beliaev, N. M. "Stability of Prismatic Rods Subject to Variable Longitudinal Forces," (in Russian), Collection of Papers: Engineering Constructions and Structural Mechanics (Inzhenernye sooruzhenilia i striotel' nais mekhanika), Leningrad, Put' (1924).

9 Weidenhammer, F. "Der Eingespante, Axial-Pulsierend Belastete Stabe als Stabilitat sproblem," Ingenieur Archiv., Vol. 19 (1951), 162-191.

10 Weidenhammer, F. "Nichtlineare Biegeschwingungen des Axial-Pulsierend Belasteten stabes, Ingenieur Archiv., Vol. 20 (1952), 315-330.

11 Bolotin, V. V. "On the Transverse Vibrations of Rods Excited by Periodic Longitudinal Forces," (in Russian), Collection of Paper: Transverse Vibrations and Critical Velocities, (Poperechnye Kolebaniia i Kriticheskie shorosti), Akademiia Nauk SSSR, Moscow, Vol. 1, 46-77.

12 Bolotin, V. V. "Determination of the Amplitudes of Transverse Vibrations Excited by Longitudinal Forces," (in Russian), Collection of Papers: Transverse Vibrations and Critical Velocities, (Poperechnye Koleboniia i kriticheskie shorosti), Akademiia Nauk SSSR, Moscow, Vol. 2 (1953), 45-64.

13 Grybos, R. "Parametric Vibration in a System with Non-linear Characteristics," (in Polish), Rozprowy Inzynierskie, Vol. 14, No. 2 (1966), 215-230.

14 Utida, I. and K. Sezawa. "Dynamical Stability of a Column under Periodic Longitudinal Forces," Rep, Aeronaut. Res. Inst., Tokyo Imp. University, Vol. 15, No 193 (1940), 139-183.

15 Somerset, J. H. "Parametric Instability of Elastic Columns," Syracuse University Research Institute Re-Report No. 1053-7 (1962).

16 Somerset, J. H. and R. M. Evan-Iwanowski. "Experiments on the Parametric Instability of Columns," Developments in Theoretical and Applied Mechanics, Proceedings of the Second Southeastern Conference on Theoretical and Applied Mechanics, Vol. 2, Pergamon Press Ltd. (1965), 503-525.

17 Einaudi, R. "Sulle Configurazioni di Equilibrio Instabili di una Piastra Sollecitata de Sforzi Tangerziale Pulsanti," Atti Accad Gioenia, J. Memoria, Vol. 20, No. 1-5 (1935-1936).

18 Bolotin, V. V. The Dynamic Stability of Elastic Systems, (English Translation), Holden Day, San Francisco (1964).

19 Bolotin, V. V. "Certain Nonlinear Problems of the Dynamic Stability of Plates," (in Russian), Izv. Adad. Nauk SSR, Otd. Tekhn. Nauk, Vol. 10 (1954) 47-59.

20 Somerset, J. H. "Large Amplitude Stabilization of Parametrically Excited Plate Vibration," Dissertation, Syracuse University (1965).

21 Somerset, J. H., and R.M. Evan-Iwanowski. "Experiments on the Large Amplitude Parametric Vibrations of Rectangluar Plates," Developments in Theoretical and Applied Mechanics, Proceedings of the Third Southeastern Conference on Theoretical and Applied Mechanics, Vol. 3, Pergamon Press, LTD., London (1966).

22 Somerset, J. H. "Transition Mechanisms Attendant to Large Amplitude Parametric Vibrations of Rectangular Plates," Presented at the A.S. M.E. vibration conference, Paper No. 67-Bibr-5 (1967).

23 Yu, Yi-Yuan, and Jai-Lue Lai. "Influence of Transverse Shear and Edge Conditions on Nonlinear Vibration and Dynamic Stability of Homogeneous and Sandwich Plates," Journal of Applied Mechanics, Transactions of the A.S.M.E., Vol.33, No.4 (1966), 934-936.

24 Yu, Yi-Yuan. "Application of Variation Equations of Motion to the Nonlinear Analysis of Dynamic Buckling," to be published in Proceedings of the Ninth Midwestern Mechanisms Conference.

25 Ambratsumyan, S. A., and V. T. Gnuni. "On the Dynamic Stability of Nonlinearly-Elastic Three-Layered Plates," (English Translation), Journal of Applied Mathematics and Mechanics, Vol 25, No. 4 (1961), 1002-1108.

26 Ambratsumyan, S. A. and V. T. Gnuni. "On the Forced Vibration and Dynamic Stability of Three-Layered Orthotropic Plates," (in Russian), Izv. Akad. Nauk SSSR, Otd. Tekh. Nauk, Mekh. i Mash., No. 3 (1961), 117-123.

27 Schmidt, G. "Nonlinear Parametric Vibration of Sandwich Plates," Proceeding of Vibration Problems, Vol. 6, No. 2 (1965), 209-228.

28 Ambratsumyan, S. A., and A. A. Khachaturian. "On the Stability and Vibrations of Anisotropic Plates," (in Russian), Dokladi Akad. Nauk Arm SSR, Vol. 29, No. 4 (1959), 159-166.

29 Ambratsumyan, S. A., and A. A. Khachaturian. "On the Stability of Vibrations of Anisotropic Plates," (in Russian), Izv. Adad. Nauk SSSR, No. 1 (1960), 113-122.

30 Francis, J. G. F. "The QR Transformation--A Unitary Analogue to the LR Transformation," Computer Journal, Vol. 4, 265-271, 332-345.

31 Parlett, B. "The Development and Use of Methods of LR Type," STAM Review, Vol. 6, No. 3, 275-295.

32 Ralston, A. A First Course in Numerical Analysis, McGraw-Hill Book Company, Inc., New York, 1965.

33 Duffield, R. C. An Investigation of Parametric Stability of Stiffened Rectangular Plates, Dissertation, University of Kansas (1968).

STUDIES IN ENGINEERING MECHANICS

1. "Vibration of Steel Joist-Concrete Slab Floor System--Part I," by Kenneth H. Lenzen and Joseph E. Keller, September, 1959.

2. "A Study of Flow Through Abrubt Expansions: Progress Report I, Mean Characteristics of Flow," by Neel Kanth D. Sharma, February, 1959.

3. "Vibration of Steel Joist-Concrete Slab Floor System--Part II," by Kenneth H. Lenzen and Joseph E. Keller, May, 1960.

4. "Damping Considerations in Vibration Response of Humans," by Joseph E. Keller, May, 1960.

5. "A Study of the Vibration of Rectangular Anisotropic Plates by the Ritz Method," by James A. Wiley, May, 1960.

6. "A Study of Flow Through Abrupt Expansions: Progress Report II, Pressure Fluctuations in Flow," by Charles L. Sanford and David W. Appel, June, 1961.

7. "A Study of Flow Through Abrupt Two-Dimensional Expansions: Progress Report III, Formation of Vortices," by Charles L. Sanford, June, 1961.

8. "A Study of the Dynamics of Flow Through Suction-Box Covers: Progress Report I, Flows Without Resistance," by Allen T. Hjelmfelt, June, 1961.

9. "Vibration Damping of Anisotropic Plates," by Gerald W. Barr, June, 1961.

10. "Stress in Unstiffened Cylindrical Shells Containing a Granular Material," by John T. Easley, June, 1961.

11. "A Study of the Dynamics of Flow Through Suction-Box Covers: Progress Report II, Flows with Resistance," by William H. Y. Lee, February, 1962.

12. "A Study of Various Damping Devices for Controlling Vibrating Floor Systems," by William C. Lyons, June, 1962.

13. "Characteristics of Flow Through Symmetrical Laterals: Progress Report I," by Carl T. Herakovich and John V. Otts, June 1, 1962.

14. "Separation of Flow at Interior Corners: Progress Report I, Geometry of Separation Zone," by Karl G. Maurer, June 1,1962.

15. "A Study of Flow Through Abrupt Expansions: Progress Report IV Effect of Gate Oscillation," by Svein Vigander, June, 1962.

16. "Vibration of Steel Joist-Concrete Slab Floor Systems: Final Report," by Kenneth H. Lenzen, August, 1962.

17. "Free-Streamline Analyses of Flow Nozzles, Flow through Side Inlets and Flow Past Corners," by David W. Appel, March, 1963.

18. "Effect of Bearing Stresses on the Fatigue Strength of a Structural Joint," Tehyu Chu, May, 1966.

19. "Pilot Study--The Applicability of the AISC Formula to the Top Chords of Steel Joists," by Kenneth H. Lenzen, 1965.

20. "Separation of Laminar and Transitional Flows at an Interior Corner," by Mack H. Gray III, March, 1965.

21. "An Experimental Study of Wall-Pressure Fluctuations in a Cavitating Turbulent Shear Flow," by Svein Vigander, May, 1965.

22. "The Jayhawk Bender--A Structural Analysis Program," by J. B. Tiedemann, February, 1966.

23. "Computer Analysis of Two Dimensional Rigid Joint Frames," by V. S. Varadachary, June, 1966.

24. "Inelastic Behavior of the Compression Chord of Open-Web Steel Joists," by W. Scott McDonald, Jr., 1966.

25. "Uniform Load Testing of Open-Web Steel Joists," by Robert D. Ohmart, 1961.

26. "Vibrations in Floor Systems of Steel-Framed Buildings," by Leslie D. Meyer, May, 1967.

27. "Design Formulas for the Top Chords of Open-Web Steel Joists: Final Report," by Kenneth H. Lenzen, April, 1968.

28. "An Investigation of Parametric Stability of Stiffened Rectangular Plates," by Nicholas Willems and Roger C. Duffield, March, 1968.